The Thesis Committee for Michelle Marie Lacks
Certifies that this is the approved version of the following thesis:

Geopolymer-Based Solutions for Coal Combustion Product Solidification and Stabilization

APPROVED BY
SUPERVISING COMMITTEE:

Maria Juenger, Co-Supervisor

Lynn Katz, Co-Supervisor

Geopolymer-Based Solutions for Coal Combustion Product Solidification and Stabilization

by

Michelle Marie Lacks, B.S.

Thesis

Presented to the Faculty of the Graduate School of

The University of Texas at Austin

in Partial Fulfillment

of the Requirements

for the Degree of

Masters of Science in Engineering

The University of Texas at Austin

May, 2017

Acknowledgements

I would like to thank my advisors Dr. Maria Juenger and Dr. Lynn Katz for your support and mentoring over the past two years. It has been a pleasure working with both of you. I would also like to thank EREF for providing the funding to work on this project.

Abstract

Geopolymer-Based Solutions for Coal Combustion Product Solidification and Stabilization

Michelle Marie Lacks, M.S.E.

The University of Texas at Austin, 2017

Supervisors: Maria Juenger and Lynn Katz

Coal combustion products (CCPs) such as fly ash have been used for years as a sustainable substitute for cement in concrete, however, significant quantities of CCPs are currently discarded into ash ponds and landfills each year. CCPs can contain heavy metals that have the potential to leach into surface and ground waters when improperly disposed of. Of further concern is that in recent years power plants have been injecting sodium carbonate compounds such as trisodium hydrogendicarbonate dihydrate (trona) into their flue gas streams to reduce SO_x emissions. Trona injection has been shown to alter the characteristics of collected fly ash and increase leaching of heavy metal compounds from the ash, posing a higher environmental threat.

Geopolymers that utilize CCPs as an aluminosilicate precursor are under consideration as an alternative to conventional Portland cement. These materials, produced by activating aluminosiliceous powders (e.g., fly ash) with highly alkaline solutions, may reduce the carbon footprint of infrastructure materials and stabilize heavy metal wastes. While previous work indicates that geopolymers can successfully stabilize heavy metal

wastes under lab conditions (i.e. reagent water), this work aims to evaluate the potential for geopolymer stabilization of heavy metal wastes in landfill environments and to identify characteristics that reduce leaching potential of geopolymers. Leaching tests on trona impacted CCP based geopolymers were performed with a simulated landfill leachate to mimic conditions within ash ponds and landfills. Batch extraction tests were used to characterize leaching at different pH's and different liquid/solid ratios (L/S) using LEAF protocols.

It was found that geopolymers made with 4M NaOH had higher reactivity than those made with 8M NaOH, and increasing the silica modulus (SiO_2/Na_2O) from 0-1.5 also increased reactivity of specimens. Cements were observed to better bind oxyanions at high pH than geopolymers, but geopolymers were capable of reducing leaching for a number of elements over a broad pH range. The extent of leaching depended on both the element and the geopolymer composition. Results also indicated that leaching of copper and selenium are affected by landfill leachate properties, which could have impacts on wastes with larger quantities of these elements.

Table of Contents

List of Tables x

List of Figures xi

Chapter 1: Introduction 1

1.1 Background 1

1.2 Objectives 2

Chapter 2: Literature Review 3

2.1 Introduction 3

2.2 Leaching of Raw CCPs 4

2.3 Stabilization Processes 5

2.3.1 Cementitious Reactions 5

2.3.2 Geopolymeric Reactions 7

2.4 Chemical Stabilization Processes 8

2.4.1 Oxyanions 9

2.4.2 Cations 13

2.5 Leaching in Landfill Conditions 15

2.6 Conclusions 16

Chapter 3: Materials and Methods 18

3.1 Mixture Development 18

3.1.1 Mixture Design 18

3.1.2 Mixing 22

3.1.3 Mini-Slump Test 23

3.1.4 Casting 23

3.1.5 Curing 23

3.1.6 Compression Testing 24

3.1.7 Particle Size Reduction 24

3.1.8 Moisture Content 24

3.1.9 Sample Ignition 25

3.2 Characterization of Materials 25

3.2.1 X-Ray Fluorescence 25
3.2.2 X-Ray Diffraction 26
3.2.3 Loss-on-Ignition 27
3.2.4 Thermogravimetric Analysis 27
3.2.5 Particle Size Distribution 28
3.2.6 Surface Area 29
3.2.7 Digestion 30
3.2.8 Porosity 31
3.3 Leaching Tests 31
3.3.1 Moisture Content 32
3.3.2 Simulated Landfill Leachate 32
3.3.3 pH Variant Leaching Test 33
3.3.4 Liquid/Solid Variant Leaching Test 35
3.3.5 Dynamic Leaching Test 35
3.3.6 pH, Conductivity, ORP Testing 37
3.3.7 Sample Collection, Dilution, and Storage 38
3.3.8 Sample Analysis 39
Chapter 4: Results and Discussion 42
4.1 Characterization of Raw Materials 42
4.1.1 Physical Characterization 43
4.1.2 Chemical Characterization 45
4.1.3 Summary 51
4.2 Characterization of Cement Pastes and Geopolymers 52
4.2.1 Physical Characterization 52
4.2.2 Chemical Characterization 55
4.2.2 Summary 59
4.3 Leaching Test Water Quality 60
4.3.1 Conductivity 61
4.3.2 Titration 61
4.3.3 ORP 63

4.4 Leaching Test Results 64
4.4.1 Major Ions 65
4.4.2 Oxyanions 69
4.4.3 Cations 74
4.4.4 Leaching in Simulated Landfill Leachate 79
Chapter 5: Conclusions 82
5.1 Conclusions 82
5.2 Future Work 83
Appendix A – Trace Metal Leaching Test Results 85
Appendix B – Characterization Results 121
Appendix C – Water Quality Data 131
References 136

List of Tables

Table 3.1: Cement Paste Mixture Design, Mini-Slump, and Initial Moisture Content 20
Table 3.2: Geopolymer Mixture Design, Mini-Slump, and Initial Moisture Content 21
Table 3.3: Alkaline Solutions 22
Table 3.4: Landfill Leachate Composition 33
Table 3.5: Dynamic Leaching Test Collection Schedule 37
Table 3.6: Typical ICP-MS Limits of Detection (determined for each sample run) 41
Table 4.1: 10%, 50%, 90% Particle Size and Surface Area of Raw CCPs 44
Table 4.2: Particle Size Distribution for Particles >1mm 44
Table 4.3: Oxide Content of Raw CCPs obtained from XRF 47
Table 4.4: Raw CCP XRD Phases and Phase Percent 49
Table 4.5: LOI Results for Raw CCPs 50
Table 4.6: Trace Metal Content of Raw CCPs Determined by Digestion 51
Table 4.7: FAH Geopolymer XRD Phases 58
Table 4.8: Geopolymer and Cement Paste Loss on Ignition Results 59
Table 4.9: pH of Increased Leaching for Cations 77

List of Figures

Figure 2.1: As(V) sorption onto goethite versus pH (Dixit and Herring, 2003 with copyright permission) (left), Arsenic adsorption on TiO_2 anatase versus pH (Wei et al., 2016 with copyright permission) (right) 10
Figure 2.2: Solubility Diagram for Metal Hydroxides (Reproduced from Porex, 2017) . 14
Figure 3.1: Dynamic Leaching Test Set-Up.....36
Figure 3.2: Typical Aluminum Standard Curve.....40
Figure 4.1: Particle Size Distributions of Raw CCPs 45
Figure 4.2: X-Ray Diffractograms for Raw CCPs 48
Figure 4.3: Geopolymer Edges Crumbling after Strength Test 54
Figure 4.4: Cement Paste Strength Results 54
Figure 4.5: Geopolymer Strength Results 55
Figure 4.6: FAH Geopolymer XRD Diffractograms 56
Figure 4.7: Raw Ash Conductivity Readings versus pH 61
Figure 4.8: Raw Ash Titration with Nitric Acid 63
Figure 4.9: Geopolymer ORP Results in MPW 64
Figure 4.10: Aluminum Species in equilibrium with Solid Al_2O_3 from Visual MINTEQ Modeling 66
Figure 4.11: Total Dissolved Ca^{2+} in equilibrium with 0.3M and 1M CO_3^{-2} from Visual MINTEQ Modeling 67
Figure 4.12: Calcium (left) and Aluminum (right) in Aqueous Solution versus pH 68
Figure 4.13: Arsenic Leaching from FAH Specimens vs pH (left) and vs L/S (right 70
Figure 4.14: Arsenic speciation and solid compounds based upon Visual MINTEQ 71
Figure 4.15: Selenium leaching from FAH (left) and FAB (right) Specimens vs pH 73
Figure 4.16: Chromium leaching from FAH Specimens vs pH (left) and vs L/S (right) . 75
Figure 4.17: Element Percent Sorbed versus pH on Ferrihydrite (Reproduced from Stumm, 1992; Dzombak and Morel, 1990) 76
Figure 4.18: Cadmium Leaching in FAH (left) and FAB (right) Systems vs pH 78
Figure 4.19: Solubility Diagram for Metal Hydroxides (Reproduced from Dyer and Scrivner, 1998)..... 79
Figure 4.20: Cadmium Hydroxide and Carbonate Aqueous Concentrations for a 4M FAH system from Visual MINTEQ..... 79
Figure 4.21: Selenium Leaching in Reagent Water and Simulated Landfill Leachate for FAH Specimens with $M_s>0$ (left) and $M_s=0$ (right) vs pH 80
Figure 4.22: Copper Leaching in Reagent Water and Simulated Landfill Leachate for FAH (right) and FAB (left) Specimens vs pH 81

Chapter 1: Introduction

1.1 Background

Cementitious materials have been used to solidify and stabilize heavy metals in contaminated soils, waste-water treatment byproducts, mining wastes and coal combustion products for decades. Many studies have tested the capacity of ordinary cement (OPC) and other typical cementitious materials (lime, slag) for solidification and stabilization of these wastes (Kogbara et al., 2013; Shi & Fernández-Jiménez, 2006; Provis, 2009). Production methods generally entail adding a small amount of binder (OPC) to a large amount of waste in order to create a weak solid that will largely prevent leaching of contaminants (Provis, 2009). However, methods other than OPC have proven more successful when it comes to stabilizing heavy metal wastes. (Shi & Fernández-Jiménez, 2006).

In the 1970's, Joseph Davidovits patented geopolymers, a new solid material that does not require the use of OPC for formation (Davidovits, 1994). Since their inception, geopolymers have been investigated as an alternative method for solidification and stabilization of hazardous wastes (Comrie et al., 1989). A number of studies highlight the successes of geopolymers in stabilizing a variety of contaminants including heavy metals (Provis, 2009; Guo et al., 2013; Zhang et al., 2008). In addition, these systems contain a larger percent waste than OPC systems. Therefore, geopolymer systems are of interest to industries that produce heavy metal wastes, such as the coal power generation and mining industries.

CCPs were solidified in both OPC and geopolymers mixtures to evaluate leaching. For both OPC and geopolymer mixes, contaminants can be physically trapped within a phase matrix, can sorb onto the surfaces of phases, and can partake in chemical

reactions by precipitating out as insoluble salts or becoming a chemically bound component of a newly formed phase. While chemical stabilization varies by element, physical encapsulation is generally dependent on matrix factors such as permeability, which can similarly affect all elements.

1.2 OBJECTIVES

The objectives off this research were to develop a number of different coal combustion product (CCP) based geopolymers, to test geopolymer leaching in both reagent water and simulated landfill leachate, to identify geopolymer characteristics that have the greatest potential for reducing contaminant leaching, and finally to determine if landfill leachate components affected leaching of contaminants. Cement pastes containing CCPs were also made and tested for comparison.

To this end, raw CCPs, geopolymers, and cement pastes were characterized with respect to physical and chemical characteristics to understand trends among those that minimized leaching. Geopolymers were made with varying sodium hydroxide (NaOH) molarity and silica moduli (SiO_2/Na_2O) to evaluate the impact of geopolymer composition. Simulated landfill leachate was based upon components and concentrations in published landfill leachate in the United States (Ghosh et al., 2006).

Chapter 2: Literature Review

2.1 INTRODUCTION

Four wastes were obtained for solidification and stabilization testing in this study, all of which were coal combustion products (CCPs): two fly ashes, one economizer ash, and one bottom ash. Bottom ash is the first to be collected from a coal power plant as it is collected at the base of the furnace. It contains large particles that settle to the bottom of the furnace and a large majority of any unburnt coal. Economizer ash is collected from particles that were light enough to fly out of the top of the furnace, but heavy enough to fall out of the air immediately after. Economizer ash also consists of large particles, but contains almost no unburnt coal (ACAA 2015). Fly ash is the last to be collected, and it contains much finer particles than either bottom or economizer ash. It is generally collected in a bag house or electrostatic precipitator.

The two fly ashes used in this study were collected from coal power plants that inject trisodium hydrogendicarbonate dihydrate (trona) into their flue gas streams. Trona is a sodium carbonate compound that is used to reduce SO_x emissions from coal power plants. While traditional coal fly ash and trona impacted ash contain similar heavy metal concentrations, trona impacted ash has been shown to leach heavy metals at higher concentrations, and is therefore a greater threat to the environment (Dan et al., 2013; Su et al., 2011).

Contaminants in CCPs that are of interest in this study are arsenic, cadmium, cobalt, copper, chromium, nickel, lead, selenium, and zinc. The metals can be analyzed in two groups: those that form oxyanions in aqueous solution, and those that are typically present as cations. Two methods of stabilization for these contaminants are analyzed,

CCP based geopolymers, and CCP-cement mixtures. Previous work discussing effectiveness of these methods for the contaminants named are outlined below.

2.2 Leaching of Raw CCPs

Of the three types of CCPs analyzed, economizer ash is mentioned least in the literature, with a majority of the literature focusing on fly ash and sometimes bottom ash. The focus on fly ash likely stems from its wide use as an additive in concrete. Economizer ash and bottom ash do not meet ASTM requirements for use in concrete and are generally either used as fill in structural engineering projects (e.g. roadway embankments), though use of CCPs as structural fill is not analyzed in this study (ACAA 2015). Moreover, utilizing trona impacted ashes in concrete is of concern due to the higher sulfur trioxide and soluble sodium compounds. However, stabilization of these wastes in cementitious products can provide viable disposal pathways.

Leaching characteristics from coal fly ash have been thoroughly studied (Blissett & Rowson, 2012; Iyer, 2002; Y. Zhang et al., 2016). Researchers have reported both the leaching of contaminants (e.g. As, Cd, Cr) and major cations (Al, Si, Ca) as increased major ion leaching can be an indicator for increased contaminant leaching (Tiruta-Barna et al., 2006). Contaminants tend to leach at to a greater extent at low and high pH. Factors that impact leaching include particle size, the presence or absence of specific solid phases that serve as adsorbents or co-precipitates, and the relative solubility of hydroxides, carbonate or sulfate solids as a function of pH (Blissett & Rowson, 2012; Y. Zhang, et al. 2016).

Typically fly ash does not leach heavy metals in concentrations that would render it a hazardous waste as classified by the Toxicity Characteristic Leaching Procedure (TCLP) set forth by the USEPA (EPA1311, 1992; Y. Zhang et al., 2016). However, the

two fly ashes used in this study were collected from coal power plants that inject trona into their flue gas streams. There are significantly fewer studies characterizing leaching from trona-impacted ashes, but it has been shown that leaching increases in ashes that are trona-impacted (Dan, et al. 2013; Su et al., 2011). Specifically, oxyanions of arsenic and selenium have been shown to leach more at high pH in trona-impacted ashes compared to non-impacted counterparts (Su et al., 2011). In addition, results show that trona-impacted ashes have a higher natural pH than their counterparts, thus increasing the possibility of oxyanion leaching (Dan et al., 2013; Su et al., 2011). This can be explained by the composition of trona fly ashes. Trona, as a sodium carbonate compound, is highly soluble and it is hypothesized that metals sorb onto the surface of the sodium compounds and then are then more easily released once the sodium compounds dissolve. It has been suggested that the "insoluble fraction of the trona ash lost its capability to adsorb… elements under the natural pH condition" due to competition from trona reaction products including chloride, carbonate, and sulfate (Dan et al., 2013).

2.3 Stabilization Processes

Two methods of stabilization and solidification of CCPs were investigated: reactions with ordinary portland cement (OPC) to form cement pastes and with alkaline solutions to form geopolymers.

2.3.1 Cementitious Reactions

OPC generally contains five major phases: tricalcium silicate (alite, Ca_3SiO_5 or C_3S in cement chemistry notation), dicalcium silicate (belite, Ca_2SiO_4, C_2S), tricalcium aluminate ($Ca_3Al_2O_6$, C_3A), tetracalcium aluminoferrite ($Ca_4Al_2Fe_2O_{10}$, C_4AF), and gypsum ($CaSO_4 \cdot 2H_2O$, $C\check{S}H_2$). When OPC is mixed with water it chemically reacts to

form new hydrated phases namely ettringite ($Ca_6Al_2(SO_4)_3(OH)_{12} \cdot 26H_2O$), calcium silicate hydrates (C-S-H in cement chemistry notation), and calcium hydroxide ($Ca(OH)_2$). While most of the phases are crystalline, C-S-H is largely amorphous, and the final product is a solid cement paste that has considerable strength. The hydration process creates an alkaline (pH > 12) environment due to the release of hydroxyl (OH^-) ions and is the step during which contaminants can chemically bond with newly formed phases or become physically trapped within a phase.

Fly ash is considered a pozzolan, or a siliceous/alumino-siliceous material that does not contain cementitious properties, but when mixed with an alkaline material will develop cementitious properties. As a pozzolan, traditional (non-trona impacted) fly ash is often added to the OPC-water mixture as the reaction creates an alkaline environment that allows pozzolanic reactions to occur. The addition of fly ash has been shown to produce positive effects in cement pastes and concrete mixes such as increased durability and decreased shrinkage (Van Jaarsveld et al., 1997). The effects of trona-impacted ash on concrete have received less attention in the literature (Pflughoeft-Hassett et al., 2009).

Porosity and permeability (hydraulic conductivity) are two characteristics that affect a cement paste or geopolymer's ability to bind contaminants. Porosity is the quantity of pore spaces within a material from nano to meso to macropores, while permeability is the ease with which a fluid can flow through the material (Glasser, 1997). The properties are related, but may not necessarily impact leaching in the same way. High permeability is an indicator that a specimen will leach more, but a highly porous material may not leach if the pores are not connected. Typically, a highly porous material also has high permeability (Roy et al., 1988). These properties can be affected by the solution/binder (S/B) ratio and concentrations of major ions in the matrix (e.g. calcium).

Permeability values for cement systems are low, making them ideal for hazardous waste stabilization (Van Jaarsveld et al., 1997). OPC systems contain a wide range of pore sizes including nanopores which are beneficial for stabilizing hazardous wastes as they can trap metals or significantly slow down the leaching process. However, the inclusion of wastes into cement matrices has been shown to increase the porosity which could enhance leaching (Poon et al., 1986). High porosity increases leaching due to increased solid surface-water contact which can accelerate contaminant leaching.

2.3.2 Geopolymeric Reactions

The concept of a geopolymer was first presented by Joseph Davidovits in 1979, and the concept of using geopolymers to immobilize toxic metals followed soon after (Van Jaarsveld et al., 1997). This research focuses on inorganic geopolymers, which are "alkali-activated alumino-silicate binders" whose strength derives from tetrahedral silicon-oxygen-aluminum bonds (Van Jaarsveld et al., 1997). When sodium hydroxide or equivalent is mixed with fly ash, the silicon, alumina oxide bonds are dissolved and new amorphous phases are formed.

Geopolymer properties depend heavily upon the silica modulus (M_s), defined here as the molar ratio of SiO_2/Na_2O, but which can also be defined as SiO_2/Al_2O_3. (Allahverdi et al., 2008). The silica modulus "plays an important role in both the mechanical and morphological characteristics of geopolymers" and affects the formation of new phases (De Vargas et al., 2011). The sodium content is varied by modifying sodium hydroxide molarity in the caustic solution, and silica content can be modified in a variety of ways including the addition of fumed silica or silicate solution.

Similar to cement systems, geopolymers have low porosity, which makes them ideal for encapsulating wastes. Geopolymer porosity has been found in the range of 0.01-

0.03 cm^3/g (Ryu et al., 2013). However, studies have shown different results with regards to physical encapsulation of heavy metal ions by geopolymers. In some cases SEM-EDX imaging has shown heavy metal ions trapped in an amorphous alumino-siliceous matrix, while in others leaching of ions is most closely associated with pH and other chemical factors indicating poor physical stabilization (Álvarez-Ayuso et al., 2008; Bankowski et al., 2004; Guo & Shi, 2013). The ability of a geopolymer to physically encapsulate heavy metals can depend upon its structural stability, porosity, and permeability among other factors. Often the silica modulus is increased to create stronger, denser, and less porous materials (A. Allahverdi et al., 2008; Gao et al., 2014). In addition, increasing alkaline solution molarity has been shown to increase compressive strength and decrease porosity of formed geopolymers (Ryu et al., 2013). When calcium is present (such as from high calcium fly ash), it can reduce geopolymerization but increase the formation of calcium based amorphous compounds, which ultimately decreases porosity (Al-Zboon et al., 2011).

2.4 Chemical Stabilization Processes

Contaminants present in CCPs include arsenic, cadmium, chromium, cobalt, nickel, lead, selenium, zinc, and mercury. The metals can be grouped into two major categories: those that form oxyanions in aqueous environments and those that remain cationic. Cations sorb to clays and clay minerals and form hydroxide and carbonate solids depending on the pH and composition of the system. Sorption of cations to clays and clay minerals increases with increasing pH. Solubility is also pH dependent and the total soluble concentration of a heavy metal cation typically decreases, reaches a minimum and then increases with pH. In contrast to cations, oxyanion sorption to oxides and hydroxides decreases with increasing pH. Formation of precipitates is dependent on the

presence of the solubility products with cationic ions such as Ca^{2+}, Mg^{2+} and Fe^{3+} (e.g. $Ca_3(AsO_4)_2$). In many cases, oxyanions can co-precipitate in precipitating phases. Goldberg and Glaubig (1988) noted increased removal of As(V) onto calcite with increasing pH; however, it is not clear whether the removal mechanism was adsorption or co-precipitation. Of the contaminants listed, arsenic, chromium, and selenium are often present in waste streams as oxyanions making them more susceptible to leaching at high pH when sorption is the primary mechanism of incorporation within the geopolymer. However, chromium is often present as a cation in fly ashes (Cr(III)). The CCPs in this study have a high natural pH (11-13), thus oxyanions have a higher potential to leach under natural conditions.

2.4.1 Oxyanions

Arsenic

Arsenic is highly toxic and has therefore been studied rigorously. It is a known carcinogen and acute arsenic poisoning symptoms can include nausea, vomiting, and diarrhea (Ratnaike, 2003). There are currently no sure treatments for chronic arsenic poisoning, making arsenic removal from drinking and surface waters an even greater topic of concern. Arsenic is generally found in two oxidation states of which As(III) is a higher threat than As(V) as it is both more toxic and more difficult to remove from water (Ratnaike, 2003). Fortunately, As(V) is the dominant form in coal fly ash (Huggins et al., 2007). Even though arsenic forms oxyanions in aqueous environments, results indicate that "increased destruction of the cement matrix at low pH has more effect on the leachate arsenic concentration than the increased solubility (of arsenic mineral phases) at

high pH" (Leist et al., 2003). Thus, leaching of arsenic at both high and low pH is of concern.

Reduced arsenic leaching at mid-range pH can be caused by sorption or the formation of precipitates. Dixit and Herring (2003) showed decreased As(V) sorption onto goethite with an increase in pH as shown in Figure 2.1, but they do not examine pH above 10. Wei et al., (2016) showed that As(V) adsorption actually increases again above pH 12, though percent adsorbed is still low. The sorbents in these systems are goethite and titanium dioxide which are not present in high concentrations in cement and geopolymer systems, but they show trends in increased adsorption at mid-range pH.

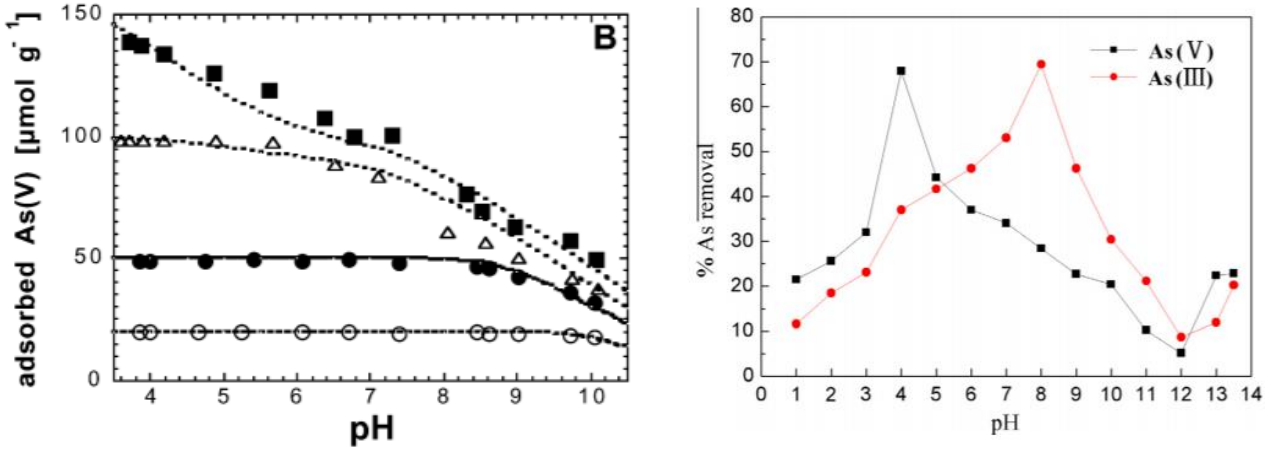

Figure 2.1: As(V) sorption onto goethite versus pH (Dixit and Herring, 2003 with copyright permission) (left), Arsenic adsorption on TiO_2 anatase versus pH (Wei et al., 2016 with copyright permission) (right)

Arsenic wastes have previously been stabilized using both OPC and geopolymers. Leaching studies indicate that arsenic stabilization is dependent on a number of factors including calcium and iron content of the stabilization matrix as well as external factors such as pH (Provis, 2009). Notably, introducing waste materials (e.g. As, Cr, Se) and matrix components (e.g. Ca, Na, Fe) in different forms can generate different leaching results (Palomo et al., 2005). For example, better results have been found for arsenic

stabilization with a base that already contains iron oxides (fly ash) versus adding iron oxides to the mixture separately (metakaolin based) (Palomo et al., 2005).

Across the board, matrices with a high calcium content stabilize arsenic better than low-calcium mixtures, and while often papers claim that OPC does not stabilize arsenic well, cement mixtures have generally outperformed geopolymers (Provis, 2009; Dutré & Vandecasteele, 1998; Leist et al., 2003). This may be due to precipitation or co-precipitation of arsenic with calcium and calcite, respectively. Indeed, geopolymers made with low-calcium ashes have achieved low oxyanion stability (Álvarez-Ayuso et al., 2008), however, geopolymer mixtures can perform just as well as cements with the addition of lime or other calcium sources (Dutré & Vandecasteele, 1998). The main factor in arsenic stabilization in both cement and geopolymer specimens is likely the formation of "hardly soluble calcium-arsenic compounds," and not binding by silica and alumina (Dutré & Vandecasteele, 1998; Leist et al., 2003a). Alexandratos et al. (2007) outline a large number of possible calcium-As(V) precipitates that could form including $CaAsO_4^-$, $CaHAsO_4$, $CaH_2AsO_4^+$, $Ca_4(OH)_2(AsO_4)_2(H_2O)_4$ and others. Amongst their compounds, $CaH_2AsO_4^+$ has the highest solubility and $Ca_5(AsO_4)_3OH$ the lowest.

Dutre & Vandecasteele (1998) tested leaching of As(III) and determined that precipitation of $CaHAsO_3$ was occurring. Similar testing has not been carried out with As(V), though it has been shown that systems containing the highest amounts of calcium are the most effective for stabilizing arsenic trioxide, pentoxide, and arsenate (Leist et al., 2003b). Similarly, fly ash based geopolymers have been shown to bind arsenic better than metakaolin (a solely alumino-siliceous material), and cement based systems have been shown to stabilize arsenic and chromium better than fly ash-based systems (slag, cement & fly ash, fly ash & lime), further suggesting that stabilization by silica or

alumina materials is not the primary mechanism for arsenic stabilization (Akhter et al., 1990; Fernández-Jiménez et al., 2005).

While increased calcium content has been clearly shown to decrease leaching of arsenic, impacts of iron content are less well defined. Iron oxides present in fly ash have been shown to adsorb arsenic, whereas iron oxides introduced separately into the system have caused no decrease in arsenic leaching (Fernandez-Jimenez et al., 2005). Arsenic was shown to be sorbed onto iron particles present in fly ash via transmission electron microscopy (TEM), but when Fe_2O_3 particles were introduced into a metakaolin system, no arsenic was visible on the particles. It has also been shown that arsenic pentoxide and trioxide leached more in a cement matrix that included additional Fe(II) suggesting that adsorbing onto or complexing with iron is not an ideal removal mechanism for arsenic (Leist et al., 2003a).

Selenium

Selenium can be found in many forms in the environment: Se(II-), Se(0), Se(IV) and Se(VI). While arsenic was predominantly found in oxidized form, in coal fly ash selenium is typically found in reduced form as Se(IV) (Huggins et al., 2007). Both selenite [Se(IV)] and selenate [Se(VI)] are highly soluble in water and have the potential to be taken up by humans. Selenium is not a carcinogen and is not toxic to humans at low levels; it is actually recommended for consumption by the World Health Organization (WHO) at around 10-70µg/day (WHO 2011). However, at high levels (mg/day) selenite and selenate can have adverse effects including growth retardation and reproductive effects (WHO 2011).

There are fewer studies on selenium than arsenic, and binding with OPC and geopolymers has been less successful. Results range from similar leaching in both fly ash

and geopolymers, to reduced leaching in geopolymers but not by a significant amount (Álvarez-Ayuso et al., 2008; Bankowski et al., 2004; Kupwade-Patil et al., 2014). Reduced leaching of selenite and selenate in soils by binding with OPC has been somewhat effective through the precipitation of calcium selenite hydrate ($CaSeO_3 \cdot H_2O$) and selenite substituted into ettringite ($Ca_6Al_2(SeO_4)_3(OH)_{12} \cdot 26H_2O$) shown by SEM-EDX and XRD (Hyun et al., 2009). However, at low pH values these compounds dissolved, and selenium was once again present in the system.

2.4.2 Cations

Chromium

Chromium is a known carcinogen with toxic effects to a number of human body systems (CDC 2011). It has two major oxidation states, Cr(III) and Cr(VI) of which hexavalent Cr(VI) is the most toxic and the most mobile (Provis, 2009). Fortunately, Cr(III) is the dominant form found in coal ash, though Cr(VI) can be found in small percentages (USGS 2015). While Cr(VI) is oxyanionic, Cr(III) is cationic.

Chromium has been successfully stabilized with OPC and geopolymers (Guo & Shi, 2013; J. Zhang, et al., 2008a). The main methods for chromium stabilization are thought to be the formation of insoluble chromium hydroxides, calcium chromium hydroxide complexes, and calcium chromate (Ca_2CrO_4), though it has been suggested that Cr(III) could be replacing aluminum in octahedrally-coordinated calcium aluminate hydrate (C-A-H) (Glasser, 1997).

As Cr(III) precipitates out more easily than Cr(VI), methods for Cr(VI) removal often entail reducing to Cr(III) first. The addition of sulfide has been shown to reduce Cr(VI) to Cr(III), which ultimately reduces chromium leaching (Glasser, 1997; J. Zhang

et al., 2008b). A majority of leaching tests with chromium have been completed by doping OPC or geopolymer pastes with soluble chromium salts (J. Zhang et al., 2008a). In the presence of sulfide, more highly soluble salts result in reduced leaching as the Cr(VI) is more available to be reduced to Cr(III) by S^{2-} (J. Zhang et al., 2008b). Overall, Cr(III) is more readily stabilized than Cr(VI) through the formation of insoluble hydroxides, and Cr(VI) can be stabilized by first reducing to Cr(III).

Other Cations

In coal fly ash, cations (Cd, Cu, Co, Ni, Pb, Zn) are generally found in the 2+ oxidation state. Of the elements listed, cadmium is toxic to humans, lead can cause developmental problems, and all elements can be toxic if consumed in large amounts (Ibrahim, 2016, CDC 2013, EPA 2008). As cations, these elements are more effectively precipitated out in the mid to high pH range than arsenic and selenium, and they tend to behave similarly in cement and geopolymer systems. Cations typically form metal hydroxides or carbonates with pH-dependent solubility as shown in Figure 2.2. For instance, cadmium has a pH of lowest solubility around 11, whereas copper has lowest solubility at pH 9.

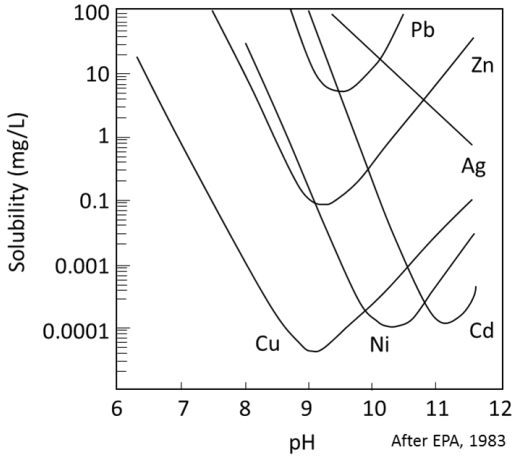

Figure 2.2: Solubility Diagram for Metal Hydroxides (Reproduced from Porex, 2017)

Metal hydroxides are amphoteric (i.e. increasing in solubility at both low and high pH), and the pH of least solubility varies by element. For the elements of interest in this study the minimum solubility occurs at relatively high (pH 10-11) though still lower than the pH range often found in cement and geopolymer systems (pH >12).

In line with this reasoning, experiments have achieved strong stabilization of cations in both OPC and geopolymer systems at high pH, and the formation of metal hydroxides has been shown with SEM images (Akhter et al., 1990; J. Zhang et al., 2008a). As would be expected, studies have found low binding of cations at low pH, with metal leachate concentrations generally following the solubility profile of formed hydroxides (Kogbara, et al., 2014; Li et al., 2001).

Outside of metal hydroxides and carbonates, it is suspected that calcium metal hydroxides are forming in OPC systems and being incorporated into the cement paste, further decreasing leaching at mid-range and high pH (Diez et al., 1997). Some promising results also show that copper, cobalt, and nickel have been incorporated into a kaolinite-based geopolymer network, and zinc has been shown to bond with silica and oxygen in geopolymer-like environments, but these results have not been directly correlated to reduced leaching at low pH (Anseau, et al., 2005; Hanzlicek & Steinerova-Vondrakova, 2006).

2.5 Leaching in Landfill Conditions

When CCPs are disposed of, they are generally deposited in landfills or ash ponds (ACAA 2015). Many of the leaching tests that have been previously carried out on raw CCPs, cement pastes, and geopolymers (such as those described in the sections above) test leaching in reagent water at natural pH, or in reagent water plus an acidifying agent (e.g. acetic acid, nitric acid, sulfuric acid) to adjust the pH. However in real-life scenarios

CCPs would be leaching not in reagent water, but into landfill leachate which can contain a vast number of components that could potentially affect trace metal leaching.

Landfill leachate can contain bicarbonate, phosphate, sulfate, silicates, and natural organic matter (NOM) (Christensen et al., 2001; Ghosh et al., 2006). In general, it is thought that the presence of additional ions in landfill leachate could cause competition for adsorption sites onto solid materials, increase aqueous complexation and increase leaching of trace elements. To date, there is little data to support these hypotheses, as the few studies that tested leaching with background ions generally showed either no difference between de-ionized water versus solutions containing salts, or less leaching in the salt solution (J. Zhang et al., 2008a; Zhao et al., 2017). In contrast, NOM has been shown to have greater effect on leaching from CCPs. NOM can bind with elements and form both adsorbable and non-adsorbable complexes, which can either increase leaching (As) or decrease leaching (Sr, Mo, V) of different elements (Zhao et al., 2017). Dissolved organic carbon (DOC) has also been shown to increase the leaching of copper from raw CCPs (Van Zomeren & Comans, 2004). While there exists a large body of work detailing relationships between specific elements and NOM, relatively few papers examine how NOM affects leaching from CCPs and even fewer discuss how NOM and other landfill conditions affect leaching from cement pastes and geopolymers.

2.6 CONCLUSIONS

There are multiple factors affecting the leaching of trace elements from geopolymer and cement systems, so it is difficult to determine exact reasons for reduced leaching of specific elements in different systems. Metals can be precipitated as hydroxides, substituted into amorphous matrices (C-S-H, C-A-H, N-A-S-H, silica-alumina systems), physically trapped within a matrix, or sorbed onto the surface of a

compound. Papers have both speculated and shown through solubility diagrams, XRD, SEM, EDS, EDX, and TEM that in most cases elements are being stabilized in multiple ways depending on the conditions of the system. pH is highly relevant to leaching in almost all systems, with low pH systems generally leaching more (even for oxyanions) than high pH systems.

A factor mentioned in many papers that appears to heavily affect trace metal leaching is the concentration of calcium. OPC systems inherently have a larger calcium concentration than geopolymer systems, and this enables the formation of insoluble calcium carbonates or calcium-metal compounds. If the pH is kept in the mid to high range, stabilization of many species in both geopolymer and OPC systems is achieved. However, if systems are exposed to low pH, stabilization is less effective. This could be due to degradation of the cement/geopolymer matrix, allowing for metals to leach out, or due to the increased solubility of hydroxide precipitates.

A majority of leaching tests have been completed following the toxicity characteristic leaching procedure (TCLP – EPA Method 1311) or similar methods put forth by non-US governments (e.g. Australian Bottle Leaching Procedure (ABLP)) and these test leaching in relatively clean environments. Tests have also been carried out in environments with background ions such as magnesium sulfate or sodium carbonate, but few if any tests have been carried out in landfill or groundwater-like conditions that include natural organic matter (NOM) (J. Zhang et al., 2008a). Only recently have tests including NOM been carried out with regards to leaching from raw fly ash, but these tests have not yet carried over to leaching from cement pastes and geopolymers (Zhao et al., 2017). This research aims to fill a gap in the literature by testing the impacts of landfill-like conditions on the leaching of heavy metals from geopolymers, and to optimize geopolymer compositions for reducing trace metal leaching.

Chapter 3: Materials and Methods

Experimental methods were carried out in four stages: characterization of raw materials, mixing of cement pastes and/or geopolymers, characterization of cement pastes and/or geopolymers, and finally leaching testing. Cement pastes and geopolymers were allowed to age for 28 days before leaching and characterization tests were conducted. Both chemical and physical characteristics of raw materials, cement pastes, and geopolymers were evaluated and methodologies are outlined in the sections below.

3.1 Mixture Development

The mixture development process began with mixture design. Cement pastes contain CCP, OPC, and de-ionized water and these can be combined in a variety of ways. Specific CCP/OPC and solution-to-binder (S/B) ratios (by weight) were mixed and tested to create a workable mixture. CCP characteristics varied and therefore different mixture designs were chosen for different CCPs in order to optimize workability. For geopolymers, similar testing was completed with varying NaOH molarity and S/B ratios. Once a design formula was established, mixtures were made (one or two at a time) and cast into cylinders according to ASTM standards. Enough cylinders were cast to allow for compression testing at 7 days and 28 days and to complete all leaching and characterization tests. Specimens were aged for 28 days at 100% humidity after which they were crushed and stored in a vacuum desiccator to slow down or stop hydration. All further characterization and leaching tests were completed on 28 day old specimens.

3.1.1 Mixture Design

Ash Pre-treatment

The economizer and bottom ashes both required pre-treatment before inclusion within cement pastes and geopolymers mixes. Both ashes had too large a particle size

distribution; therefore, they were crushed with a ceramic mortar and pestle to a particle size of <250μm. The bottom ash arrived in a slurry and was dried in an oven at 60°C for 24 hours before use.

Cement Pastes

Cement pastes for different CCPs were mixed according to workability, and mixes are outlined in Table 3.1, with de-ionized water as the solution. Initially, it was attempted to use the same solution/binder ratio (S/B; which is calculated by weight) for each cement paste, however the characteristics of each ash did not allow for this. Fly ash H was much drier than fly ash B, requiring a higher S/B in order to obtain a workable mixture. It was attempted to create a mixture with fly ash B and the same S/B used for the fly ash H mixture, but the mix was too watery and would not combine well. Therefore, another mixture was created for fly ash B with a lower S/B as outlined in Table 3.1. The economizer and bottom ashes also required lower S/B ratios, likely due to their higher particle size distributions lowering their ability to react.

Table 3.1: Cement Paste Mixture Design, Mini-Slump, and Initial Moisture Content

Ash	% Ash (dry weight)	% OPC (dry weight)	S/B	Mini-Slump Area (in^2)	Initial Moisture Content
Fly Ash H	30%	70%	0.45	4.6	22.3%
Fly Ash H	60%	40%	0.45	3.8	24.3%
Fly Ash B	30%	70%	0.40	-	22.3%
Fly Ash B	60%	40%	0.35	-	22.4%
Economizer Ash	30%	70%	0.40	8.7	17.5%
Economizer Ash	60%	40%	0.40	14.7	14.3%
Bottom Ash	30%	70%	0.35	4.2	18.3%
Bottom Ash	60%	40%	0.35	2.3	22.9%

In order to quantify workability, mini-slump testing was carried out and results are recorded in Table 3.1. Mini-slump testing methodology is outlined in Section 3.1.3, but it consists of measuring the area over which a specific volume of a mixture spreads when on a flat surface. Mini-slump data are not available for FAB 30% and 60% pastes as originally mini-slump testing was not completed on mixtures. Only after it was determined that different S/B ratios would be required for different ash mixes was the mini-slump test implemented. Mini-slump values for the original FAH 30% and 60% mixtures were also not recorded, but these mixtures were remade at a later date and data was recorded then.

Geopolymers

4M and 8M sodium hydroxide (NaOH, 50% w/w, extra pure, ACROS Organics) solutions were prepared in 1L batches by diluting 50% by weight sodium hydroxide with ultrapure Millipore Water (MPW). Dilutions were completed according to Table 3.3. 4M

and 8M NaOH batches were mixed in a 1L volumetric flask on a stir plate and allowed to combine for a minimum of 12 hours (overnight). The NaOH/water reaction is exothermic which causes water to evaporate, so additional MPW was added over time to keep the volume at exactly one liter. Glassware and the stirbar were cleaned in 10% nitric acid and rinsed with MPW prior to use.

Table 3.2: Geopolymer Mixture Design, Mini-Slump, and Initial Moisture Content

Ash	Sodium Hydroxide (NaOH, ACROS Organics) Molarity	Silica Modulus (M_s)	S/B	Mini-Slump	Initial Moisture Content
Fly Ash H	4M	0	0.55	3.8	30.7%
Fly Ash H	4M	0.15	0.55	13.9	30.3%
Fly Ash H	4M	1.5	0.55	30.0	22.3%
Fly Ash H	8M	0	0.65	3.4	31.2%
Fly Ash B	4M	0	0.45	3.3	28.2%
Fly Ash B	8M	0	0.55	3.0	26.3%

As with the cement pastes, different S/B ratios (by weight) were required to generate workable geopolymer mixtures. Silica modulus (M_s), defined as the molar ratio of SiO_2/Na_2O of the solution, was varied through the addition of fumed silica. Fumed silica was dissolved in the NaOH solution prior to mixing with fly ash. The solution was allowed to mix for a minimum of 12 hours (overnight) before use.

Table 3.3: Alkaline Solutions

Solution	Volume NaOH (mL)	Volume MPW (mL)	Fumed Silica (g)
4M	213.3	786.7	0.0
4M M_s= 0.15	213.3	786.7	18.0
4M M_s= 1.5	213.3	786.7	180.0
8M	426.6	573.4	0.0

3.1.2 Mixing

Cement paste and geopolymer mixes were cast into pre-prepared 5.1 cm x 10.2 cm plastic cylinders. Enough mix was made to fill five cylinders: two for compression testing at 7 days, and three for compression testing at 28 days which were also used during leaching tests. Prior to mixing, a small hole was drilled into the bottom of each cylinder which was covered with tape. The inside of the cylinder was then coated with form oil using a brush. After cylinder preparation, mixes were prepared following ASTM C305 Part 7: Procedure for Mixing Pastes.

1. Add activating solution to the mixing bowl (for cement pastes this was de-ionized water (DI) and for geopolymers this was 4M or 8M NaOH).
2. Add dry ingredients (CCP, OPC) to solution and allow to hydrate for 30 seconds, during which time the mixing paddle and bowl are attached to the mixer.
3. Turn the mixer on at low speed for 30 seconds.
4. Stop the mixer for 15 seconds and use a spatula to scrape down the sides of the bowl.
5. Increase mixer to high speed and mix for one minute.

3.1.3 Mini-Slump Test

Immediately after mixing mini-slump testing was performed. The mini-slump test was completed quickly to keep the paste from hardening in the bowl before it could be transferred to cylinders.

1. Set up mini slump mold on an acrylic sheet.
2. Use a spoon or spatula to place paste into mini slump mold.
3. Insert spatula 15 times into paste to ensure no air bubbles in the paste.
4. Level off the top of the mold and lift mold.
5. Measure and record diameter of resulting pat across two perpendicular axes. Complete measurements within 30 seconds of lifting the mold.

3.1.4 Casting

Each cylinder was cast into a 5.1cm x 10.2cm cylinder according to ASTM C192.

1. Fill cylinder halfway with paste.
2. Insert steel rod into cylinder 15 times and tap the side of the cylinder using rod.
3. Fill cylinder to the top and rod 15 more times. Tap the side of the cylinder again.
4. Level off the top of the cylinder with the tamping rod.
5. Put cap on cylinder.

3.1.5 Curing

Cast cylinders were left at room temperature for one hour before curing at 38ºC and 100% relative humidity for 24 +/- 0.5 hours. After 24 hours, specimens were removed from their molds by removing the caps and applying pressurized air to the hole in the bottom of the cylinder. The form oil applied to cylinders at the beginning of the process allowed the pastes to slide out easily. Specimens were then stored at 23ºC and 100% humidity for 27 more days (28 days of curing total).

3.1.6 Compression Testing

Two cylinders were tested for compressive strength each at 7 days and either two or three were tested at 28 days according to ASTM C39 using a Forney FX 700 compression testing machine.

1. Specimens are removed from 100% humidity and tested immediately.
2. Testing is completed at 7 days +/- 6 hours and 28 days +/- 20 hours.
3. Specimens are placed in 2" cylinder holders with neoprene pads.
4. The machine is turned on with the load at zero.
5. Load is increased at a rate of 88-132 lb/ft^2-s
6. Load and stress are recorded when specimen breaks.

3.1.7 Particle Size Reduction

Particle size reduction was required for leaching tests as well as for storage in a vacuum desiccator. Specimens were stored in a vacuum desiccator to prevent further hydration of the material and drying much more easily achieved with small particles than with big chunks. Broken specimens were placed into a plastic Ziploc bag and a plastic hammer was used to break them into small chunks. The small pieces were further crushed using a ceramic mortar and pestle and sieved to 2mm. Plastic and ceramic materials were used to prevent metal contamination of the specimens. Sieved material was stored in open plastic bags in a vacuum desiccator. The vacuum desiccator was used to prevent further hydration of the material so that additional testing could be completed at later dates. Mortar and pestles were cleaned with ZEP Calcium, Lime and Rust stain remover.

3.1.8 Moisture Content

After particle size reduction, but prior to desiccation, some sample was removed and set aside to test for initial moisture content. A 1 gram sample was placed in a pre-

dried porcelain crucible. The combined weight of the crucible and sample was recorded. Uncovered crucibles were dried in an oven at 110 +/- 2°C for 24 hours and then re-weighed. The difference between the initial and final mass was recorded as the moisture content. Samples were completed in triplicate and were disposed of after testing.

3.1.9 Sample Ignition

To determine the amount of bound water in the pastes, sample ignition tests were completed. The procedure is similar to that outlined in Section 3.1.3. Dried samples were ignited in an oven at 1000°C for one hour, with a ramp up time of two hours. Samples were brought back to room temperature and their weights recorded. The difference between the final weight and dried weight was taken as the weight of water chemically bound to the dry material (Fagerlund, 2009). Samples were completed in triplicate and were disposed of after testing.

3.2 Characterization of Materials

Characterization of four raw CCP materials, four cement pastes, and six geopolymers was completed. Raw CCPs were fly ash H (FAH), fly ash B (FAB), an economizer ash (EA), and a bottom ash (BA). FAH, EA, and BA were obtained from Headwaters Construction Materials, and FAB was obtained from Boral Material Technologies. Additional obtained materials include a slag, a calcium aluminate cement, and a Type I Ordinary Portland Cement (OPC).

3.2.1 X-Ray Fluorescence

X-Ray Fluorescence (XRF) was completed by Wyoming Analytical Laboratories on three of the raw CCPs, a Lafarge slag, and a calcium aluminate cement (CAC). XRF results for FAH were provided by the supplier.

3.2.2 X-Ray Diffraction

Both qualitative and quantitative X-Ray Diffraction (XRD) analyses were run on each raw CCP as well as mixed cement pastes and geopolymers to determine the phases present in each sample as well as the relative percent concentrations of each phase.

Preparation of two samples was completed for each sample type, one for qualitative analysis and one for quantitative analysis. To begin sample preparation for both analyses, slightly more than 1 gram of ash was crushed using a ceramic mortar and pestle and sieved through a #325 sieve (45μm). Any amount that did not pass through the sieve was re-crushed until the entire sample passed through the sieve to ensure that all crystalline phases were included in the sample.

For quantitative analysis, a specific concentration of reference material was then included in the sample. For these analyses zincite (ZnO, Acros Organics, ACS grade) was included at a percentage of 10% by mass. The powders were mixed in an agate mortar and pestle and a small amount of ethanol was added to mix the two together evenly. Samples were then dried in an oven at 60°C for a short period of time (less than 5 minutes).

After crushing, samples were placed into glass slides for analysis in a Rigaku Miniflex 600 x-ray diffractometer. There are several possibilities for error in sample preparation for XRD including preferred orientation and peak shifting. To prevent preferred orientation, a razor blade was used to cut across the sample in perpendicular directions after which a flat glass plate was used to press down on the sample without twisting. The razor blade cutting motion helps randomize the direction that particles are facing, which reduces preferred orientation. The glass plate ensures that the sample lies flat against the glass to prevent shifting of peaks.

Samples were run with a 2-theta range of 4-70, a step size of 0.02 degrees, and at 1.5-2 degrees per minute. After analyzing the first few patterns it was determined that more precise results were required for quantitative analysis. The following patterns were analyzed at 0.5-1 degrees per minute in order to obtain more precise results. Qualitative analysis was completed using Jade and the PDF 2015 database as well as referencing Snellings (2015). Quantitative analysis was completed using PDXL2 and importing Crytallographic Information Files (CIF). CIFs were obtained from the American Mineralogist Crystal Structure Database and the Crystallography Open Database.

3.2.3 Loss-on-Ignition

Loss on ignition (LOI) measures the weight loss of a material when it is ignited to 750°C, and is typically used as an estimate for carbon content. Testing was only completed on FAH, as the LOI was provided for the other CCPs by the supplier. LOI was completed following ASTM Standard D7348. Ashes were weighed, dried for 24 hours in an oven at 110°C, weighed, heated to 750°C over two hours, maintained at 750°C for two hours, cooled, and weighed again. Samples were heated in uncovered pre-dried porcelain crucibles. After heating, samples were put into a vacuum desiccator for 24 hours at room temperature and weighed a final time. The difference between the dry weight and the final weight represents the LOI. Samples were completed in triplicate.

3.2.4 Thermogravimetric Analysis

Thermogravimetric Analysis (TGA) is similar to LOI as it measures the weight loss of a material when ignited to 1000ºC. TGA is different than LOI as it continually measures weight loss while the temperature is increased, so the temperature at which different compounds are volatilized is recorded. TGA was completed on raw fly ashes and geopolymer mixes. Mixed pastes were crushed to 150μm before analysis while raw

fly ashes were analyzed with their existing particle size. Approximately 20µg of undried sample was weighed in a porcelain crucible. Measurements were taken in a N_2 gas atmosphere using a Mettler Thermogravimetric Analyzer, Model TGA/DSC 1. Measurements were taken from 30-1000ºC and the temperature was increased at a rate of 10ºC per minute.

3.2.5 Particle Size Distribution

Particle size distribution of the raw CCPs was determined using laser diffraction in a Mastersizer 2000. Particles were dispersed in isopropyl alcohol (>95% concentration by weight) to prevent hydration of particles during the test. Dispersion was accomplished through pumping and sonication Pump speeds were varied from 2000-2500 rpm depending upon the CCP. Higher pump speeds were used on CCPs with larger particle sizes (the bottom and economizer ash) to keep the larger particles suspended in the dispersant. Ultrasonic dispersion was used for 30 seconds and particles were allowed to disperse for a minimum of 15 minutes before measurements were taken to allow bubbles to clear and to provide even dispersion of particles.

The refractive index for both the particles and the dispersant are required for particle size calculation. The refractive index of isopropanol has been studied in numerous papers and a value of 1.39 was used (Chu & Thompson, 1962). Refractive indices for fly and bottom ash can vary, but generally range between 1.5-1.7 (Jewell & Rathbone, 2009). A refractive index of 1.7 was used as this gave a good residual value of less than 1% for all ashes. A residual of less than 1% indicates that there is a good fit between the measured and calculated data.

Two ashes, the bottom ash and the economizer ash, had particles of size greater than 1000µm, which is the highest size accurately measured by the instrument. To correct

for this, the ashes were sieved through a No. 18 sieve (1mm) before running in the instrument. Any ash that was greater than 1000µm was then passed through a series of sieves and weighed to determine a general particle size distribution for the larger particles.

3.2.6 Surface Area

Surface area of the raw CCPs was determined using Brunauer–Emmett–Teller (BET) theory and a NOVA 2000 series instrument by Quantachrome Instruments. Samples were weighed, placed in a glass bulb, and degassed under vacuum at 170°Cfor 24 hours. Bulbs were pre-cleaned using soap and water, sonicated, rinsed with ethanol and dried in an oven at 105ºC. For some samples degassing in the NOVA instrument did not fully remove the water content. If this occurred, samples were pre-dried in an oven at 105°C for 12-24 hours before degassing. Degassed samples were re-weighed and placed under vacuum in the NOVA instrument, at which point the attached decanter attached was filled with liquid nitrogen.

The NOVA 2000 measures the volume of N_2 gas adsorbed onto the surface of the material. Volumes adsorbed at relative pressures $0.05 < P/P_0 < 0.3$ were used to determine the surface area of the material. For some CCPs the surface area was low with values of < $1m^2$/gram. Thus, a significant amount of sample was required for use (approx. 5 grams) as the test required surface area values of 2-25m^2 to provide accurate results. Results were analyzed using AutoSorb 1. Results were deemed acceptable when C values of greater than 20 were obtained. The C value is a dimensionless constant in the BET adsorption isotherm equation that is related to the energy of adsorption in the first adsorbed layer, and it must be a positive number (Particle Analytical, 2017). When not

enough material was used, or when the materials had not been sufficiently degassed, negative C values were obtained.

3.2.7 Digestion

Raw CCPs were digested to determine trace metal contents according to EPA method 3050b. Digestion was completed with nitric acid (HNO_3, 67-70% w/w, trace metal, Fisher), and hydrogen peroxide (>30% H_2O_2, trace metal, Sigma Aldrich). A 1-gram sample (dry weight) was added to a pre-weighed 250mL fluorinated ethylene propylene (FEP) bottle. A mixture of 1:1 HNO_3 was prepared and 10mL added to the bottle. The bottle was capped, submerged in a hot water bath, and heated at approximately 95°C for 15 minutes under a fume hood. After 15 minutes the bottle was allowed to vent under the fume hood to release any brown fumes that had been generated due to oxidation of the sample. An additional 5mL of HNO_3 was then added to the sample and put back into the water bath for 30 minutes. If more brown fumes were generated, additional HNO_3 was added in 5mL increments. When no more brown fumes were generated, the bottle was uncapped and heated in the water bath for two hours to allow the mixture to evaporate.

After two hours, 10mL of hydrogen peroxide was added to the mixture in 1mL increments, waiting in between additions to allow for more brown fumes to escape. The bottle was uncapped and resubmerged in the hot water bath for another four hours to allow some of the liquid to evaporate. After four hours, the remaining liquid was filtered to 20 µm using Whatman^R No. 41 filter paper into 100mL volumetric flasks and then diluted with Millipore water to 100mL. Samples were then transferred into 125mL LDPE bottles for storage. For all CCPs some solids remained undissolved. Samples were further diluted by a factor of 10 prior to analyzing on the Inductively Coupled Plasma – Mass

Spectroscopy (ICP-MS). Samples were completed in triplicate along with a blank. All materials (bottles, volumetric flasks, funnels) were pre-cleaned in 10% nitric acid and rinsed with Millipore water.

3.2.8 Porosity

Porosity can be an indicator for geopolymer and cement paste stabilization, and low porosity can be associated with decreased leaching of contaminants. Porosity of geopolymer and cement pastes were measured according to a procedure outlined by Day and Marsh (1987). An approximately 10 gram sample was submerged under de-ionized water for 24 hours and then weighed under water and in the saturated surface dry state. A system was designed to weigh the sample under water as it was hanging from a stand. The level of the water was kept constant and the length of the line the sample was hanging from was also kept constant. The sample was then submerged in isopropyl alcohol (>95% concentration by weight) for a period of approximately two weeks. The sample was weighed under isopropyl alcohol over time to determine the change in weight from water saturation to alcohol saturation. After the weight in isopropyl alcohol remained constant at least one day, samples were dried in an oven at 105°C for 24 hours to determine the dry weight. The porosity was calculated based upon the differences in weight of the water-saturated and alcohol-saturated samples.

3.3 Leaching Tests

Three different leaching tests were completed: EPA Method 1313 (variable pH), EPA Method 1314 (dynamic testing), and EPA Method 1316 (variable liquid/solid ratio). EPA Methods 1313 and 1314 were completed with both reagent water (ultrapure Millipore water) and with a simulated landfill groundwater leachate.

3.3.1 Moisture Content

Before setting up a leaching test the moisture content of the prepared geopolymer or cement paste mix to be tested was determined. Materials had often been sitting in the vacuum desiccator for several days and therefore the moisture content had decreased from the initial moisture content tested at 28 days. When possible, moisture content was tested the day prior to the start date of the test as it takes 24 hours to confirm moisture content. When moisture content was not tested the day prior, the moisture content test as outlined in Section 3.2.8 was begun and materials were weighed after approximately 1 hour to gain an estimation of the moisture content. When moisture content was completed the day prior, it was also completed the day of the test in order to account for drying that occurred during the additional 24 hours in the desiccator.

3.3.2 Simulated Landfill Leachate

Leaching tests were completed with MPW and with simulated landfill leachate. Leachate components were based upon (Ghosh et al., 2006) who examined typical landfill leachate extracts. There are wide range of typical values, so median values were chosen. Landfill leachate was made in 1L batches using a volumetric flask. Multiple batches were mixed and stored in a 4L plastic container. 400mg of Humic Acid was dissolved in 1L of water which gave a reading of approximately 100mg/L as TOC. The pH of the simulated landfill leachate was in the range of 8.7-8.9, versus that of Millipore water which had a pH of 5.8-6.0.

Table 3.4: Landfill Leachate Composition

Component	Concentration (mmol/L)	Source
Bicarbonate	30	$NaHCO_3$ (Sigma-Aldrich, ACS grade, 99.7%)
NOM	400 mg/L (as TOC)	Aldrich Humic Acid™
Hydroxylamine Hydrochloride	0.4	NH_2OH-HCl (Aldrich, 99.999% trace metal)
Silicate	0.3	Silicic Acid (Sigma-Aldrich, 99.9%, 20μm)
Mg	4.1	$MgCl_2$-$6H_2O$ (Amresco, ACS grade)
Ca	2.5	$CaCl_2$ (Spectrum, FCC grade, Anhydrous)
Phosphate	0.02	NaH_2PO_4 (Fisher, >99%, Anhydrous)
Sulfate	2.6	Na_2SO_4 (Fisher, ACS grade, Anhydrous)
Background ions (Ionic Strength = 0.1M)	42.3	$NaNO_3$ (Sigma-Aldrich, ReagentPlus, >99.0%)

3.3.3 pH Variant Leaching Test

The goal of EPA Method 1313 is to determine the leaching of different constituents of potential concern (COPCs) in a pH range of 2-13. The raw CCPs, cement pastes, and geopolymers tested were highly alkaline with a natural pH above 12, but the materials varied in alkalinity and required differing amounts of acid to reach specific pH

values. To determine the acid titration behaivor of the materials, acid titrations were completed prior to running the full scale batch test. The EPA test method also calls for the addition of a base to reach high pH values, but this was found unnecessary due to the alkaline nature of the materials tested.

125mL high-density polyethylene (HDPE) bottles were used for pre-titration and 250mL HDPE bottles were used for the full scale batch test. Nitric acid (HNO_3, 67-70% w/w, Trace Metal, Fisher) was used to adjust the pH in each bottle. Two blanks were run with each test (but not with the pre-titration test). One blank was run with pure reagent water (MPW or simulated landfill leachate), and one with reagent water plus the maximum amount of nitric acid required to reach the lowest pH. Tests were run with a liquid/solid (L/S) ratio of 10.

For a particle size of <2mm, the method calls for a total of 360mg (dry weight) per test. The method was modified to use180mg (dry weight) per test to save raw CCPs and to reduce the amount of material required to be crushed. 20 gram (dry weight) samples were added to pre-weighed and labeled bottles, followed by reagent water (MPW or simulated landfill leachate) and nitric acid. Reagent water was added by weight assuming a density of 1.0 g/mL, and nitric acid was added by pipette under a fume hood. Bottles were weighed after the addition of each new component.

Bottles were placed into a rotator at 38 +/- 2 rpm for 48 +/- 2 hours. The 48 hour clock was begun when the rotator was turned on. After 48 +/- 2 hours, bottles were removed from the rotator and allowed to settle for 10-15 minutes before testing and sample collection. Testing and sample collection are the same for all leaching tests and are described in Sections 3.3.6 through 3.3.7.

3.3.4 Liquid/Solid Variant Leaching Test

The goal of EPA Method 1316 is to determine the leaching of different COPCs for various liquid/solid (L/S) ratios. For a particle size of <2mm, the method calls for a total of 1.5 kg (dry weight) per test. The methodology was modified to use less material to save raw CCPs and reduce the amount of material required to be crushed. A 10 gram minimum (dry weight) sample was used for a total of 370 mg (dry weight) per test. Tests were run with L/S ratios of 1, 2, 5, 10, and 20. One blank was run with pure reagent water (MPW) for each test. Tests were not run with simulated landfill leachate.

Cement paste and geopolymer specimens were added to pre-weighed and labeled fluorinated ethylene propylene (FEP) bottles, followed by reagent water (MPW). Both 250mL and 1L FEP bottles were used depending upon the amount of specimen required. Reagent water was added by weight assuming a density of 1.0 g/mL. Bottles were weighed after the addition of each new component.

Bottles were placed into a rotator at 38 +/- 2 rpm for 48 +/- 2 hours. The 48 hour clock was begun when the rotator was turned on. After 48 +/- 2 hours, bottles were removed from the rotator and allowed to settle for 10-15 minutes before testing and sample collection.

3.3.5 Dynamic Leaching Test

The goal of EPA Method 1314 is to measure the leaching of constituents over time. The dynamic test required eluent to be pumped through an upflow column over approximately two weeks. Four 5cm x 30cm borosilicate glass columns with polypropylene filters covering either end were connected to a Cole Parmer Masterflex pump via 1/16” polytetrafluoroethylene (PTFE) tubing. PTFE tubing was connected to 0.89mm Viton tubing at the pump head via PTFE adaptors. Teflon tape was used over adaptors to prevent leaking.

Materials were sieved to 1-2.38mm to obtain a column diameter to particle diameter ratio of 20. 300 grams (dry weight) of material was added to the column with a layer of silica sand at the bottom and top to fill remaining space. PTFE tubing was attached to the top of the column and led into 1L or 250mL FEP bottles. The entire set up was in a fume hood.

Eluent was either MPW or simulated landfill leachate and was pumped at a rate of approximately 0.16mL/min. Samples were collected according to Table 3.5.

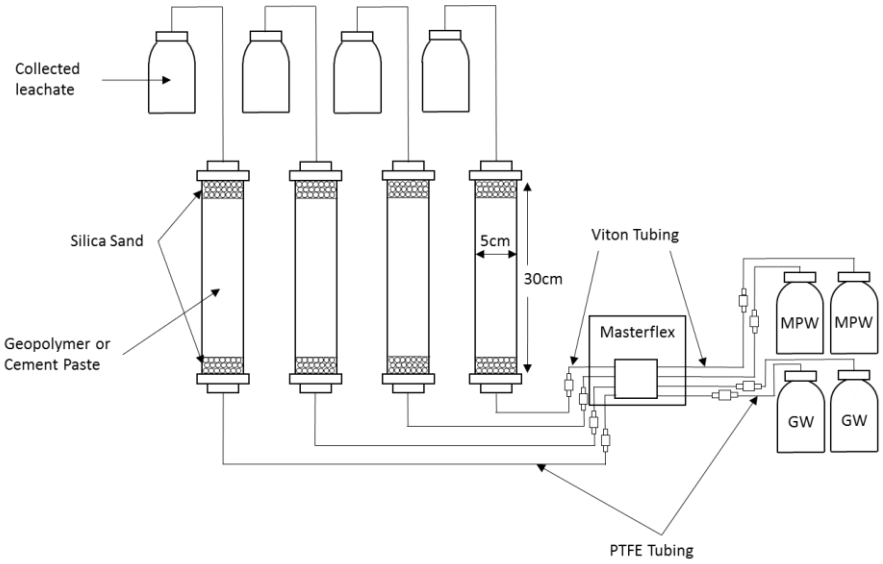

Figure 3.1: Dynamic Leaching Test Set-Up

Table 3.5: Dynamic Leaching Test Collection Schedule

	End Point	Fraction L/S	Fraction Volume (mL)	Time (hours)
T1	0.2 +- 0.1	0.2	60	6.4
T2	0.5 +- 0.1	0.3	90	9.6
T3	1.0 +- 0.1	0.5	150	16.0
T4	1.5 +- 0.2	0.5	150	16.0
T5	2.0 +- 0.2	0.5	150	16.0
T6	4.5 +- 0.3	2.5	750	80.0
T7	5.0 +- 0.2	0.5	150	16.0
T8	8.8 +- 0.3	3.3	1000	106.7
T9	9.3 +- 0.2	0.5	150	16.0
T10	10.0 +- 0.2	1.2	350	37.3
Total		10	3000	320

3.3.6 pH, Conductivity, ORP Testing

For each test, the pH was measured *in situ* using an Orion Star™ A211 pH benchtop meter with ROSS Ultra Triode glass-body pH/ATC electrode. The probe was calibrated before each test using ThermoScientific pH 4.01, 7.00, and 10.01 buffer solutions. The pH was measured directly after removing bottles from the rotator or after collecting bottles at their specified time in EPA Method 1314. The probe was maintained with Ross electrode filling solution and was stored in Ross storage solution between uses.

Conductivity and ORP were tested with a Myron L® Company Ultrameter III 9P™. The conductivity meter was calibrated with Myron L® Company TDS/conductivity standard at 3900µS. Conductivity is dependent upon temperature with measurements typically changing 1-2%/ºC (Barron & Ashton, 2007). Measurements were taken at room

temperature and values within one experiment varied by less than 0.5ºC. Across all experiments temperature varied from 20-25ºC. The ORP meter was calibrated with a pH 7.0 buffer solution. The conductivity and ORP were measured after the pH was measured and before filtering the solution. Sample was left in the ORP measuring cup for as long as it took the reading to stabilize (generally 5-10 minutes). The unit was rinsed three times with DI water between each use and rinsed three times with sample before completing a measurement. The ORP probe was stored with Myron L® pH/ORP storage solution.

3.3.7 Sample Collection, Dilution, and Storage

Samples were filtered through 0.45 µm GH Polypro (GHP) membrane disc filters from Pall Laboratory using a 250mL polysulfone reusable filter holder by Nalgene. The filter was connected to a Cole-Parmer vacuum pump. Between the collection of each sample the filter holder was rinsed with 10% nitric acid and MPW, and dried with KimWipes.

Filtered samples were pipetted with FisherBrand Elite pipettes and polypropylene pipette tips into pre-weighed and labeled 15mL or 50mL plastic vials for dilution and analysis or for saving. Samples were diluted for analysis with inductively coupled plasma mass spectroscopy (ICP-MS) in 15mL plastic vials and for cold vapor atomic fluorescence spectroscopy (CVAFS) in 50mL plastic vials. Two samples were collected each for analysis using ICP-MS and CVAFS. One sample was diluted upon collection for immediate analysis, and another sample of larger volume (25mL for ICP-MS and 30mL for CVAFS) was collected to store for use in the event of future analysis. Samples were preserved in either 2% nitric acid for ICP-MS or 1% bromine chloride (BrCl) for CVAFS.

For analysis using ICP-MS samples were diluted based upon their conductivity. The maximum total dissolved solids (TDS) allowable in the ICP-MS is 2000ppm (200ppm preferred). Samples were diluted with MPW to 10mL and acidified with 2% nitric acid. For analysis using CVAFS samples were diluted with MPW to 30mL and acidified with 1% bromine chloride (BrCl).

Bromine chloride solution was made according to EPA Method 1631. In a fume hood, 5.4 grams of potassium bromide (KBr, ACS grade, Fisher) was dissolved in 0.5L of hydrochloric acid (HCl, trace metal, Fisher). An acid-rinsed magnetic stir bar was placed in the bottle and stirred on a stir plate for approximately 1 hour in the fume hood. 7.6 grams of potassium bromate ($KBrO_3$, ACS grade, Fisher) was slowly added to the acid while stirring. When all of the $KBrO_3$ was added, the solution color changed from yellow to red to orange. The bottle was loosely capped and allowed to stir another hour before tightening the lid. Bromine chloride and sample vials were stored in plastic Ziploc bags at 4ºC.

3.3.8 Sample Analysis

Samples were analyzed with ICP-MS for trace metal concentrations and with inductively coupled plasma-optical emission spectroscopy (ICP-OES) for major cation concentrations. Mercury was measured with cold vapor atomic fluorescence spectroscopy (CVAFS). ICP-MS measurements were completed by Dr. Nathan Miller in the Jackson School of Geosciences at the University of Texas at Austin. ICP-MS limits of detection are in Table 3.6.

For ICP-OES and CVAFS measurements, a standard calibration curve was completed for each element prior to analysis and a blank (MPW with 2% nitric acid) was measured every 5-6 samples to rinse the probe and prevent carry-over. Elements analyzed

on ICP-OES were Ca, Al, Si, and Mg. 1000ppm stock solutions from Inorganic Ventures were used to generate standards for the calibration curve. A typical standard calibration curve used on the ICP-OES is shown in Figure 3.2.

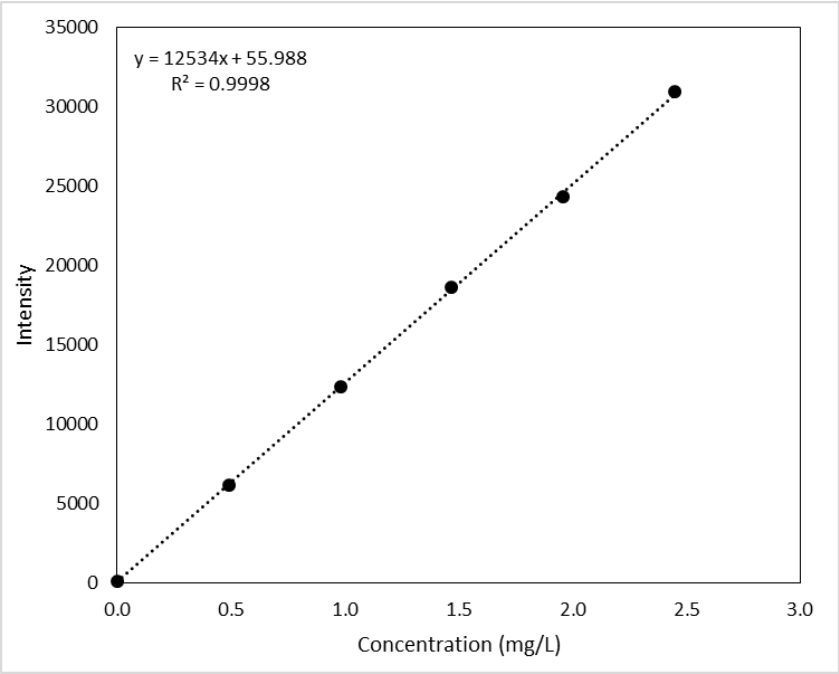

Figure 3.2: Typical Aluminum Standard Curve

Table 3.6: Typical ICP-MS Limits of Detection (determined for each sample run)

Element	**Limit of Detection (µg/L)**
As	<0.1
Cd	<0.01
Co	<0.01
Cu	<0.1
Cr	<0.1
Ni	<0.1
Pb	<0.01
Se	<0.1
Zn	<0.1

Chapter 4: Results and Discussion

The potential for stabilizing trona fly ashes by incorporating coal combustion products into geopolymers was evaluated. The evaluation required chemical and physical characterization of both the fly ash and the resulting geopolymers as well as quantification of the leaching potential of the geopolymers. Assessment of the relative performance of geopolymers to cement pastes was conducted by simultaneously producing, characterizing and quantifying the leaching potential of cement pastes containing the trona based fly ash. Chemical characterization of the raw materials was performed to identify the mineralogy of the fly ashes and to quantify the concentration of hazardous contaminants within each ash. These results served as a baseline for assessing the potential leaching and changes in mineralogy resulting from formation of the geopolymers and cement pastes. Physical characterization was performed to evaluate the relative stability of the materials (strength, surface area, porosity etc.) to weathering, erosion and structural failure as well as the potential for diffusion of contaminants from the matrix. Leaching tests were selected that would provide an assessment of the potential for contaminant release from the geopolymers relative to baseline leaching from cement based materials. To this end, major ion and minor element concentrations were analyzed from leaching tests conducted for geopolymers and cement pastes over an extended range of pH and liquid-to-solid ratios (L/S).

4.1 Characterization of Raw Materials

Four raw materials were characterized: fly ash H (FAH), fly ash B (FAB), an economizer ash (EA), and a bottom ash (BA). The CCPs were obtained from coal power plants within the United States and the ashes both come from plants that inject trona into their flue gas streams. The physical properties of surface area and particle size were

analyzed as they can indicate material reactivity. Higher reactivity indicates that a larger portion of the material is transformed into amorphous sodium-alumino-siliceous (N-A-S-H) or calcium (C-S-H) based compounds during the geopolymer or cementitious reaction leading to better solidification and better stabilization of contaminants. X-ray fluorescence (XRF), x-ray diffraction (XRD), loss-on-ignition (LOI), and digestion were completed to determine chemical composition and minerology. Trace element chemical composition was necessary to know which contaminants were present in the ash and at what concentration, while major elements and phases can indicate ash reactivity and help show which chemical reactions are controlling contaminant stabilization.

4.1.1 Physical Characterization

Particle Size and Surface Area

Particle size distributions (PSD) have been shown to significantly affect the reactivity of fly ash during geopolymerization, with finer particles leading to higher reactivity and ultimately higher compressive strength (Diaz et al., 2010). PSDs for the raw CCPs were determined by laser diffraction and are shown in Figure 4.1. The particle diameters for which 10%, 50%, and 90% of particles are smaller than are summarized in Table 4.1. The two fly ashes had significantly smaller particle sizes than the economizer and bottom ash indicating that they had a greater capacity to react. The PSDs were typical of coal fly ash (Ramenzanianpour, 2014). The economizer and bottom ash both had particles with diameters greater than 1mm, obtained by sieving, and the particle size distributions for particles >1mm are shown in Table 4.2.

Surface area was calculated using Brunauer-Emmett-Teller (BET) theory which includes surface area due to porosity. The surface area of the raw CCPs is directly related to the PSD, with finer particles having larger surface area and ultimately greater

reactivity. Surface areas found were typical of coal fly ash, and the economizer ash had significantly lower surface area than the fly ashes (Ramenzanianpour, 2014). Previous studies have found that fly ash is largely non-porous, and surface area is mostly dependent upon particle size (Schure et al., 1985).

Table 4.1: 10%, 50%, 90% Particle Size and Surface Area of Raw CCPs

CCP	d_{10} (µm)	d_{50} (µm)	d_{90} (µm)	Surface Area (m^2/g)
FAH	3.2	15.6	68.1	4.40
FAB	3.1	15.7	88.1	3.51
EA	36.5	134	557	0.57
BA	23.5	164	529	-

Table 4.2: Particle Size Distribution for Particles >1mm

Particle Size (mm)	Percentage by Weight	
	Economizer Ash	**Bottom Ash**
< 1	75.3%	77.1%
1-2	8.6%	11.1%
2-2.8	6.1%	4.3%
>2.8	9.9%	7.5%

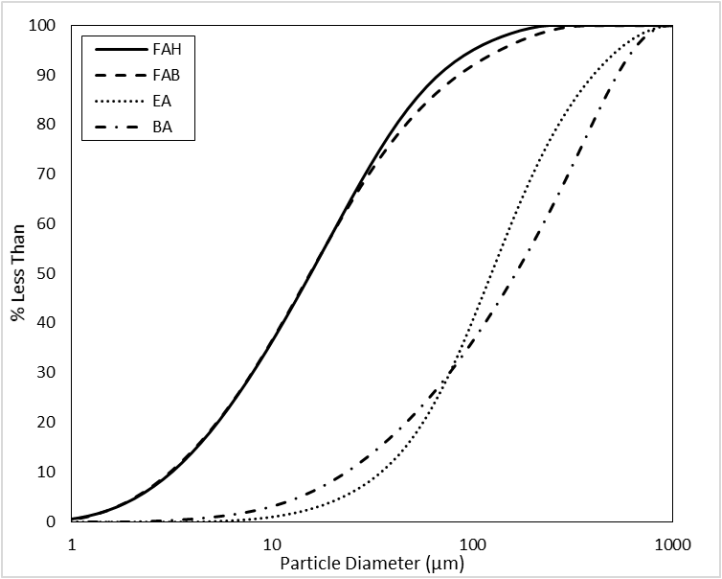

Figure 4.1: Particle Size Distributions of Raw CCPs

4.1.2 Chemical Characterization

X-Ray Fluorescence

X-ray fluorescence (XRF) provided the oxide content of raw CCPs from which the elemental content could be calculated. The oxide and elemental contents can help determine the origin of the CCPs, and give insight into what phases or compounds might be available to react. Results are shown in Table 4.3. While the coal source of the fly ashes is unknown, the bulk composition most closely aligned with that of lignite (Blissett & Rowson, 2012). The two fly ashes were both Class C ashes with greater than 50% but less than 70% SiO_2, Al_2O_3, and Fe_2O_3 as classified by ASTM C618. Class F ashes have greater than 70% SiO_2, Al_2O_3, and Fe_2O_3. The reduced alumino-siliceous content of Class C ashes is typically due to their having a higher calcium content, as is the case for FAH and FAB.

There are a number of studies discussing the effects of high calcium content on both cements and geopolymers (Li et al, 2013, Blissett & Rowson, 2012). Class C coal

fly ashes (CFAs) are typically regarded as less favorable for inclusion within concrete as they are not as good at improving concrete durability as class F ashes, however they can still be used to increase concrete strength. A high calcium content in geopolymers has been associated with shorter setting times, but lower ultimate compressive strength (Diaz et al., 2010). Depending upon other ash characteristics (e.g. particle size), higher compressive strength can still be achieved with class C ashes (Li et al., 2013). It has also been suggested that a high calcium content aids in the formation of calcium silicate hydrate (C-S-H) compounds in addition to typical geopolymer alumino-siliceous compounds (Li et al., 2013).

The two fly ashes both have larger than typical sodium and sulfur content due to the addition of trona (Na_2CO_3•$NaHCO_3$•$2H_2O$) to the flue gas stream at the coal power plant. The ordinary portland cement (OPC) is a Lehigh Type I cement. Oxide composition for the OPC was typical for Type I cement.

Table 4.3: Oxide Content of Raw CCPs obtained from XRF

	Fly Ash H	Fly Ash B	Economizer Ash	Bottom Ash	OPC
SiO_2	30.13%	30.68%	39.90%	40.70%	20.36%
Al_2O_3	16.70%	15.81%	16.79%	14.54%	5.82%
Fe_2O_3	5.35%	4.53%	4.99%	4.29%	2.3%
CaO	25.00%	25.39%	25.45%	16.57%	62.49%
MgO	5.73%	4.85%	4.81%	3.33%	3.3%
Na_2O	8.55%	6.28%	1.56%	1.07%	0.89%
K_2O	0.43%	0.37%	0.33%	0.35%	0.15%
TiO_2	-	1.42%	1.61%	1.24%	0.28%
Mn_2O_3	-	0.10%	0.10%	0.08%	0.04%
P_2O_5	-	0.95%	0.81%	0.70%	0.16%
SrO	-	0.40%	0.40%	0.28%	0.08%
BaO	-	0.66%	0.60%	0.46%	-
SO_3	5.31%	6.14%	2.52%	0.83%	3.30%

X-Ray Diffraction

X-ray diffraction (XRD) was completed to determine crystalline phases present in the raw CCPs and percent amorphous content. Amorphous or glassy content is of interest as a high percentage indicates a higher reactivity. Amorphous content of fly ash can vary from 50-95% (Ramenzanianpour, 2014). Diffractograms of raw CCPs are shown in Figure 4.2. CCPs contained a number of crystalline components shown as sharp peaks with the amorphous component shown as a large bump between 25-35°2θ. High calcium

ashes have been shown to have an amorphous maximum centered around 30-34°2θ, whereas low calcium ashes tend to be centered between 21-25°2θ (Ramenzanianpour, 2014). The difference in the 2θ values is due to either siliceous glassy content, or a calcium aluminate glassy structure (Diaz et al., 2010). Both glassy structures are reactive. FAH and FAB are known to have high calcium content from the XRF data, and correspondingly the amorphous maximum are centered slightly above 30°2θ as shown in Figure 4.3.

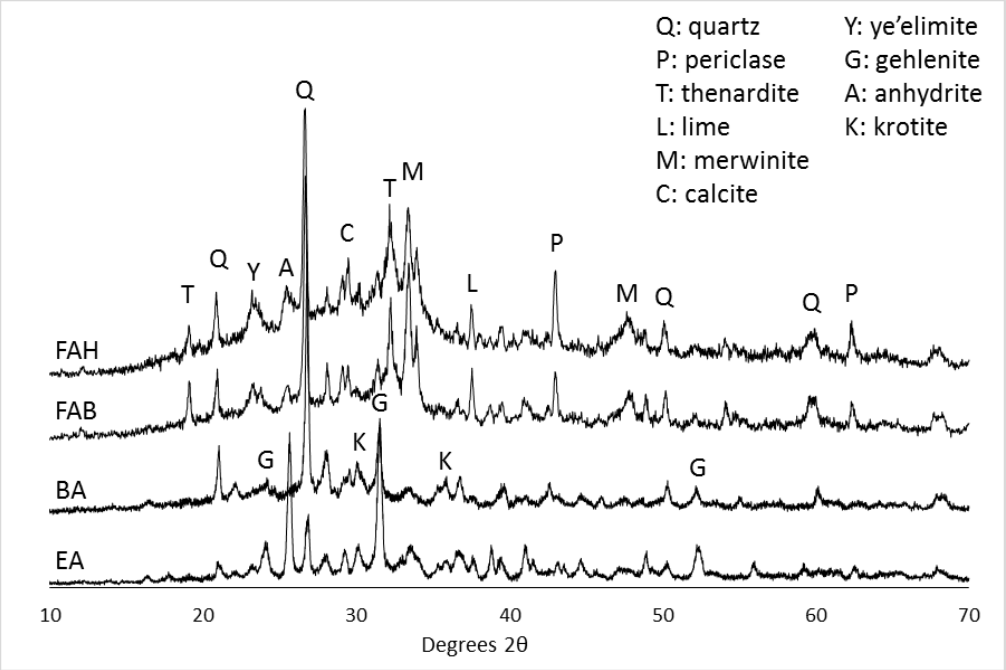

Figure 4.2: X-Ray Diffractograms for Raw CCPs

The two fly ashes had highly similar diffractograms and crystalline components including quartz, periclase, lime, calcite, and merwinite. Periclase and merwinite are commonly found phases in class C fly ash (Chancey, 2008). Phases and associated chemical formulas for the two fly ashes are shown in Table 4.4. Results for the bottom and economizer ash are in Appendix B. The majority of crystalline phases contained aluminum, silica, or calcium which complements the XRF data as these elements were present in the

ash at the largest percent. Thenardite was found in both of the trona-impacted fly ashes, as trona (Na_2CO_3• $NaHCO_3$•$2H_2O$) reacts with sulfate and sulfite to form thenardite (Na_2SO_4) (Su, Shi, & Wang, 2011). The largest component of all CCPs was amorphous, and could not be quantified by XRD.

$2(Na_2CO_3$• $NaHCO_3$•$2H_2O)$ + heat → $3Na_2CO_3 + CO_2 + 5H_2O$

$Na_2CO_3 + SO_2 + ½\ O_2 \rightarrow Na_2SO_4 + CO_2$

$Na_2CO_3 + SO_3 \rightarrow 2Na_2SO_4 + CO_2$

Table 4.4: Raw CCP XRD Phases and Phase Percent

Phase Name	Phase Formula	PDF#	FAH Phase Percent (%)	FAB Phase Percent (%)
Amorphous	N/A	-	65.1	59.6
Anhydrite	$CaSO_4$	37-1496	1.6	13.1
Calcite	$CaCO_3$	5-586	2.3	2.3
Gehlenite	$Ca_2Al(AlSiO_7)$	37-755	-	6.3
Lime	CaO	37-1497	2.3	2.3
Merwinite	$Ca_3Mg(SiO_4)_2$	35-591	8.6	27.2
Periclase	MgO	45-0946	4.0	5.7
Quartz	SiO_2	33-1161	9.3	4.5
Thenardite	Na_2SO_4		4.1	1.9
Ye'elimite	$Ca_4(AlO_2)_6SO_4$	33-0256	2.7	1.7

Data quality including Rwp, Rp, and Chi^2 values are shown in Appendix B.

Loss on Ignition

Loss on ignition (LOI) is generally used as an estimate for the unburnt carbon content in CCPs, but in total it also shows the water, bound water, and inorganic carbonate mineral content (Mohebbi, Rajabipour, & Scheetz, 2015). The results in Table 4.5 do not include the free water content as CCPs were dried before testing. The higher LOI for the bottom ash indicates that it had a higher unburnt carbon content. Bottom ash is the "heavier portion of coal ash that settles on the ground in the boiler" and generally contains the non-combustible portion of coal, so a higher LOI was expected (Palmer, 2015).

ASTM C618 requires an LOI of less than 6% for fly ash to be used in concrete. A high carbon content is detrimental to the formation of concrete and geopolymers due to the high specific surface area of carbon as compared to fly ash and cement (Blissett & Rowson, 2012). The carbon tends to absorb water present in the system, preventing it from allowing the fly ash or cement to react. The addition of trona has been shown to slightly increase the LOI of fly ash (Dan et al., 2013; Pflughoeft-hassett et al., 2009).

Table 4.5: LOI Results for Raw CCPs

CCP	LOI
FAH	3.99%
FAB	2.43%
EA	0.14%
BA	15.57%

Digestion

Average trace metal content of the raw CCPs determined by digestion are shown in Table 4.6. FAH generally had the highest content of trace metals with the exception of copper. Cadmium was present at the lowest concentrations for all CCPs with concentrations in the 1 mg/kg range. Samples were completed in triplicate for FAH and FAB, and in duplicate for the economizer ash (EA) and bottom ash (BA).

Trace element contents are similar to those found in trona-impacted ashes in the literature and generally fall within the range of typical coal fly ash trace element compositions (Blissett & Rowson, 2012a; Su et al., 2011).

Table 4.6: Trace Metal Content of Raw CCPs Determined by Digestion

Element	FAH	FAB	EA	BA	OPC
As (mg/kg)	28.9	13.3	9.8	4.5	16.0
Cd (mg/kg)	1.2	1.0	2.0	0.3	0.3
Co (mg/kg)	17.3	18.0	14.8	9.0	43.2
Cu (mg/kg)	124.8	140.6	108.4	65.4	6.1
Cr (mg/kg)	74.1	56.5	41.9	22.9	31.6
Ni (mg/kg)	50.7	42.7	33.5	20.1	26.7
Pb (mg/kg)	26.7	20.9	18.0	5.9	19.2
Se (mg/kg)	18.1	13.6	0.2	1.5	0.8
Zn (mg/kg)	134.0	52.7	36.1	37.7	123.5

4.1.3 Summary

Based solely upon physical characteristics, the economizer and bottom ash could be expected to be less reactive and therefore form weaker cements pastes and/or geopolymers than the two fly ashes. Fly ash H (FAH) had slightly finer particles and

larger surface area than fly ash B (FAB), but the differences were small enough that the two could be expected to perform similarly without further information.

Examining chemical characteristics furthers the conclusion that the economizer and bottom ash are less suitable for geopolymerization than the two fly ashes. The bottom ash had a large LOI indicating a high unburnt carbon content which hinders reactivity, and both the economizer and bottom ash had lower amorphous content than the two fly ashes. In addition, they contained lower concentrations of almost every trace element of concern than the two fly ashes meaning that stabilization is less of an issue for these ashes. The two fly ashes are likely significantly more reactive, and contained higher metal contents so the focus of the majority of the leaching tests was on these materials.

4.2 Characterization of Cement Pastes and Geopolymers

Four cement pastes and six geopolymers were made and characterized. Two cement pastes were made each for FAH and FAB with 30% and 60% ash content (70% and 40% cement). For each of the fly ashes, two geopolymers were made using 4M sodium hydroxide (NaOH) and 8M NaOH. Two additional geopolymers were made with 4M NaOH and silica moduli (M_s) of 0.15 and 1.5 respectively for FAH to reach a total of 6 geopolymer specimens. The silica modulus is defined as SiO_2/Na_2O and was obtained by added fumed silica into the NaOH solution prior to mixing.

Similarly to raw CCPs, cement pastes and geopolymers were characterized with respect to both physical and chemical traits. Strength and porosity were tested to confirm solidification of the specimens. Low porosity can also be associated with reduced leaching of contaminants as they may become trapped within inaccessible pores. Chemical characterization tests included XRD and LOI, which helped determine which

new phases had formed during geopolymerization as compared to phases present in the raw CCP. Phases can then be associated with either reduced or increased leaching.

4.2.1 Physical Characterization

Strength

While strength testing was completed mainly to confirm solidification of specimens, stronger specimens also likely have a higher amorphous content which could be beneficial for stabilization of heavy metals. Amorphous compounds are mainly calcium silicate hydrates (C-S-H) for cements and alumino-siliceous compounds for geopolymers which contribute significantly to specimen strength and have the potential to bind contaminants within their matrix during formation.

Strength results for cement pastes and geopolymers are shown in Figure 4.4 and Figure 4.5. Two specimens were broken at 7 days, and either two or three were broken at 28 days. Average values are shown. It would be expected for the specimens to be stronger at 28 days than at 7 days, but this was not always the case. The discrepancy is likely due to specimen preparation and the low strength of geopolymers. Specimens were prepared in 5.1cm x10.2cm cylinders and the top was leveled off during casting. However, due to evaporation of water and potential drainage of water out of the bottom of the cylinder, the tops of the cylinders did not always harden completely level. Compression testing carried out on cylinders with uneven surfaces can yield lower results as load will not be dispersed evenly throughout the cylinder causing it to break faster. In addition, it was found that due to the low strength of geopolymers often the edges on the top and bottom of the cylinder would crumble during testing before the main body of the geopolymer actually cracked (Figure 4.3). Therefore, the strengths are likely artificially low.

Figure 4.3: Geopolymer Edges Crumbling after Strength Test

Cement pastes were significantly stronger than geopolymers which could be attributed to the cement reacting more than the fly ash or could also partially be due to the high S/B ratio for geopolymers. 4M geopolymers were stronger than 8M geopolymers, and 4M FAB was the strongest of the geopolymers as it had the lowest S/B at 0.45. In addition, the geopolymer with M_s=1.5 had higher strength than others, though it appears that decreasing the S/B had a larger impact on strength than increasing the M_s.

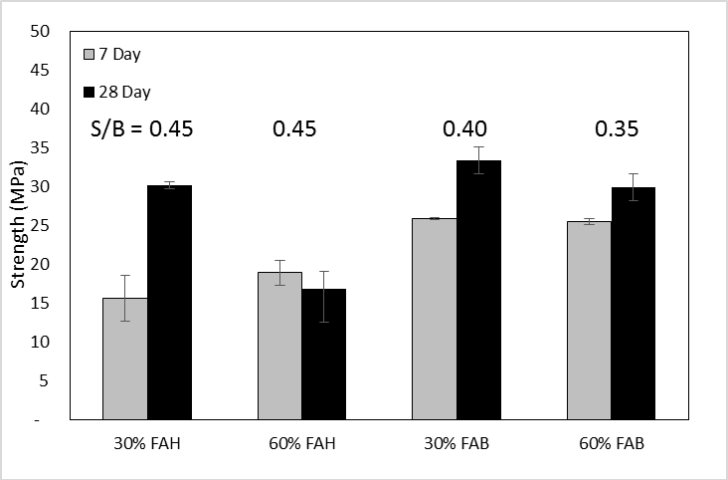

Figure 4.4: Cement Paste Strength Results

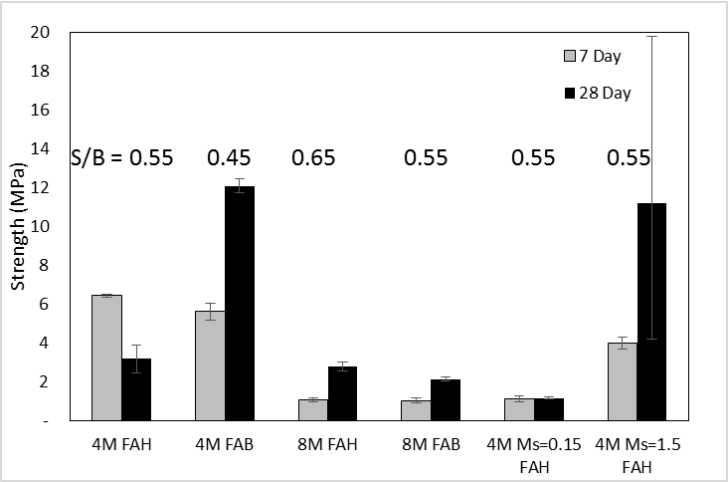

Figure 4.5: Geopolymer Strength Results

Porosity

Porosity was calculated based upon a difference in weight between specimens saturated with water and isopropanol and dry weight. Trends indicated that cement pastes and the 4M M_s = 1.5 geopolymer had lower porosity than did 8M geopolymer and the 4M M_s = 0.15 geopolymer.

4.2.2 Chemical Characterization

X-Ray Diffraction

Crystalline phases and amorphous content obtained from XRD for geopolymers and cements can be compared to those found in the raw CCPs to help determine changes responsible for reducing leaching. Some phases present in raw ashes were also present in geopolymers such as quartz, periclase, calcite and ye'elimite. Quartz and periclase are both insoluble and their presence in both raw CCP and geopolymers indicates that they did not react. Similar results have been found by others (Bankowski et al., 2004; Swanepoel & Strydom, 2002). Calcite concentrations increased from raw CCPs to geopolymers, but the lime peak present in CCPs is gone. While carbonate concentrations

in the system are unknown, the NaOH used to make geopolymers likely contained a significant amount of carbonate due to dissolution of CO_2 from the atmosphere, so the increase of calcite is not unexpected. Both calcite and C-S-H have peaks at approximately 29.4° 2θ, but the calcite peak would be expected to be much sharper as C-S-H is mostly an amorphous compound (Snellings et al., 2015). A portion of the calcite peak could be attributable to C-S-H, but here it is assumed that the whole peak is calcite.

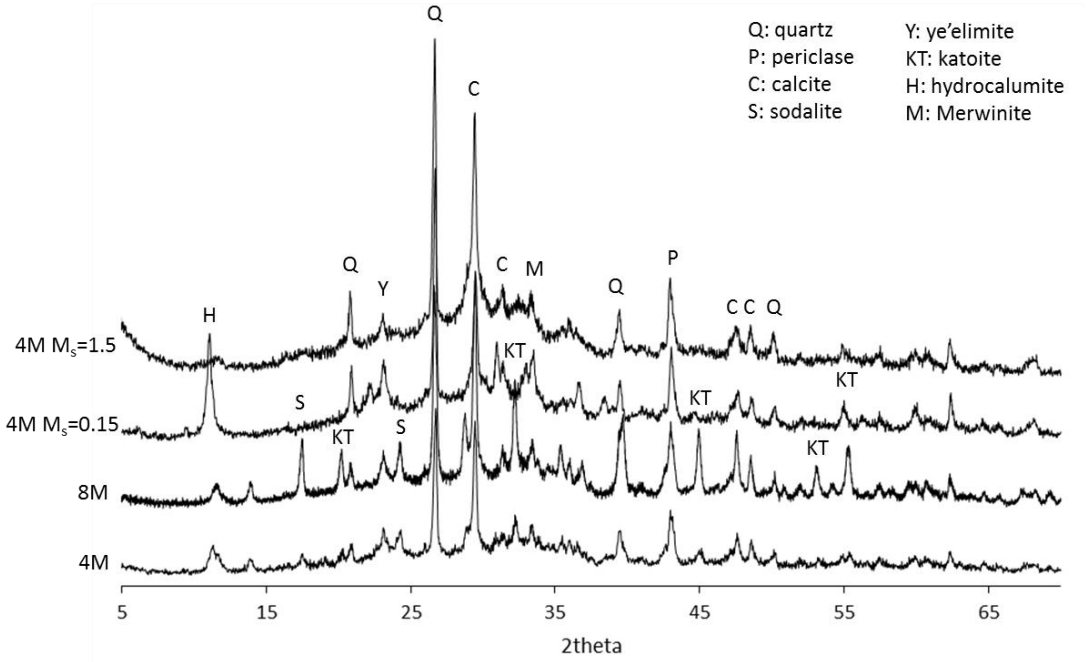

Figure 4.3: FAH Geopolymer XRD Diffractograms

Thenardite in raw CCPs is now gone, and a new sodium phase sodalite is present. Sodalite contains chloride which was expected to be present in the system only at low concentrations. It is possible that the sodalite peaks are incorrectly identified and is actually a different phase that does not contain chloride, however the peak fits well and chloride could potentially be present in the system as trona is known to react with HCl in flue gas streams. In addition to having a higher sodalite content than other geopolymers, the 8M geopolymer had a higher katoite content as well.

The geopolymer with M_s=1.5 had a higher amorphous content than other geopolymers and also had a higher strength as shown in Section 4.2.1. The geopolymer with M_s=0.15 had a composition different than that of other geopolymers, and it is unclear why. It had a large peak at approximately 11° 2θ, which is attributed to hydrocalumite, but could be hydrotalcite, AFm solid solution or a C-A-H phase, though the hydrocalumite peak fits best (Snellings et al., 2015). Similarly to sodalite, hydrocalumite contains chloride and it is likely that chloride is available at such low quantities that forming hydrocalumite would be infeasible. The phase was also present in 4M geopolymers with M_s=0, and 8M geopolymers to a lesser extent. It was originally assumed that the phase formed due to the addition of fumed silica, however when more fumed silica was added (M_s=1.5) the peak decreased. The geopolymer would need to be re-made to confirm the results.

Table 4.7: FAH Geopolymer XRD Phases

Phase Name	Phase Formula	4M FAH Phase %	8M FAH Phase %	4M FAH M_s = 0.15 Phase %	4M FAH M_s = 1.5 Phase %
Amorphous C-S-H/ N-A-S-H	N/A	61.6	60.8	47.9	70.2
Calcite	$CaCO_3$	10.7	10.8	11.5	15.2
Katoite	$Ca_3Al_2(SiO_4)_{(3-x)}(OH)_{4x}$	5.7	13.1	-	-
Hydrocalumite	$Ca_2Al(OH)_6[Cl-x(OH)_x]-3H_2O$	3.8	1.5	13.8	-
Merwinite	$Ca_3Mg(SiO_4)_2$	3.6	2.1	-	-
Periclase	MgO	3.2	2.8	4.0	2.6
Quartz	SiO_2	4.2	4.4	11.2	7.7
Sodalite	$Na_8Al_6Si_6O_{24}Cl_2$	3.0	2.6	-	-
Ye'elimite	$Ca_4(AlO_2)_6SO_4$	4.3	1.8	-	4.3

Data quality including Rwp, Rp, and Chi^2 values are shown in Appendix B.

Loss on Ignition

The LOI is an indicator of reaction as it can be assumed to be an approximation of the amount of water chemically bound to the dry material (Fagerlund, 2009). Cement paste and geopolymer samples were ignited to determine the percent bound water in the system. Samples were completed in triplicate and average values are shown in Table 4.8. The percentage of bound water in all systems was in the range of 10%. The geopolymer with the highest silica modulus had the largest percent LOI and cement pastes with 60%

CCP had the lowest percent LOI. All values were somewhat low, with reported literature values around 20-40% for cement pastes (Fagerlund, 2009).

With LOI as an indicator of reaction it would be expected that a higher reaction would be correlated with higher strength. This was somewhat the case, as the geopolymer with M_s=1.5 had the highest LOI and had one of the highest strengths. In addition, 4M geopolymers had higher LOI and higher strength in both cases. However, 4M FAB had the highest strength of all the geopolymers and it had a lower LOI than 4M FAH. Also in agreement, 30% cement pastes were stronger and had a larger LOI than 60% pastes. It is possible that a similar amount of solution reacted with geopolymers and cement pastes, but that the compounds formed in cement had higher strength than those formed in geopolymers.

Table 4.8: Geopolymer and Cement Paste Loss on Ignition Results

Averages	% LOI	Standard Deviation
30% FAH	10.8%	0.1%
60% FAH	9.1%	0.1%
30% FAB	10.3%	0.8%
60% FAB	9.2%	0.1%
4M FAH	11.2%	0.2%
4M FAB	10.6%	0.2%
8M FAH	10.7%	0.2%
8M FAB	9.3%	0.4%
4M FAH M_s = 0.15	9.3%	0.7%
4M FAH M_s = 1.5	12.9%	0.1%

4.2.2 Summary

Among geopolymers, XRD, LOI and strength testing indicate that raising the silica modulus to 1.5 increased reactivity and created a stronger, more amorphous solid. Increasing the silica modulus to only 0.15 had varying results and less can be concluded. Results also indicated that 4M geopolymers had a more complete reaction than 8M geopolymers due to their increased LOI and higher strength. Similar results have been found in the literature for high calcium fly ash based geopolymers (Winnefeld et al., 2010, Williamson et al., 2016). Both FAH and FAB contained a high calcium content at approximately 25%, as seen from XRF results. Typically geopolymers are made with low-calcium ashes, and these increase in reactivity with increasing NaOH molarity due to the increased formation of N-A-S-H phases. High calcium ashes however, tend to generate calcium based amorphous phases in addition to sodium based phases, and increasing the NaOH molarity beyond what is required for dissolution leads to a decrease in compressive strength.

In general, it is expected that increased reactivity of cement pastes or geopolymers is beneficial with respect to leaching (i.e. results in less leaching of contaminants) due to the higher potential to form new phases that can physically or chemically bond with contaminants in the ash. Based on characterization results, geopolymers made with 4M NaOH would therefore be expected to stabilize elements better than geopolymers made with 8M NaOH, and the geopolymer made with 4M NaOH and M_s=1.5 would be expected to perform the best.

4.3 Leaching Test Water Quality

Leachate water quality can give insight into whether conditions favor or disfavor leaching of particular elements. Conductivity measurements can indicate dissolution of major ions, titrations indicate alkaline components of materials and ultimately of

leachate, and oxidation reduction potential (ORP) indicates the potential of a water to oxidize or reduce compounds. Oxidation state is of relevance as for several contaminants including as arsenic and chromium one oxidation state is significantly more toxic than the others.

4.3.1 Conductivity

Conductivity is the capacity of a solution to conduct electricity and is directly proportional to the concentration of ions in the water. For almost all samples, conductivity increased with decreasing pH, except for above pH 12 where it increased slightly. Increasing conductivity is due to dissolution of cations such as calcium, sodium and aluminum. To confirm this, major cation concentrations are shown to increase with decreasing pH in Section 4.4.1, and also at times increase at high pH as is the case for aluminum. Notably, conductivity measurements versus pH varied between raw FAH and FAB. FAB had higher conductivity readings at higher pH than did FAH (see Figure 4.7). This indicates that FAB was dissolving more at high pH than was FAH. Conductivity results for geopolymer specimens are included in Appendix C.

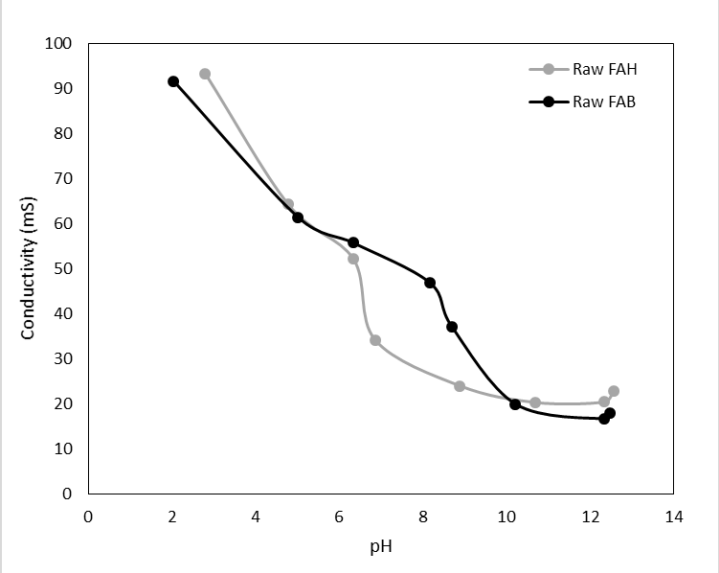

Figure 4.7: Raw Ash Conductivity Readings versus pH

4.3.2 Titration

Raw CCPs were titrated with nitric acid as an estimate of alkaline compounds within the ash. Titration curves were obtained based on pH values from the pH variant leaching test (EPA Method 1313). Figure 4.8 shows that more acid was required to reduce the pH of raw FAB than FAH in the pH 6-10 range. From Figure 4.7 we know that FAB was dissolving more in the pH range 6-10 than was FAH. It can be deduced that through dissolution, FAB was releasing more hydroxide and carbonate groups that buffered the pH. FAH and FAB had approximately equal total alkaline content with roughly 22.4 meq acid/g-dry and 21.4 meq acid/g-dry required to titrate to a pH of 4.3 respectively. FAB had over twice the bicarbonate alkaline content however as it required 10.9 meq acid/g-dry to reach a pH of 8.3 and FAH only required 5.2 meq acid/g-dry. Titrations were completed over 48 hours and calculations assume that equilibrium was reached.

Titration curves of cement pastes and geopolymers are in Appendix C and all are generally similar. Cement pastes had the highest alkaline compound content and geopolymers the lowest, with raw ashes falling in between. 30% pastes had notably higher alkalinity than 60% pastes, but 4M and 8M geopolymer titration curves followed each other closely with few differences.

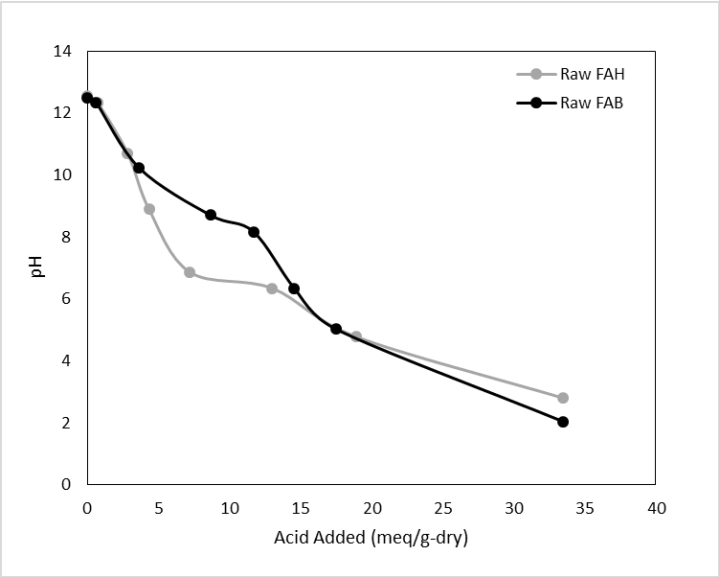

Figure 4.8: Raw Ash Titration with Nitric Acid

4.3.3 ORP

Oxidation-reduction potential (ORP) is the ability of a solution to oxidize or reduce chemical species. Positive readings indicate an oxidizing solution, and negative readings indicate a reducing solution with a reading of zero indicating a neutral solution. ORP was measured to determine if the raw CCPs and/or cement and geopolymer mixtures were creating highly oxidizing or reducing environments that might change the speciation of contaminants (e.g. As(V) to As(III)). A majority of leachates had positive ORP readings, and for the pH leaching test where the liquid/solid (L/S) ratio was 10, experimental values ranged from about +20-500mV. Reagent water blanks at pH 5.8-6.0 gave readings around +220-250mV. Overall, ORP increased with decreasing pH as shown in Figure 4.9. Lower, and occasionally negative, values were found when the L/S was decreased and the pH was higher (>12.5). The lowest recorded reading was -22mV, which is quite close to zero, indicating a mostly oxidizing environment. Obtained ORP values do not indicate either highly oxidizing or highly reducing environments over the pH range. Results were consistent and a similar trend of increasing ORP with decreasing

pH has been found in fly ash systems by others (Kazonich, n.d.). Results for leaching in reagent water versus the simulated landfill leachate were highly similar indicating that components of the landfill leachate used in this study did not affect the ORP of solution.

Additional ORP data are contained in Appendix C. Some ORP points in Figure 4.9 and figures in Appendix C appear to be higher than would be expected based on the overall curve. It often took 5-10 minutes to obtain a stable reading on the probe and it is possible the value was still decreasing when the reading was recorded. The value could appear to be stable on the instrument over the course of a shorter amount of time (30 seconds to 1 minute), but if a long enough time were given it could still decrease so higher than actual readings may have been recorded.

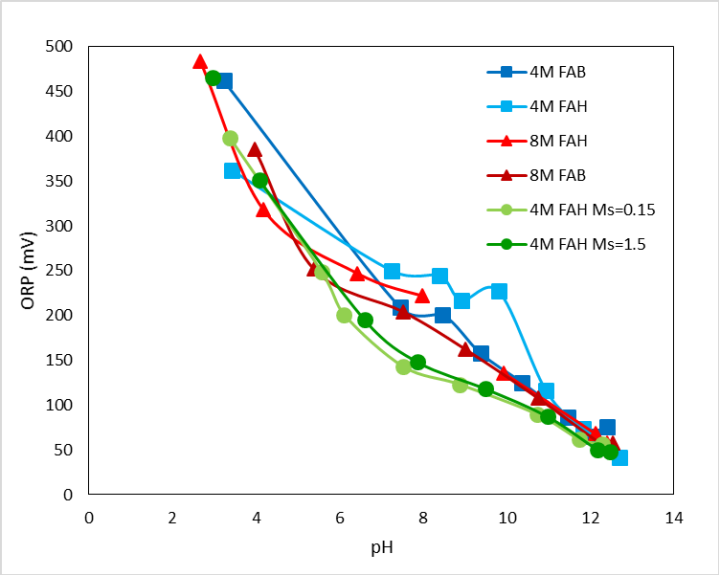

Figure 4.9: Geopolymer ORP Results in MPW

4.4 Leaching Test Results

Leaching test results are presented in multiple ways for both varying pH and liquid/solid (L/S) testing. Results are presented in Appendix A as raw concentrations, with the resulting elemental concentrations plotted against either pH or L/S. Results were also normalized by total metal concentration to show percent leaching. Total metal

concentrations were determined by taking the grams of CCP and cement within the geopolymer or cement paste and multiplying by the concentration of each element found by digestion. Grams of CCP and cement paste were calculated by taking into account the percent bound water as found in Section 4.2.2.

OPC was digested and results are shown in Section 4.1.2. Several elements were present in the OPC at high enough concentrations to affect the results, and impacts are mentioned where relevant. NaOH and DI water blanks were also run to ensure that the solutions were not contaminated and impacting the results.

In addition to the experimental leaching tests, equilibrium chemical speciation simulations were run in Visual MINTEQ to help understand how element concentrations compared to expected mineral solubilities for compounds over varying pH. Solubility modeling and analysis of the resulting precipitate formation/dissolution considered three potential mechanisms that can affect leaching of oxyanions and cations across varying pH:

1. Cement and geopolymer matrix dissolution.
2. Adsorption of trace elements onto solid surfaces.
3. Trace metal hydroxide formation.

Analyses were carried out to help determine the extent to which each of these components was contributing to the leaching of metals.

4.4.1 Major Ions

First, solubility diagrams for aluminum and calcium were examined to observe the general trends and to determine the approximate pH corresponding to the lowest solubility for a particular mineral. Figure 4.10 shows the solubility diagram for aluminum assuming an infinite amount of solid aluminum oxide (Al_2O_3). Aluminum oxide was used

as a majority of aluminum phases in the fly ash and geopolymer systems were amorphous, for which solubility data is less well defined. The diagram shows that total dissolved aluminum is at a low point at approximately pH 6.

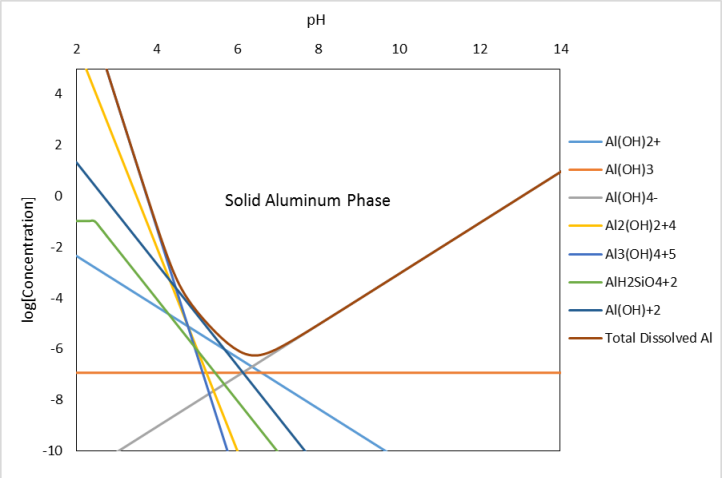

Figure 4.10: Aluminum Species in equilibrium with Solid Al_2O_3 from Visual MINTEQ Modeling

Figure 4.11 shows the dissolution of calcium in equilibrium with varying amounts of carbonate, as the carbonate concentration in the system is unknown. The calcium concentration was input into the system based upon XRF data and quantities were used for the 4M FAH geopolymer. Up until approximately pH 5, calcium concentrations are high as calcite is not expected to form but then they drop off significantly corresponding to the precipitation of calcite. Increasing the carbonate concentration can drastically decrease the dissolution of calcium. As indicated in the literature review, oxyanions of arsenic can be incorporated into calcite during precipitation.

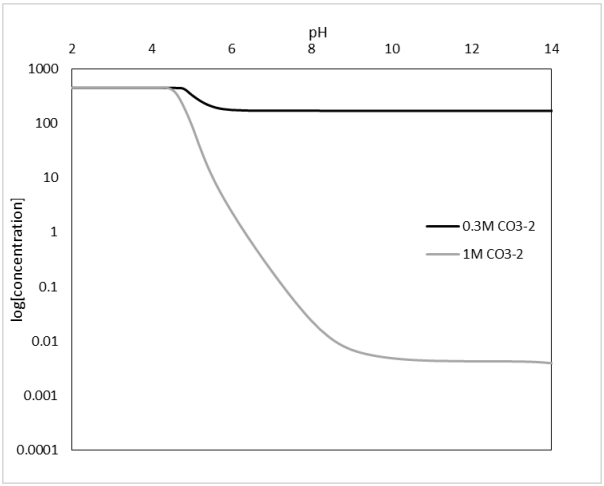

Figure 4.11: Total Dissolved Ca^{2+} in equilibrium with 0.3M and 1M CO_3^{-2} from Visual MINTEQ Modeling

Figure 4. shows measured aluminum and calcium leachate concentrations which can be compared to the theoretical solubility diagrams. Aqueous calcium concentrations decreased with increasing pH consistent with the precipitation of calcite. While the data do not match either of the equilibrium speciation plots for calcite, at pH 12 the concentration of calcium in solution is consistent with approximately 0.4M carbonate in the system.

Aluminum matched the trends for the solubility curve presented in Figure 4.11, as it increased at both low and high pH as shown in Figure 4.10. Lowest aluminum concentrations were found in the 10^{-2} mmol/L or 10^{-5}mol/L range, while Figure 4.10 indicates that aluminum concentrations are as low as 10^{-6} mol/L. The difference is likely due to the various aluminum compounds present in the actual system, whereas only Al_2O_3 was assumed present in Figure 4.10. The increase in calcium and aluminum concentrations at low pH are indications of the breakdown of geopolymer matrices and thus an increase in metal ions is expected.

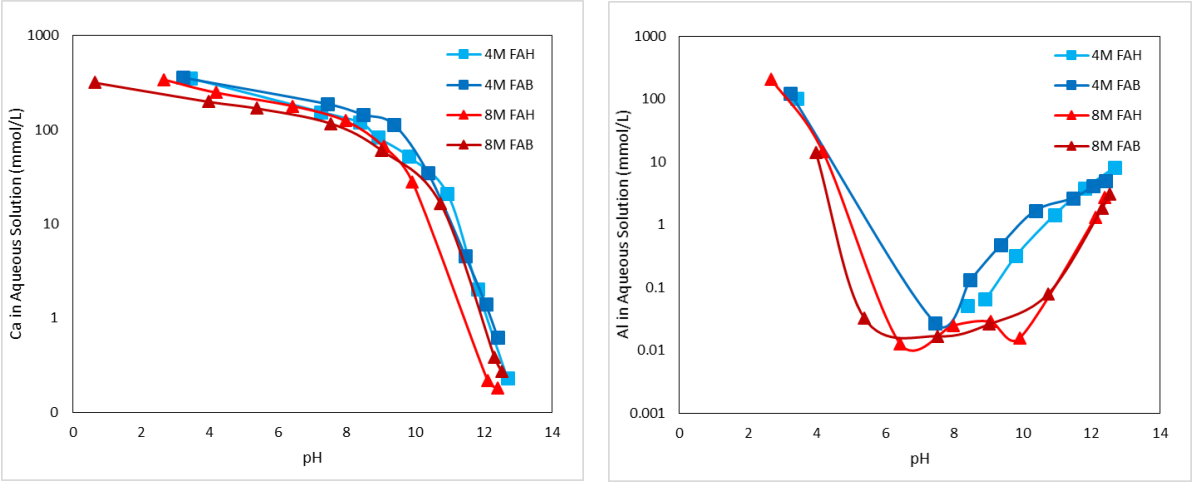

Figure 4.12: Calcium (left) and Aluminum (right) in Aqueous Solution versus pH

In addition, theoretical solubility diagrams were developed using Visual MINTEQ based upon actual concentrations of elements in the system. As a first step, concentrations of major ions present in the system were determined based upon XRF data and input into Visual MINTEQ. Sulfite (SO_3^{2-}) concentrations were available from XRF data, and carbonate (CO_3^{2-}) concentrations were estimated by assuming that all sodium present in the fly ash was due to trona ($Na_2CO_3 \bullet NaHCO_3 \bullet 2H_2O$). A low chloride concentration (10^{-6}M) was added, since it is possible that chloride is in the system, but the concentration is unknown. The speciation modeling was then conducted to determine possible phases present with a specified pH of 12.5 as this was the pH obtained by most geopolymers in reagent water with an L/S of 10. Ionic strength was specified at 0.7M. The initial list of possible formed phases was large and is included in Appendix A. Minerals that were found to precipitate included quartz, calcite, and periclase which were also found in geopolymer XRD patterns as shown in Figure 4.6 and Table 4.7. Several possible solids were not available in the MINTEQ database including katoite ($pK_s = 22.3$) and C-S-H ($pK_s = -11.625$). These solids were also input into the database with solubility

data taken from Meyers et al. (2015) and Narayan (2017). Elemental diagrams are shown in applicable later sections.

4.4.2 Oxyanions

Trace metals are divided into anions and cations for analysis. Results are discussed in relation to how well geopolymers and cement pastes performed compared to each other, and in reference to which mechanisms are thought to cause increased leaching for various elements.

Arsenic

The toxicity characteristic leaching procedure (TCLP) limit for arsenic put forth by the USEPA is 5.0 mg/L using an L/S of 20:1 (EPA 2015). The 5.0 mg/L value was only exceeded by raw ash in more stringent conditions than required by the TCLP (i.e. L/S < 20), and was never exceeded by geopolymer or cement pastes. With an L/S of 10, arsenic concentrations were less than 1 mg/L across all pH's, and at mid-range pH (6<pH<11) values were typically less than 50 µg/L. In all cases specimens made with FAH leached more than those made with FAB, and this is attributed to the higher arsenic concentration in FAH as shown in Section 4.1.2. From the literature, As(V) is expected in the fly ash, and ORP values in Section 4.3.3 are in agreement.

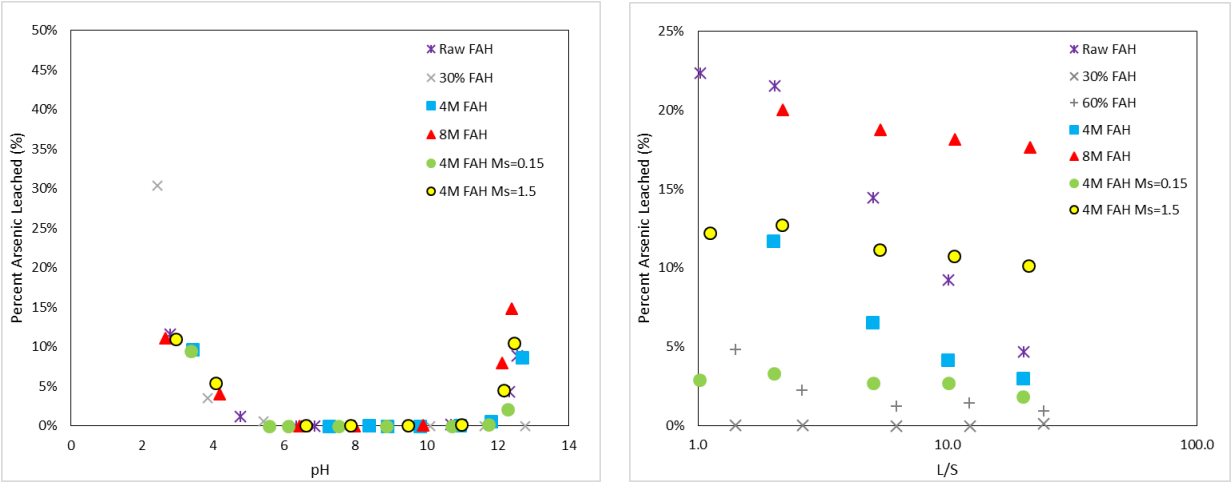

Figure 4.13: Arsenic Leaching from FAH Specimens vs pH (left) and vs L/S (right

The OPC used to make cement pastes had 16.0 mg/kg arsenic which is significant compared to arsenic in the CCPs (28.9 and 13.3 for FAH and FAB, respectively). Despite this, at high pH the cement pastes bound arsenic better than geopolymers for both FAH and FAB as shown in Figure 4.13 on the right. This is likely due to the presence of calcite in the cements. The exception was the 4M geopolymer made with FAH that had an M_s of 0.15. This geopolymer performed notably better than other geopolymers at high pH, and bound arsenic at a level similar to the 60% FAH cement paste. Decreased leaching could be due to differences in XRD results outlined in Section 4.2.2, but ultimately reasons are unknown and the specimen would need to be re-made to confirm results. Other characteristics of the geopolymer with M_s=0.15 included low strength, and somewhat low LOI as compared to the other geopolymers which would not be expected to be associated with decreased leaching, as both are associated with low reactivity. Also unexpected was that increasing the silica modulus from 0.15 to 1.5 did not further decrease arsenic leaching. Increasing the silica modulus caused an increase in reactivity and higher strength as outlined in Section 4.1, therefore the higher silica modulus would be expected to perform better due to increased binding of contaminants in reaction products.

However, the 4M geopolymer with M_s=1.5 performed similarly to the 4M geopolymer with M_s=0.

Of the geopolymers, those made with 8M NaOH leached the most for both FAH and FAB, and even leached more than raw ashes at high pH. This is not surprising based upon strength and LOI results of 4M and 8M geopolymers, as 8M geopolymers had lower strength and lower LOI results indicating less reaction. 30% fly ash cement pastes leached less than 60% fly ash cement pastes, which could be attributed to the increased C-S-H content that would be present in 30% pastes from the higher cement content. There were few significant differences in leaching between specimens at mid and low pH.

While both FAH and FAB had high calcium contents for coal fly ash (approx. 25% CaO) the OPC had over twice this concentration at 62.5% CaO. Matrices with a high calcium content have been shown to stabilize arsenic better, so it is not unexpected that the cement pastes bound arsenic better at high pH than the geopolymers did (Provis 2009). The calcium present likely helped to form low-solubility calcium-arsenic compounds which was briefly looked at via Visual MINTEQ modeling as shown in Figure 4.14.

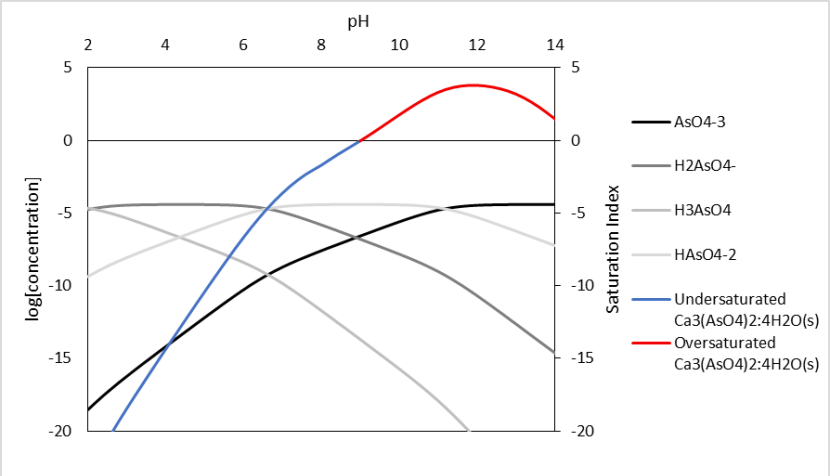

Figure 4.14: Arsenic speciation and solid compounds based upon Visual MINTEQ

Figure 4.14 was created by entering all compounds present in the 4M FAH geopolymer leachate system into Visual MINTEQ based upon XRF and digestion concentrations and plotting all compounds that Visual MINTEQ found that contained arsenic. MINTEQ found one solid calcium-arsenic compound that is oversaturated above approximately pH 9. Arsenic did not begin to increase leaching in geopolymer systems until above pH 12 as shown in Figure 4.13, and the calcium-arsenic compound also begins to dissolve more above pH 12. The figures indicate that dissolution of calcium-arsenic compounds could be a potential reason for increased arsenic leaching above pH 12.

Selenium

The TCLP limit for selenium is 1.0 mg/L (EPA 2015). The 1.0 mg/L limit was exceeded by raw ash, cement pastes and geopolymers, but only in more stringent conditions than required by the TCLP (i.e. L/S < 20). Selenium is amphoteric, but in most cases concentrations were higher at high pH than at low pH. Only at extremely low pH (<2) did concentrations increase again. At mid-range pH (6<pH<11) concentrations were typically less than 200 µg/L for cement and geopolymer pastes, and less than 500 µg/L for raw CCPs. FAH specimens leached at higher concentrations than FAB specimens, due to a higher selenium content of the FAH (Table 4.6). Interestingly, raw FAH leached at high concentrations at high pH, whereas FAB leached at similar concentrations at high pH and at mid-range pH (Figure 4.15).

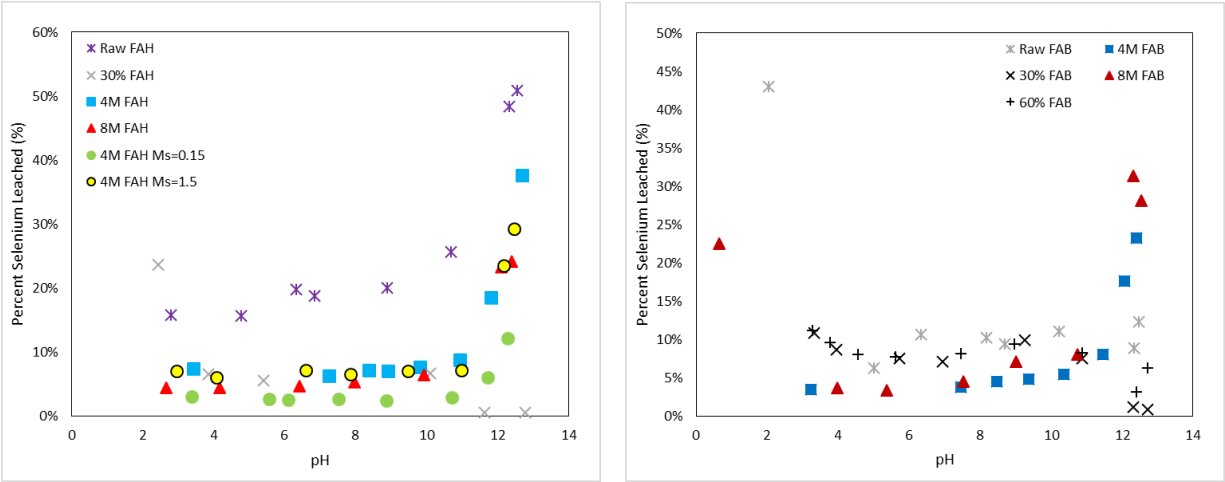

Figure 4.15: Selenium leaching from FAH (left) and FAB (right) Specimens vs pH

FAB geopolymers leached more selenium at high pH than they did at low pH, but raw FAB leached similarly over a wide pH range (pH 4-13). Therefore, at high pH, geopolymers wound up leaching more than the raw ash. For FAH however, all geopolymers and cement pastes reduced leaching as compared to the raw CCP. As with arsenic, the 4M FAH geopolymer with M_s=0.15 reduced selenium leaching considerably more than the other geopolymers. All other geopolymers performed approximately the same, and at high pH cement pastes bound selenium better than geopolymers, with 30% fly ash cement pastes binding more than 60% fly ash cement pastes. Literature has shown reduced leaching of selenium in high calcium matrices, and the formation of low solubility calcium compounds such as $CaSeO_3$-H_2O, is likely a reason for reduced leaching (Hyun et al., 2009).

Oxyanion Summary

Arsenic and selenium had differing concentration profiles versus pH. Arsenic leached similarly at both low and high pH while selenium leached noticeably more at high pH. Cement pastes bound oxyanions better at high pH than geopolymers did, and in every case 30% fly ash pastes reduced leaching more than 60% fly ash pastes. This result

fits neatly into the literature as high calcium systems have been shown to bind oxyanions better due to the formation of insoluble calcium compounds. However, OPC is not the preferable binder because less fly ash is incorporated in the resulting solid. The best geopolymer overall was the geopolymer made with 4M NaOH and an M_s=0.15. It reduced leaching of arsenic and selenium significantly more than other tested geopolymers and sometimes reduced leaching to concentrations on-par with the 60% fly ash cement pastes. This geopolymer was only made with FAH and not FAB, so it is unknown if the same results would be found with FAB. It is unclear why increasing the silica modulus above 0.15 did not cause a further decrease in leaching. The geopolymers would need to be re-made and re-tested to confirm results. 8M geopolymers typically performed slightly worse than 4M geopolymers, but this varied and generally leaching concentrations were similar.

4.4.3 Cations

Chromium

The TCLP limit for chromium is 5.0 mg/L (EPA 2015). The 5.0 mg/L value was only exceeded by raw ash in more stringent conditions than required by the TCLP (i.e. L/S < 20), and was never exceeded by geopolymer or cement pastes. However, at low pH, some specimens got close to the limit (approx. 4 mg/L). Chromium is amphoteric, but concentrations were higher at low pH than high pH (see Figure 4.16), whereas arsenic concentrations were similarly high at low and high pH. At mid-range pH (6<pH<11) concentrations were typically less than 100 µg/L. Leachate concentrations from FAH and FAB specimens were similar.

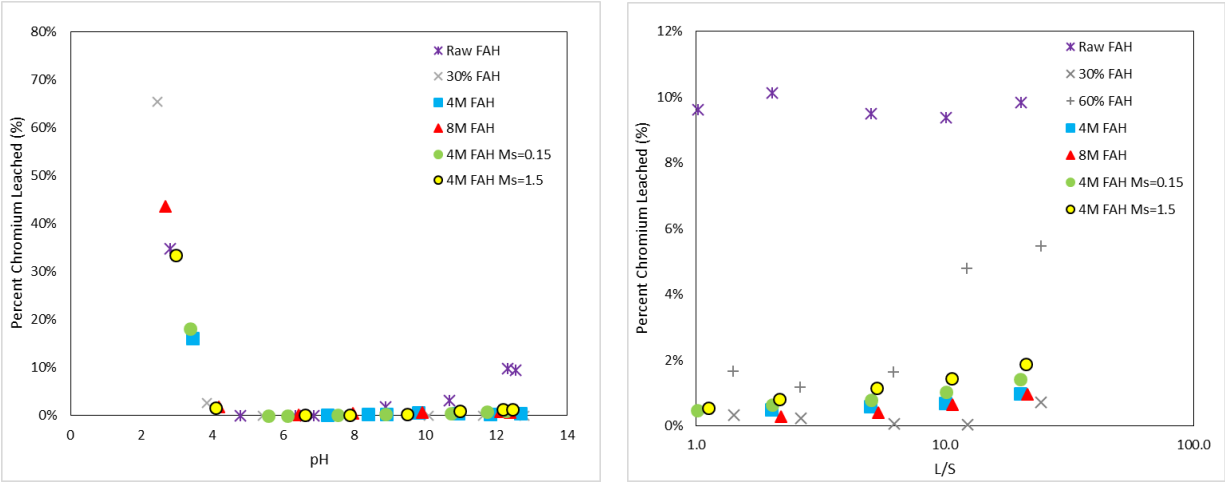

Figure 4.16: Chromium leaching from FAH Specimens vs pH (left) and vs L/S (right)

As opposed to majority of other cations measured, raw ashes leached chromium at high pH, and geopolymer and cement specimens were able to reduce this leaching. Especially at low L/S ratios, specimens kept concentrations below 1 mg/L, while raw ash leached up to 7-8mg/L, which is above the TCLP limit. Even though the OPC used to make cement pastes had 43.2 mg/kg chromium, which is high and nearly comparable to the amount contained within CCPs (Table 4.6), cement pastes still had lower chromium leaching than the raw ash. Again, 30% fly ash cement pastes leached less than 60% fly ash cement pastes, but unlike arsenic leaching, no one geopolymer considerably outperformed another. All geopolymers adequately reduced leaching at high pH as compared to raw CCPs. The 8M geopolymers tended to do slightly better than the others, and geopolymers with an increased silica modulus did slightly worse.

Literature indicates that chromium is present in fly ash as Cr(III), and ORP values are in agreement. The reduction in chromium leaching at high pH could have been due to being bound within the geopolymer matrix or due to precipitation out as chromium hydroxide, however Cr(III) has also been shown to adsorb significantly onto different minerals with increasing pH as shown in Figure 4.17 (Griffin et al., 1977; Rajurkar et al.,

2011). While Figure 4.17 only applies to adsorption on ferrihydrite, it shows that Cr(III) begins to desorb significantly around pH 4-4.5, which is the pH that chromium concentrations increased in leachate (Figure 4.16). Iron content in the fly ashes was only approximately 5%, but there would be iron phases present for sorption to occur, therefore it is possible that the decrease in chromium concentrations at high pH was due to adsorption.

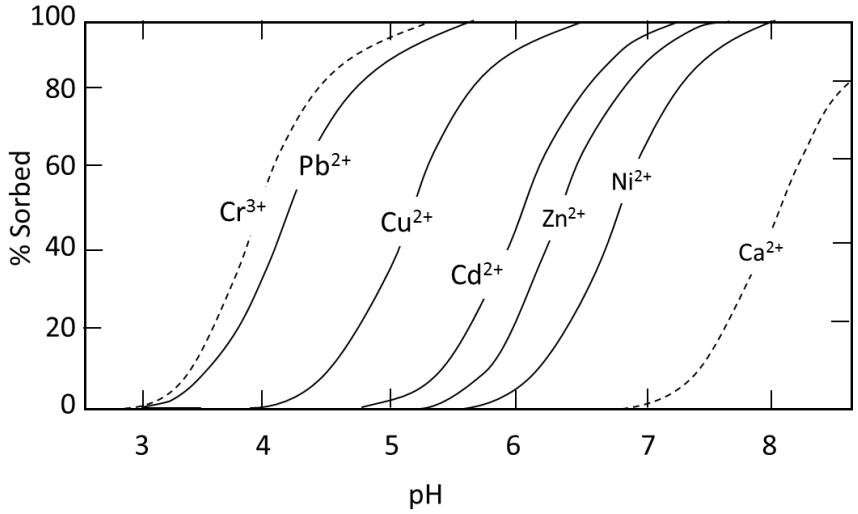

Figure 4.17: Element Percent Sorbed versus pH on Ferrihydrite (Reproduced from Stumm, 1992; Dzombak and Morel, 1990)

Other Cations

Leaching trends were similar among most other cations examined as these elements (Cd, Co, Cu, Ni, Pb, Zn) had essentially no leaching at high pH, and concentrations only began increasing once the pH dropped below 7, likely due to dissolution of C-S-H and N-A-S-H. Figure 4.18 shows cadmium as an example where leaching increased below pH 7. For some elements the pH was lower than 7 before any significant leaching occurred. Table 9 shows the approximate pH at which each element showed an increase in leaching. For each element FAH and FAB specimens gave similar

results. The OPC used for cement pastes contained many of the cations tested, and this became clear at low pH. In many cases, the cement pastes were leaching at higher concentrations than would be possible if the OPC did not contain any metals. To account for this, concentrations of elements within the OPC were included in the normalized graphs. In general, raw CCPs leached more than geopolymers at low pH. Lead was the exception to this, where the raw ash tended to leach at lower concentrations than geopolymers, though all concentrations were low.

Table 4.9: pH of Increased Leaching for Cations

Element	**pH of Increased Leaching**	**pH of Lowest Metal Hydroxide Solubility**
Cd	<7	11
Co	<7	11
Cu	<5	9
Ni	<7	10.2
Pb	<4	9.5
Zn	<6	9

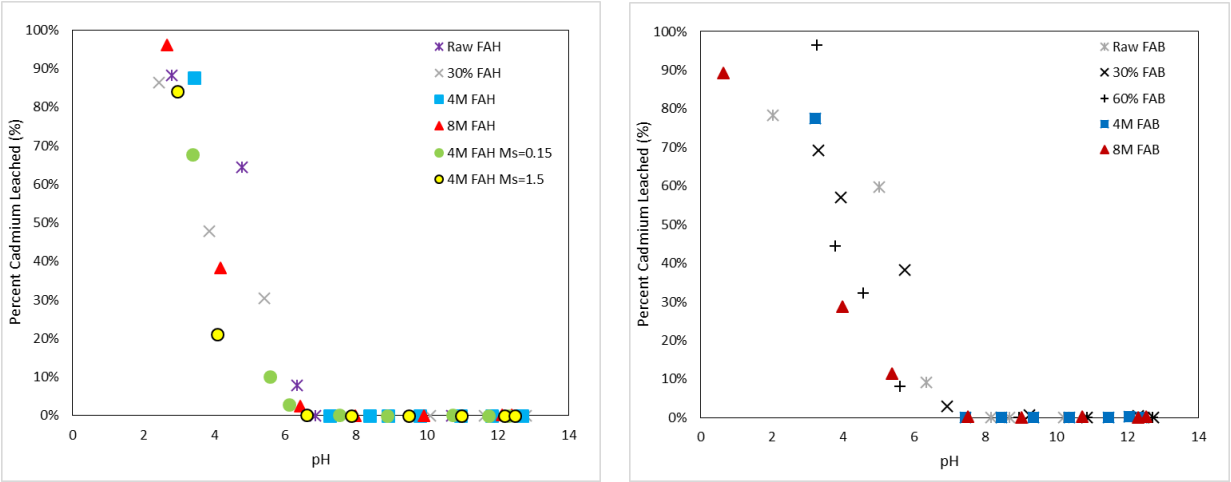

Figure 4.18: Cadmium Leaching in FAH (left) and FAB (right) Systems vs pH

While most cations showed no leaching at high pH, in Section 4.4.1 the aluminum phases were predicted to be dissolving at high pH. Therefore, it is expected that either adsorption or formation of metal hydroxides are reducing cation leaching, and not only binding within the amorphous N-A-S-H or C-A-S-H phases. Both adsorption and hydroxide formation of cations have both been found in the literature (Frost & Griffin, 2008). Cations generally adsorb strongly at high pH due to the negative charge associated with solid surfaces.

Figure 4.19 shows a solubility diagram for a number of different metal hydroxides (Dyer and Scrivner 1998). Many of the cations of interest (e.g. Cd, Co, Ni, Zn) have a pH of lowest solubility that is high (pH 9-11) which could account for some of the low leaching observed at high pH. A metal hydroxide/carbonate diagram was made based upon element concentrations in a 4M FAH geopolymer system and results are shown for cadmium in Figure 4.20. Figure 4.19 and Figure 4.20 are consistent as cadmium hydroxide is shown to precipitate in the pH range 10-13. Cadmium carbonate and cadmium sulfate tend to dominate the dissolved forms in pH range 8-10, while hydroxides dominate above pH 10.

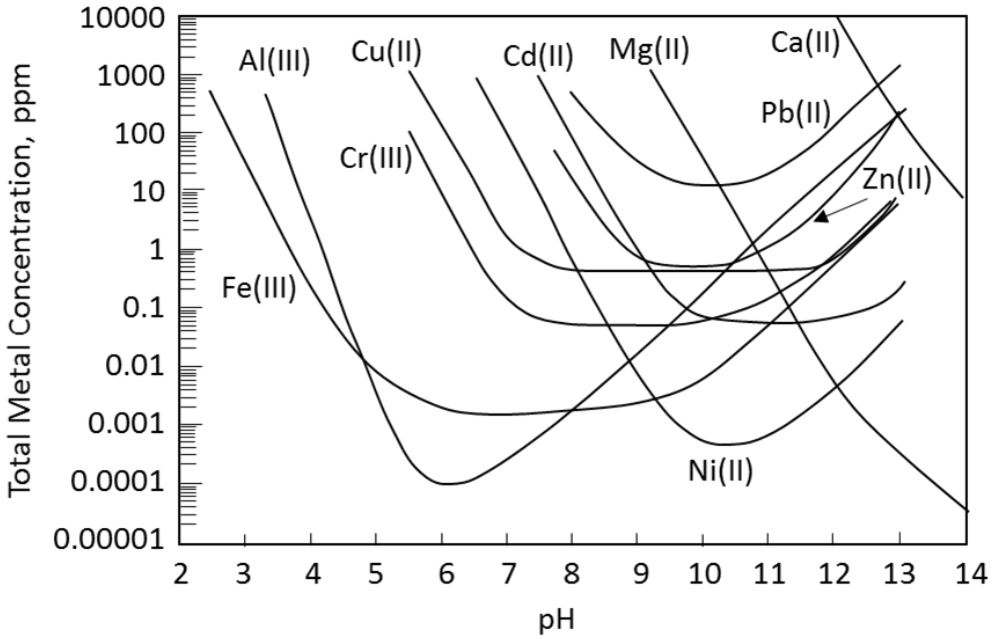

Figure 4.19: Solubility Diagram for Metal Hydroxides (Reproduced from Dyer and Scrivner, 1998)

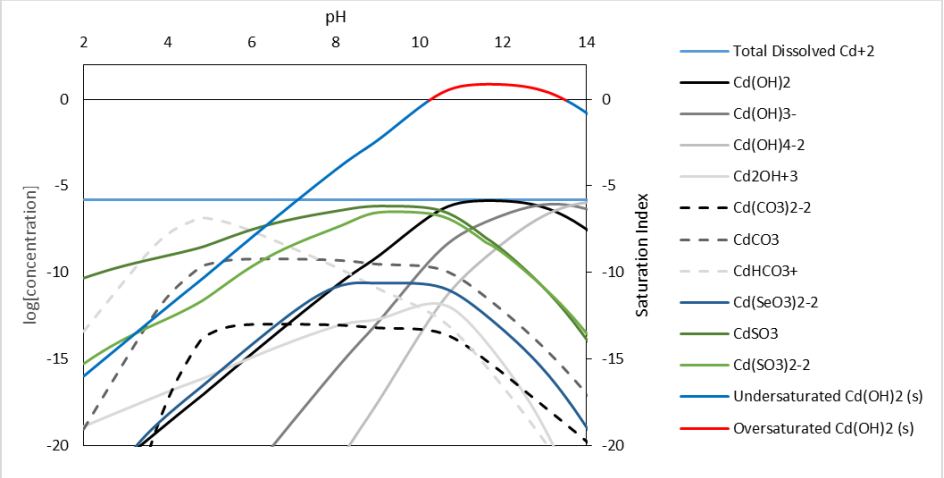

Figure 4.20: Cadmium Hydroxide and Carbonate Aqueous Concentrations for a 4M FAH system from Visual MINTEQ

4.4.4 Leaching in Simulated Landfill Leachate

Leaching tests were also run versus pH in a simulated landfill leachate to determine if leaching in real landfill scenarios might differ from that in reagent water. For

all graphs enclosed shapes represent leaching in reagent water and open shapes represent leaching in simulated landfill leachate.

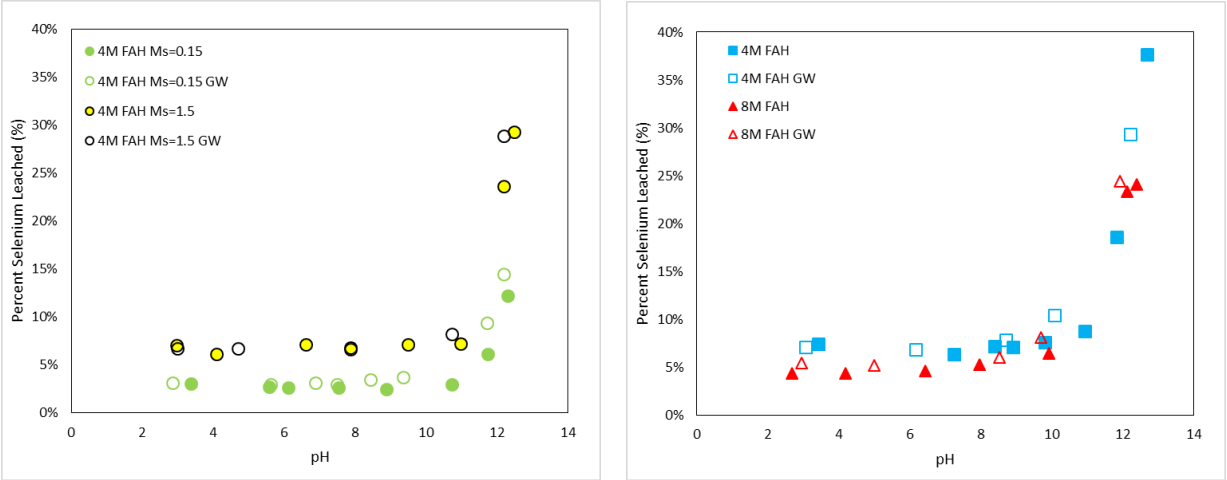

Figure 4.21: Selenium Leaching in Reagent Water and Simulated Landfill Leachate for FAH Specimens with M_s>0 (left) and M_s=0 (right) vs pH

Among oxyanions, only selenium showed a difference between reagent water and simulated landfill leachate. Selenium appeared to leach slightly more in the simulated landfill leachate than reagent water at high pH. The trend shown in Figure 4.21 is more obvious in geopolymers that contained a higher silica modulus (Figure 4.21 left) than those where the silica modulus was zero (Figure 4.21 right).

Among cations, copper showed increased leaching in simulated landfill leachate in all tests and across a wide pH range. Studies have shown that copper binds with NOM, and it is expected that the copper in the fly ash was complexing with NOM keeping it dissolved in solution (Wang et al., 2015, Holm 1990). Effects were similar across all tested geopolymers as shown in Figure 4.22.

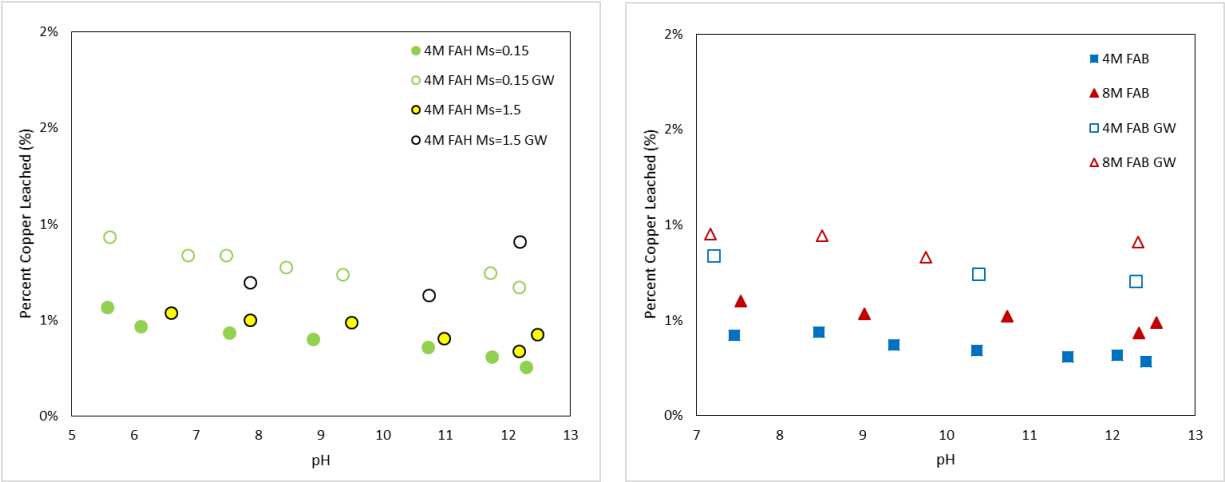

Figure 4.22: Copper Leaching in Reagent Water and Simulated Landfill Leachate for FAH (right) and FAB (left) Specimens vs pH

As there were many components in the simulated landfill leachate, it was difficult to determine effects of a single component on the leaching of various elements. However, the simulated landfill leachate did not drastically change leaching results as compared to reagent water. The difference in selenium leaching was minimal, and total copper leaching at mid-range pH was low at less than 2%. Copper and selenium were the only two elements that notably changed their leaching characteristics in the simulated landfill leachate.

Chapter 5: Conclusions

5.1 Conclusions

Of the CCPs characterized, the two trona impacted ashes (FAH and FAB) had more desirable traits for geopolymerization due to their finer particle size, lower carbon content, and larger surface area. Thus, the fly ashes were used to make a majority of the geopolymer and cement specimens tested in this research. The two ashes also contained the highest contaminant content, though they did not leach in their original/raw state to an extent where they would be considered a hazardous waste according to the TCLP. Concentrations above TCLP limits were obtained during some testing conditions used in the EPA 1313 method, but these conditions were always more stringent than required by the TCLP.

Of the geopolymers, geopolymers made with 4M NaOH appeared to have reacted more and were stronger than geopolymers made with 8M NaOH, but only slightly and neither performed significantly better than the other at binding contaminants. The high S/B ratio and low degree of reaction was likely the greatest contributor to the low strengths achieved by geopolymers. Increasing the silica modulus improved strength and decreased porosity of geopolymers, but also did not greatly impact leaching for the case where M_s=1.5.

Three main mechanisms were identified by which metals could be bound in fly ash cement pastes or geopolymers: they can be physically trapped within or chemically bonded to a geopolymer or cementitious matrix, adsorbed onto the surface of a solid phase, or precipitated out as a metal hydroxide or other salt. The mechanisms tend to overlap and reduced leaching of contaminants in most cases could be due to multiple mechanisms. For example, results indicated that, at high pH, cations were either adsorbed

onto a solid surface or precipitated out as a metal hydroxide, though leaching at low pH could also be due to the dissolution of aluminum-based phases.

For oxyanions, arsenic was bound better in fly ash cement systems at high pH, likely due to the formation of insoluble calcium-arsenic compounds. Chromium was bound well by all systems at high pH, possibly due to the formation of chromium hydroxide and due to adsorption at high pH. Reduced selenium leaching was obtained across a wide pH range, though raw FAB leached less at high pH than raw FAH did.

The only geopolymer that significantly outperformed the others was 4M FAH M_s=0.15 and these results need to be confirmed because the results were surprising. Therefore, few conclusions can be made regarding an optimal geopolymer matrix for binding metal contaminants. However overall, geopolymer systems bound metals better than the raw ash, which is a promising result.

5.2 Future Work

Several aspects of this research were not fully resolved and require additional testing. It is unclear why the 4M FAH geopolymer with a silica modulus of 0.15 bound oxyanions better than other tested geopolymers and it should be re-made and re-tested to confirm that it is truly a better binder. Geopolymers could also be remade with lower S/B ratios which would likely increase strength and potentially decrease porosity. Second, additional testing should be carried out with regards to the simulated landfill leachate. Due to the large number of components within the simulated landfill leachate it was difficult to isolate any one reason for differences in leaching of contaminants. It would be beneficial to carry out testing with individual components of the landfill leachate such as testing in reagent water with added NOM, and testing in waters of different ionic

strengths. More specific testing would help determine the mechanisms behind increased leaching of selenium and copper.

Anions including carbonate, chloride, and sulfate should be analyzed from leaching tests to better understand what phases are present in the system. For instance a high carbonate concentration would increase the likelihood of forming insoluble calcium or metal carbonate compounds which could cause a decrease in leaching at high pH.

Appendix A – Trace Metal Leaching Test Results

A.1 FAH, ARSENIC

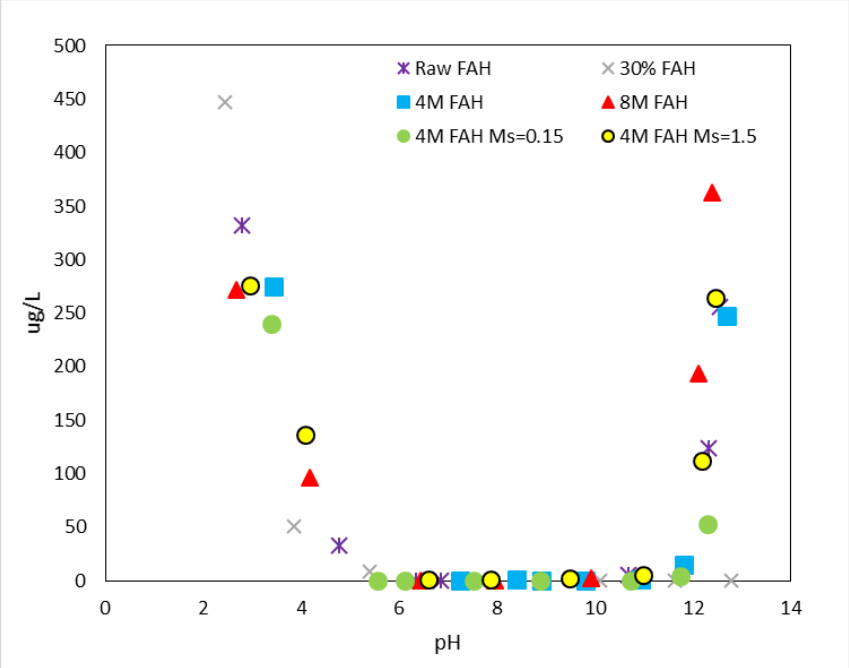

Figure A.1: Raw Arsenic Concentrations in Leachate from FAH specimens versus pH

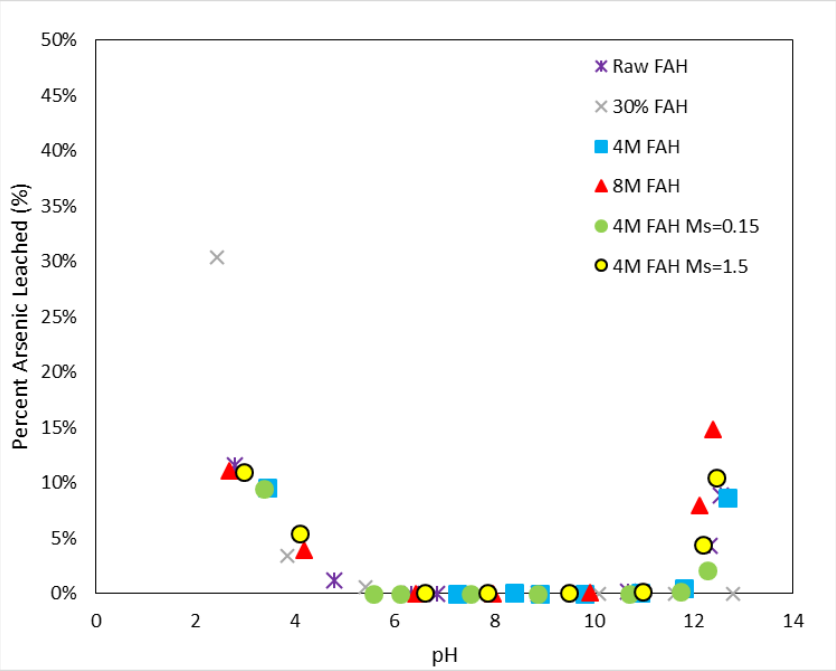

Figure A.2: Percent Arsenic Leached from FAH specimens versus pH

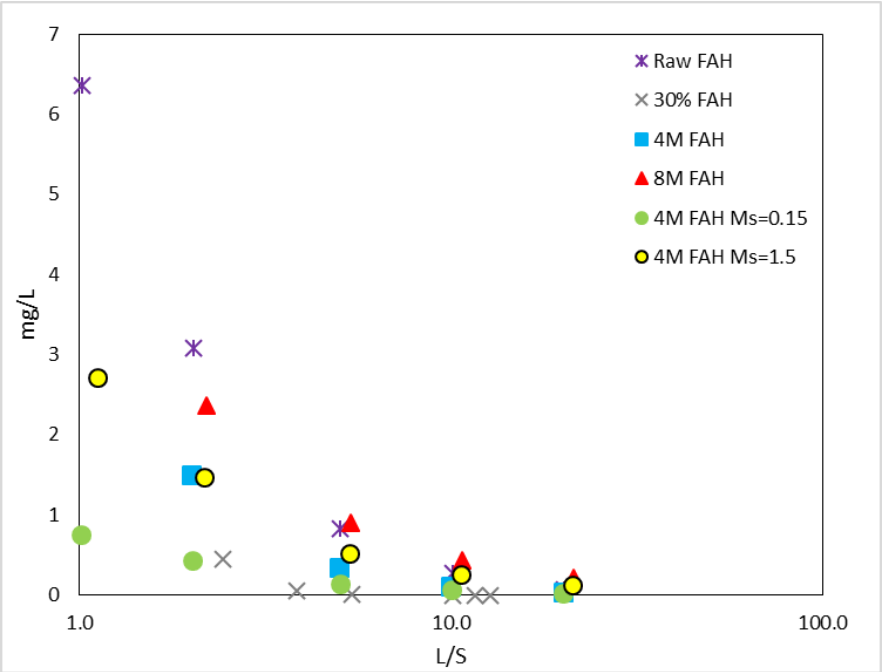

Figure A.3: Raw Arsenic Concentrations in Leachate from FAH Specimens versus L/S

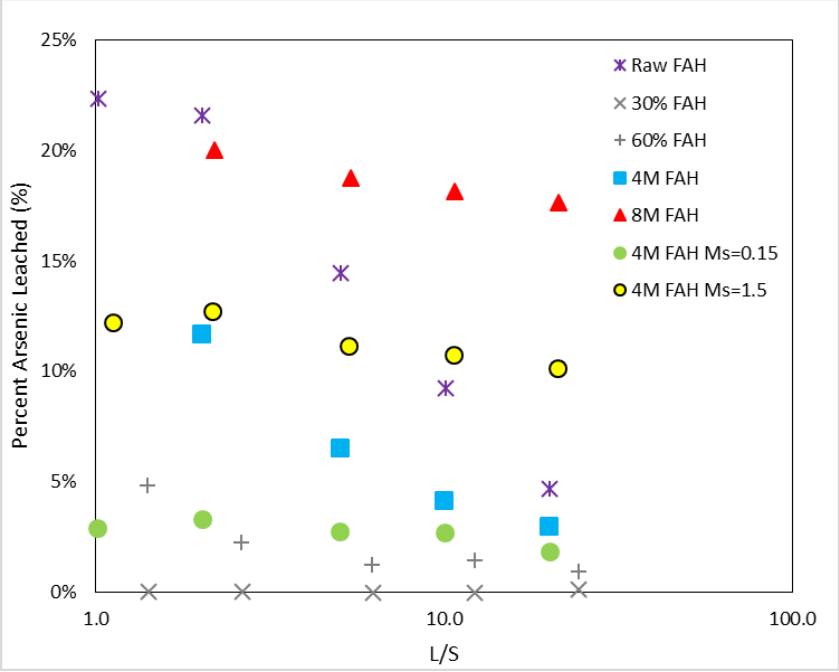

Figure A.4: Percent Arsenic Leached from FAH Specimens versus L/S

A.2 FAB, ARSENIC

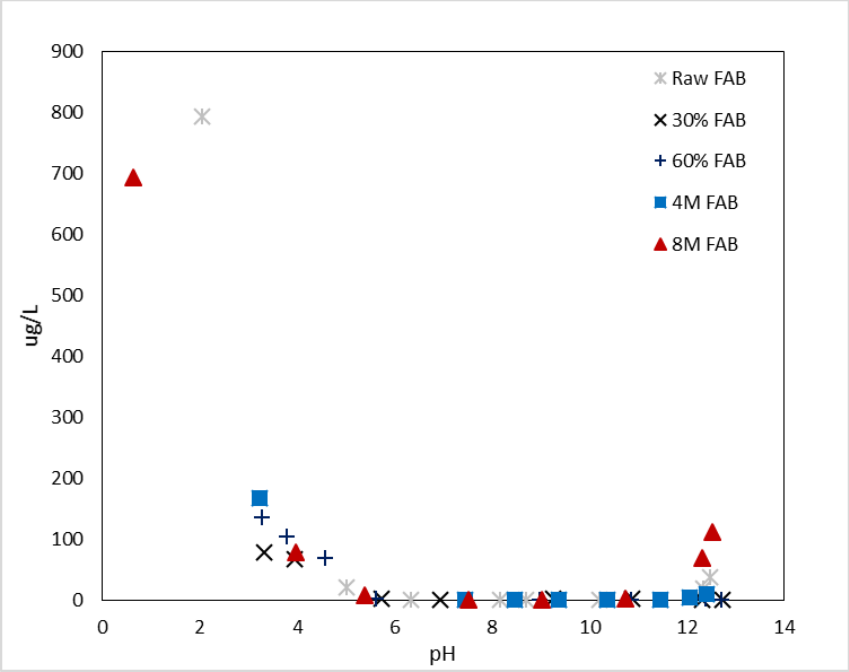

Figure A.4: Raw Arsenic Concentrations in Leachate from FAB Specimens versus pH

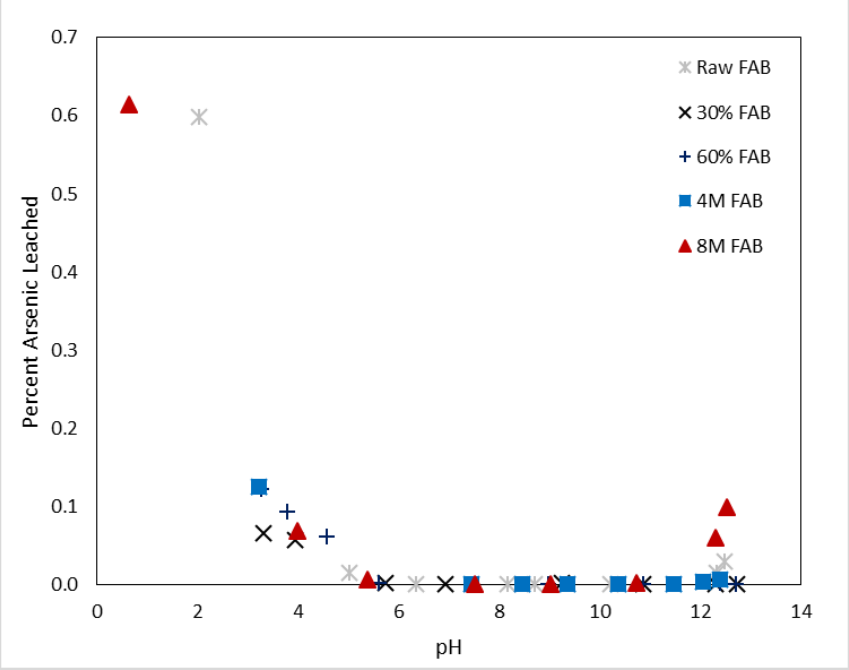

Figure A.5: Percent Arsenic Leached from FAB Specimens versus pH

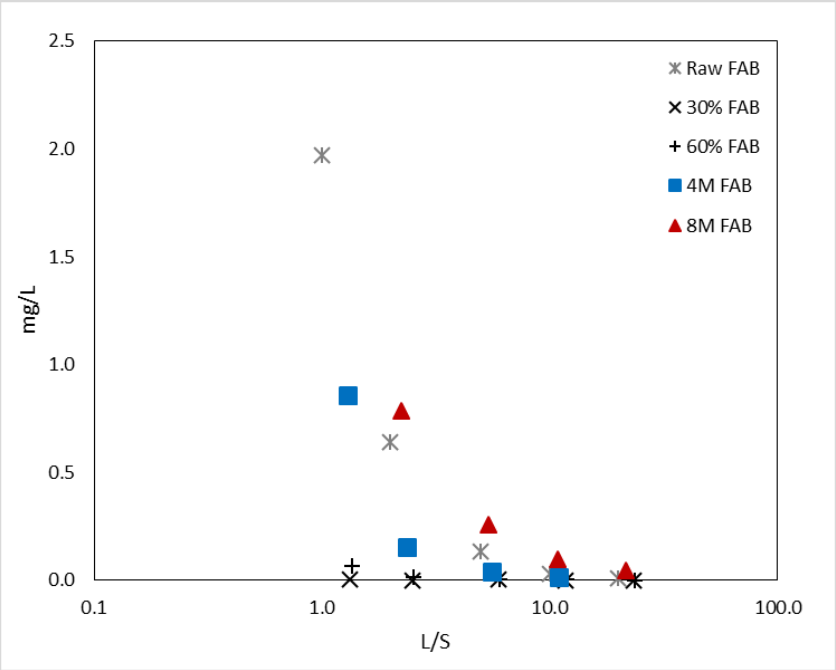

Figure A.6: Raw Arsenic Concentrations in Leachate from FAB Specimens versus L/S

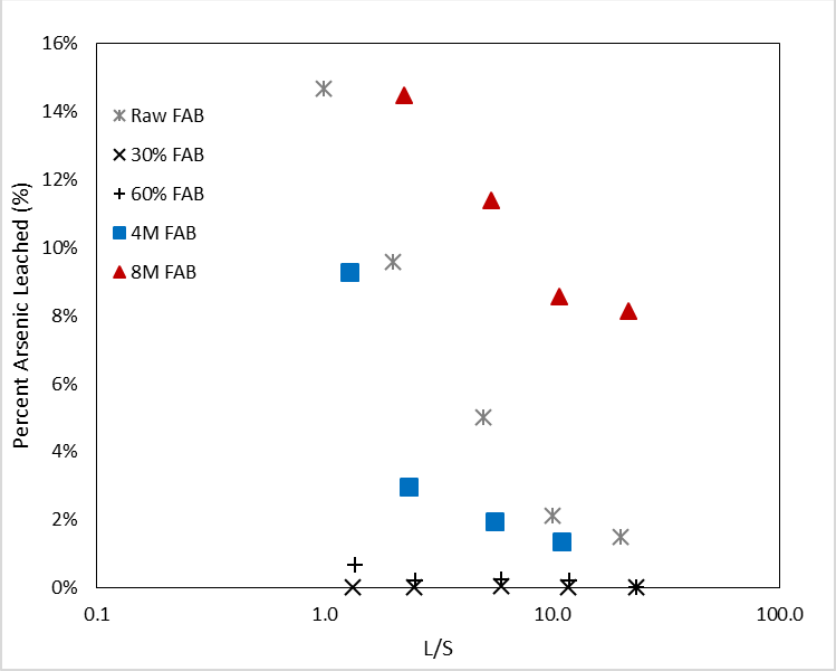

Figure A.7: Percent Arsenic Leached from FAB Specimens versus L/S

A.3 FAH, CADMIUM

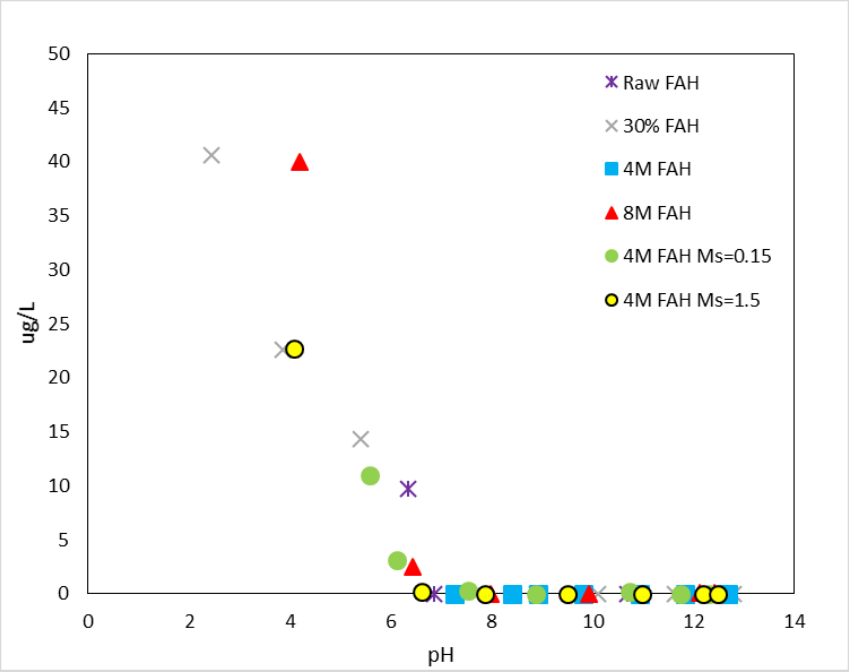

Figure A.8: Raw Cadmium Concentrations in Leachate from FAH Specimens versus pH

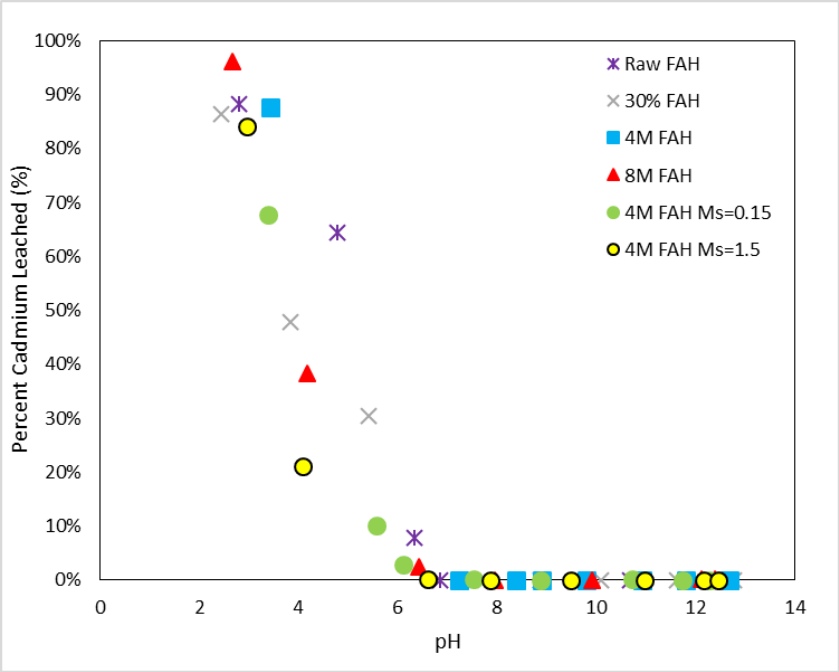

Figure A.9: Percent Cadmium Leached from FAH Specimens versus pH

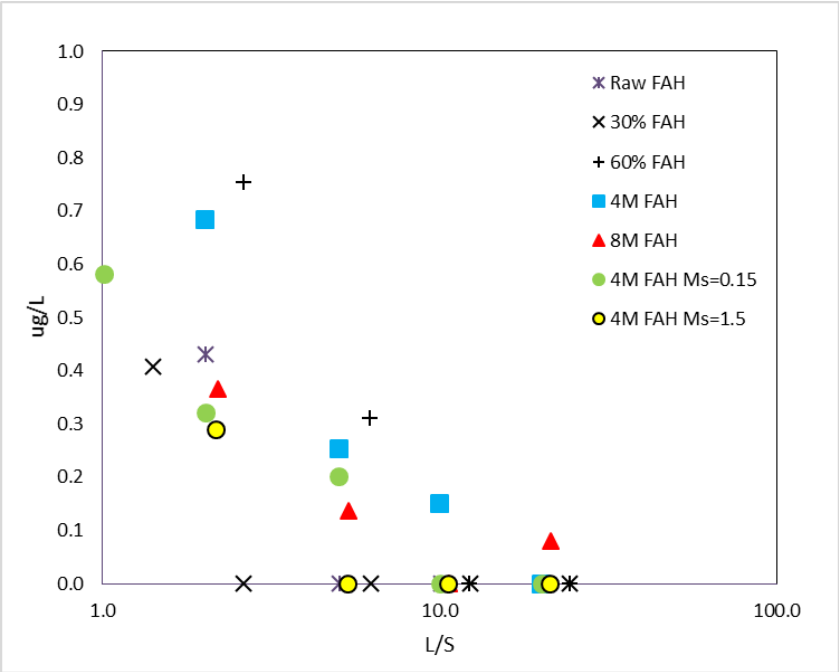

Figure A.10: Raw Cadmium Concentrations in Leachate from FAH Specimens versus L/S

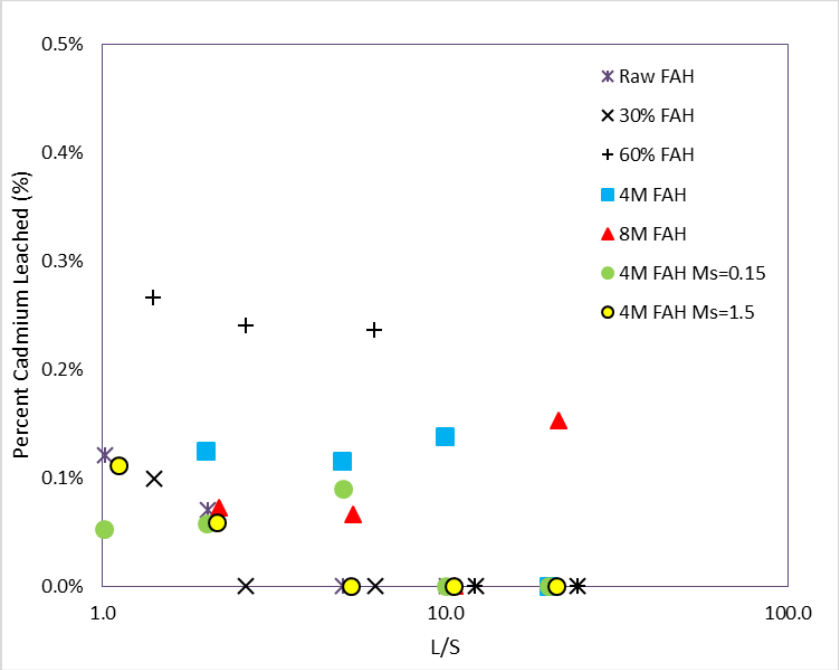

Figure A.11: Percent Cadmium Leached from FAH Specimens versus L/S

A.4 FAB, CADMIUM

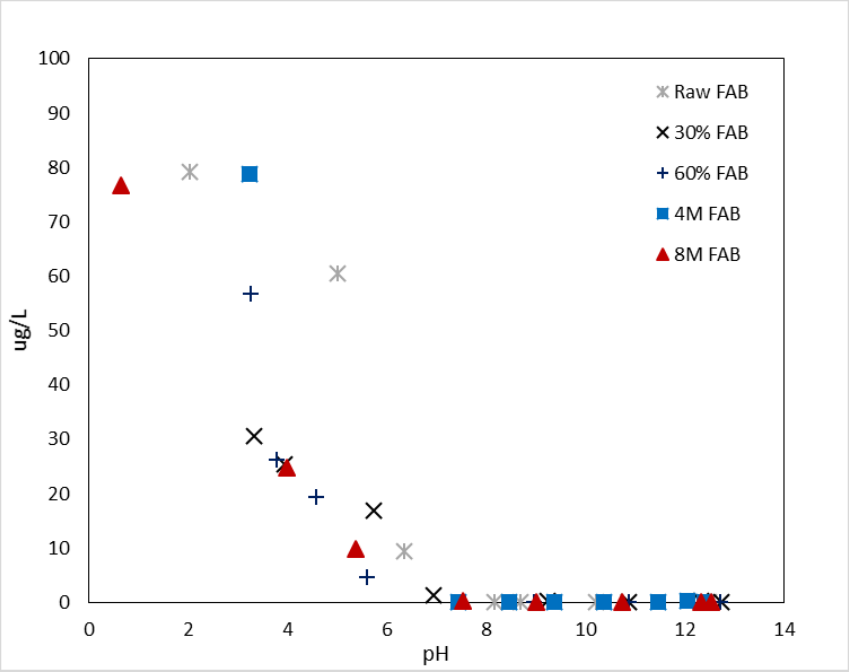

Figure A.12: Raw Cadmium Concentrations in Leachate from FAB Specimens versus pH

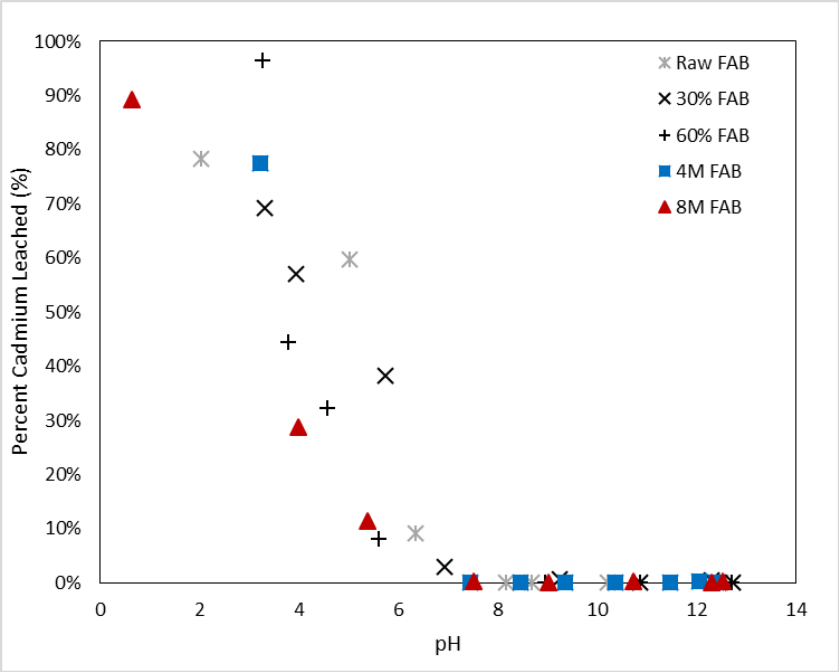

Figure A.13: Percent Cadmium Leached from FAB Specimens versus pH

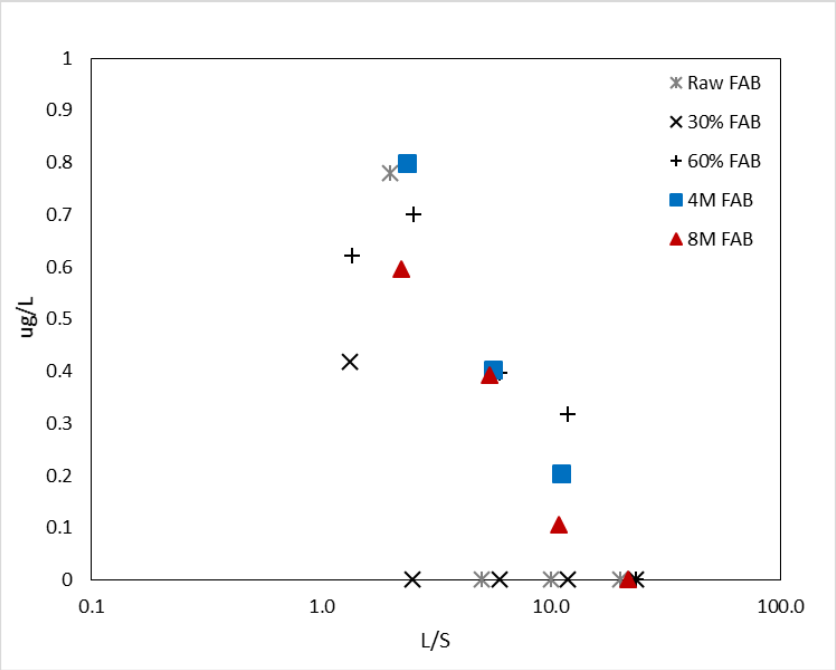

Figure A.14: Raw Cadmium Concentrations in Leachate from FAB Specimens versus L/S

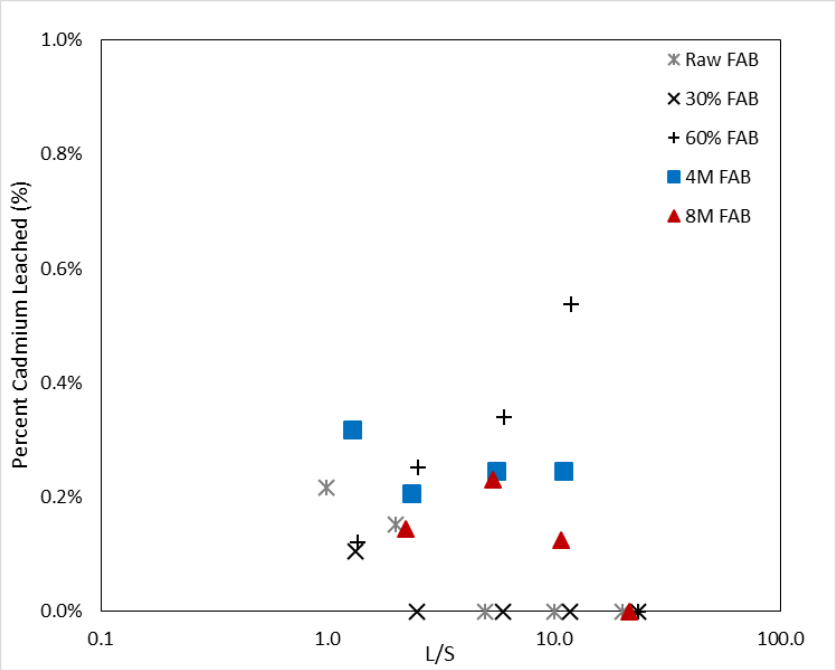

Figure A.15: Percent Cadmium Leached from FAB Specimens versus L/S

A.5 FAH, COBALT

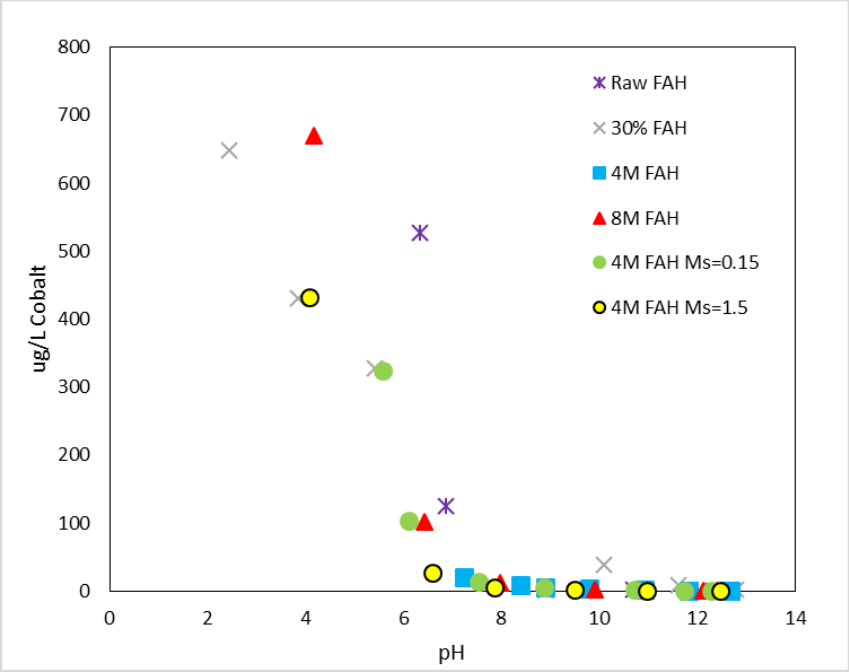

Figure A.16: Raw Cobalt Concentrations in Leachate from FAH Specimens versus pH

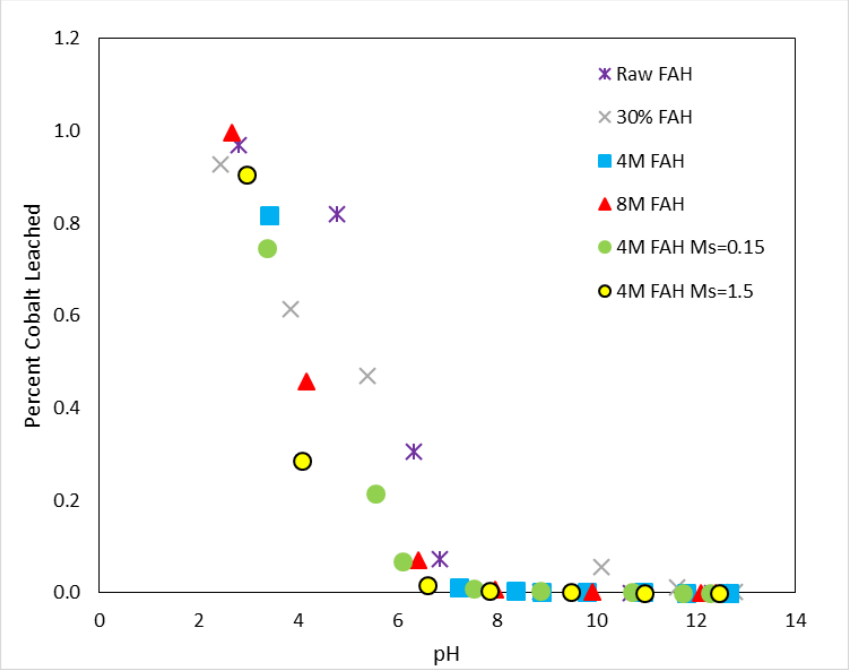

Figure A.17: Percent Cobalt Leached from FAH Specimens versus pH

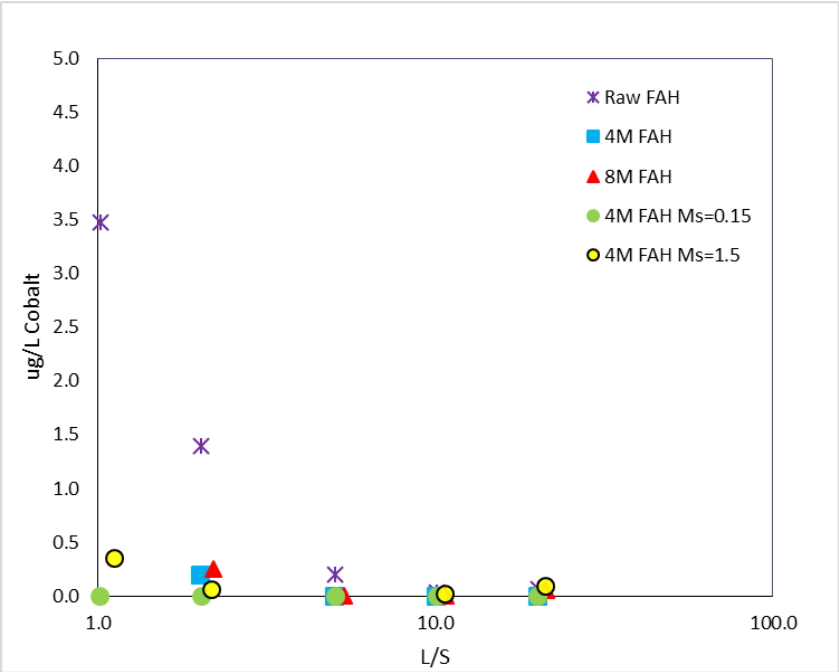

Figure A.18: Raw Cobalt Concentrations in Leachate from FAH Specimens versus L/S

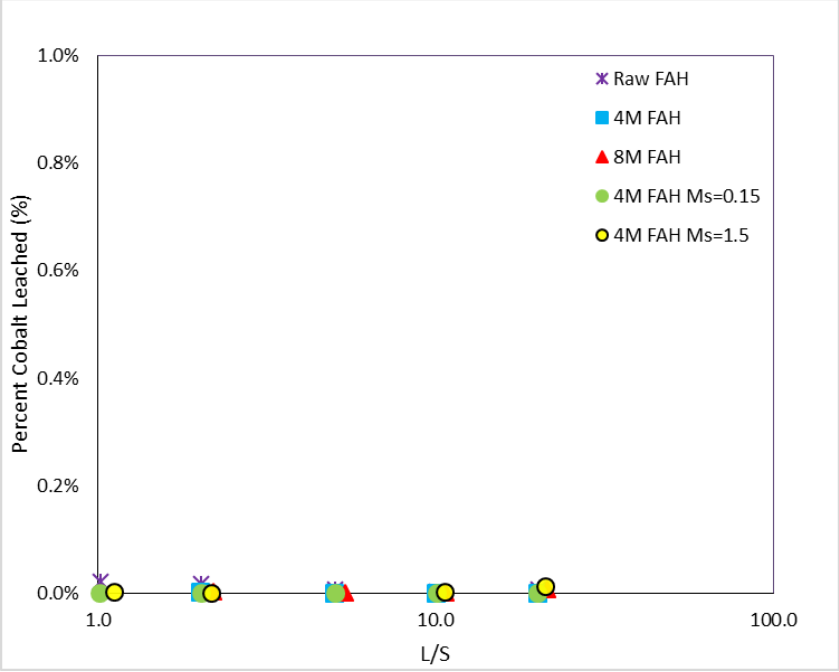

Figure A.19: Percent Cobalt Leached from FAH Specimens versus L/S

A.6 FAB, COBALT

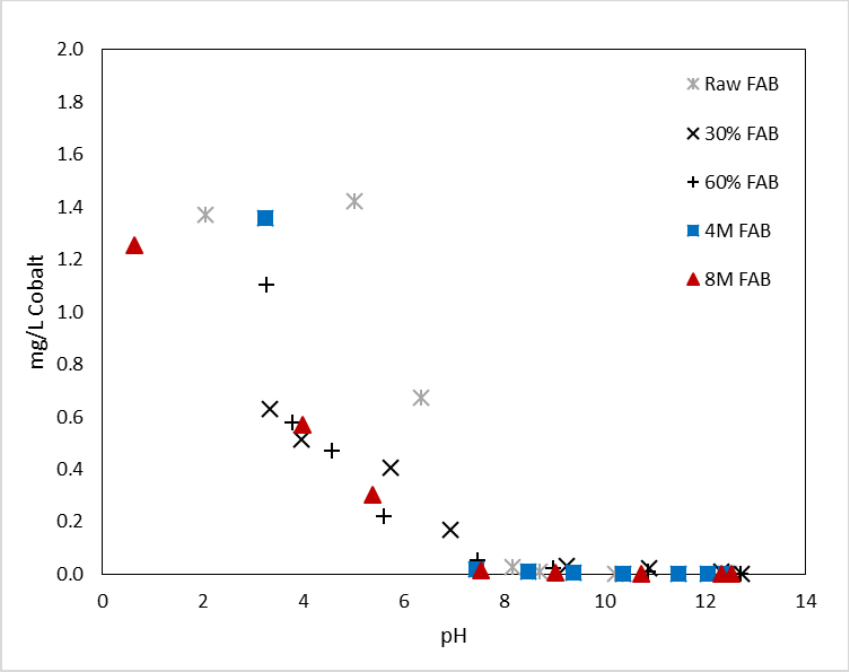

Figure A.20: Raw Cobalt Concentrations in Leachate from FAB Specimens versus pH

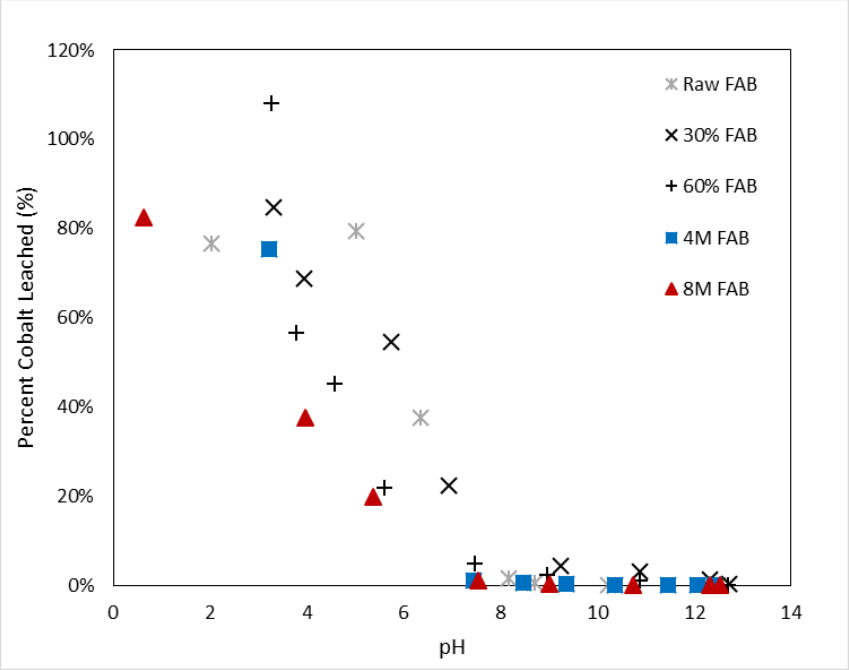

Figure A.21: Percent Cobalt Leached from FAB Specimens versus pH

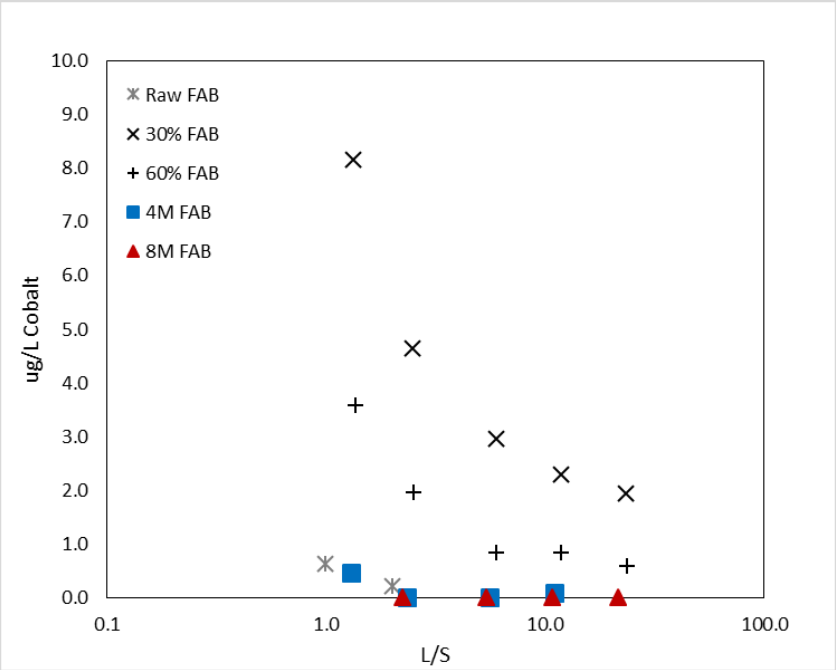

Figure A.22: Raw Cobalt Concentrations in Leachate from FAB Specimens versus L/S

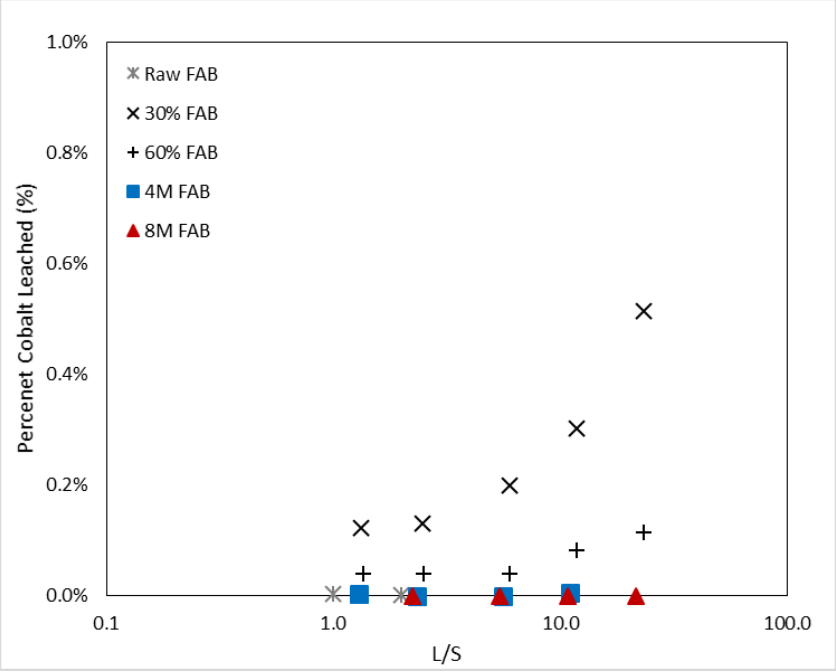

Figure A.23: Percent Cobalt Leached from FAB Specimens versus L/S

A.7 FAH, COPPER

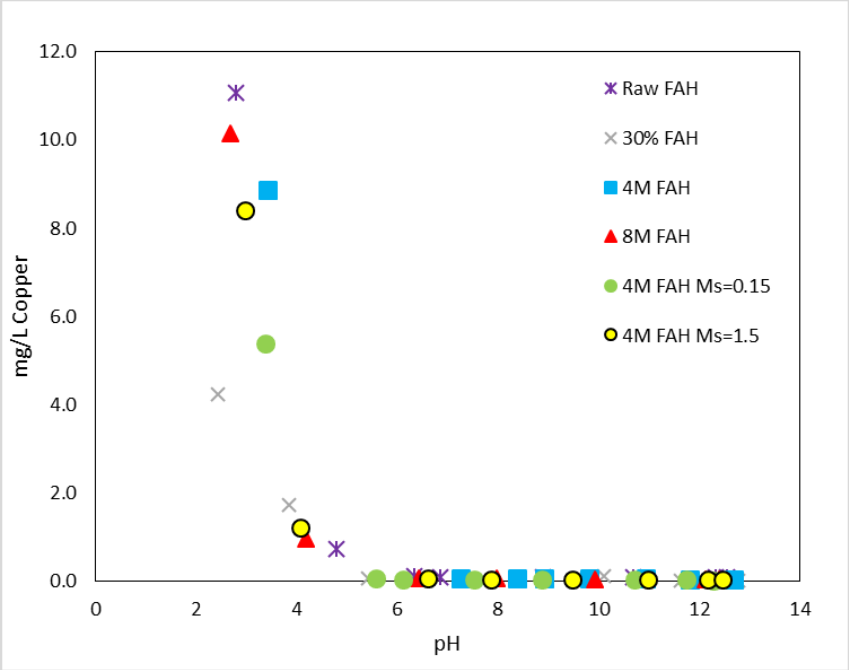

Figure A.24: Raw Copper Concentrations in Leachate from FAH Specimens versus pH

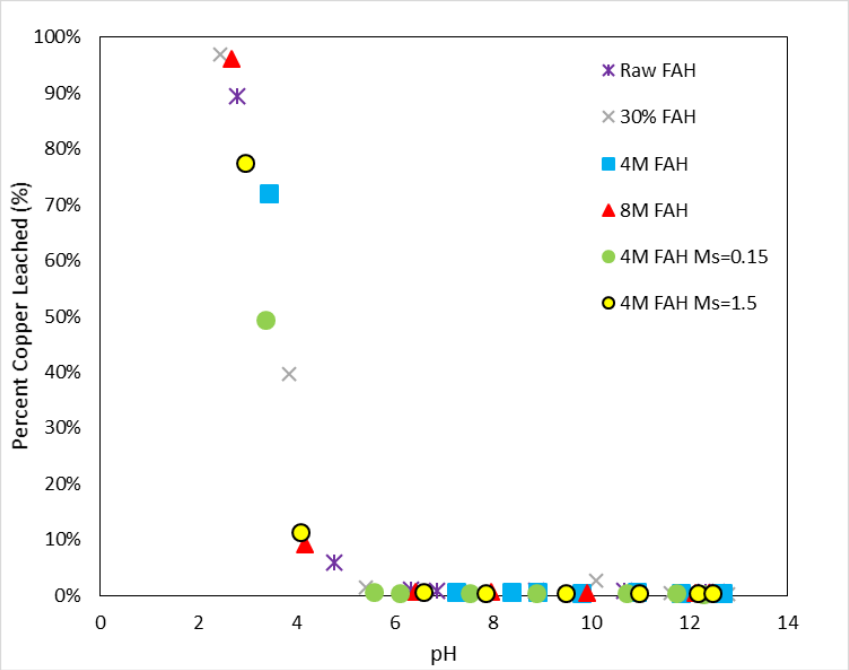

Figure A.25: Percent Copper Leached from FAH Specimens versus pH

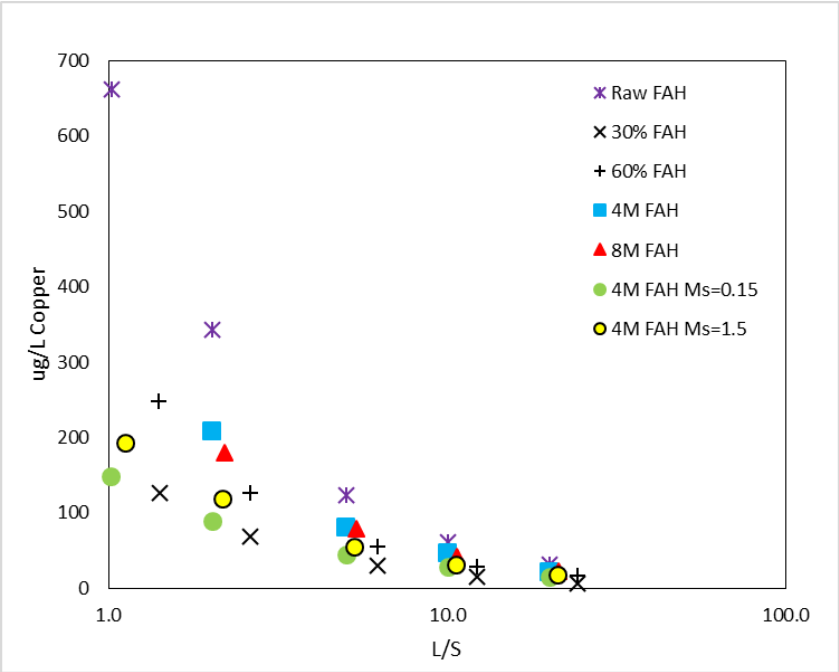

Figure A.26: Raw Copper Concentrations in Leachate from FAH Specimens versus L/S

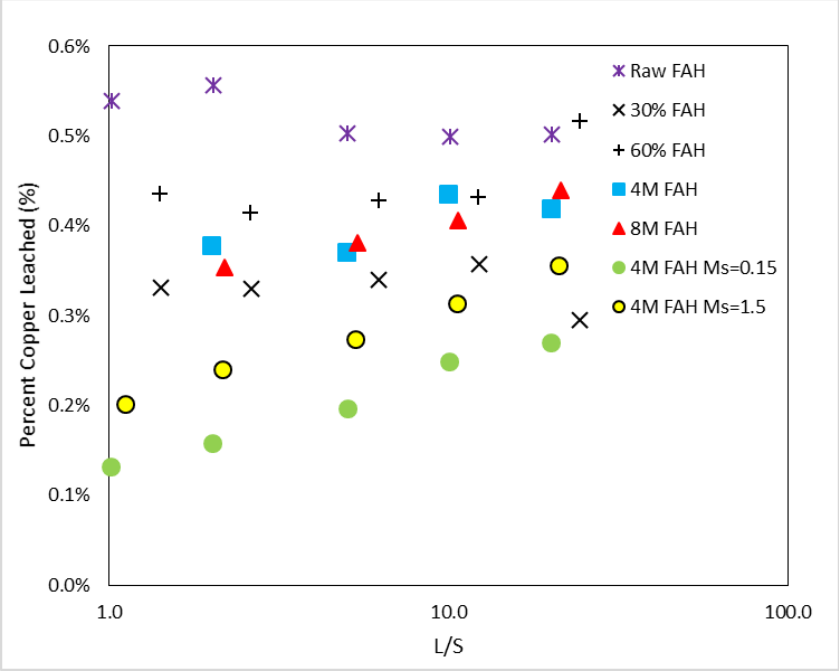

Figure A.27: Percent Copper Leached from FAH Specimens versus L/S

A.8 FAB, COPPER

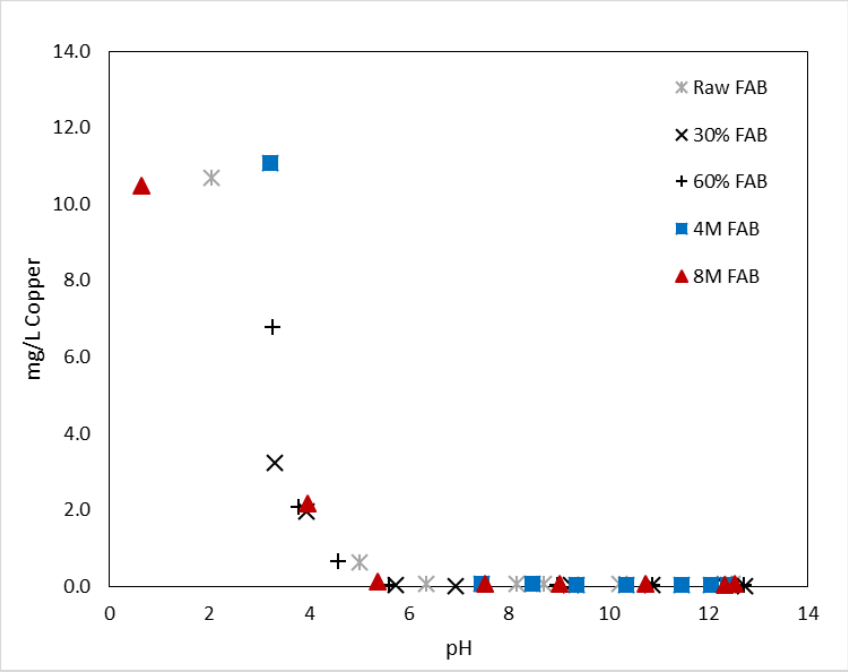

Figure A.28: Raw Copper Concentrations in Leachate from FAB Specimens versus pH

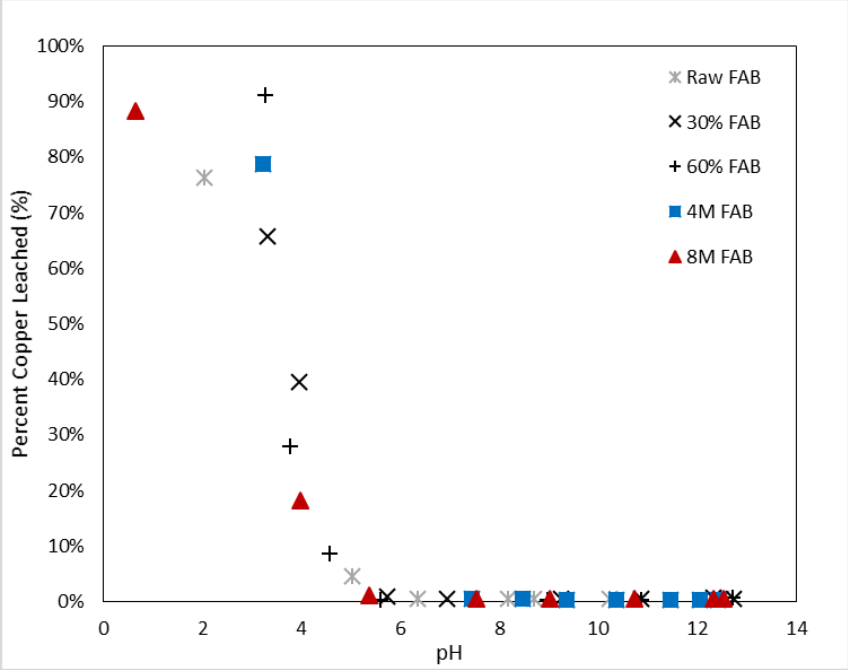

Figure A.29: Percent Copper Leached from FAB Specimens versus pH

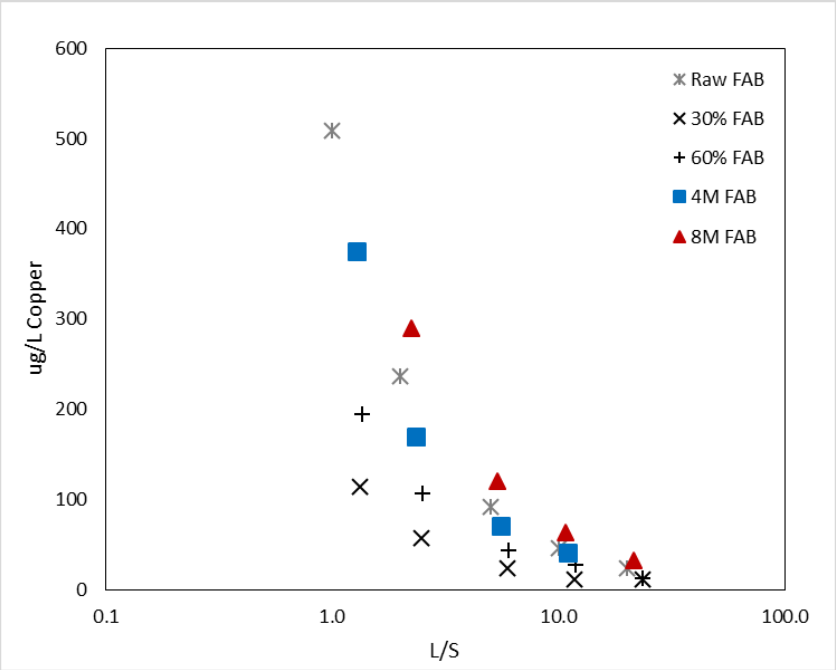

Figure A.30: Raw Copper Concentrations in Leachate from FAB Specimens versus L/S

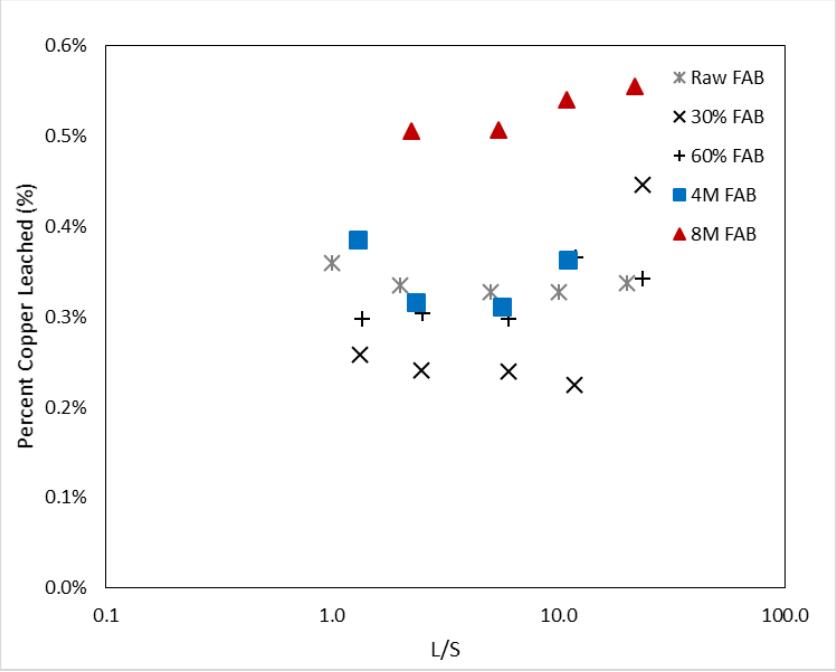

Figure A.31: Percent Copper Leached from FAB Specimens versus L/S

A.9 FAH, CHROMIUM

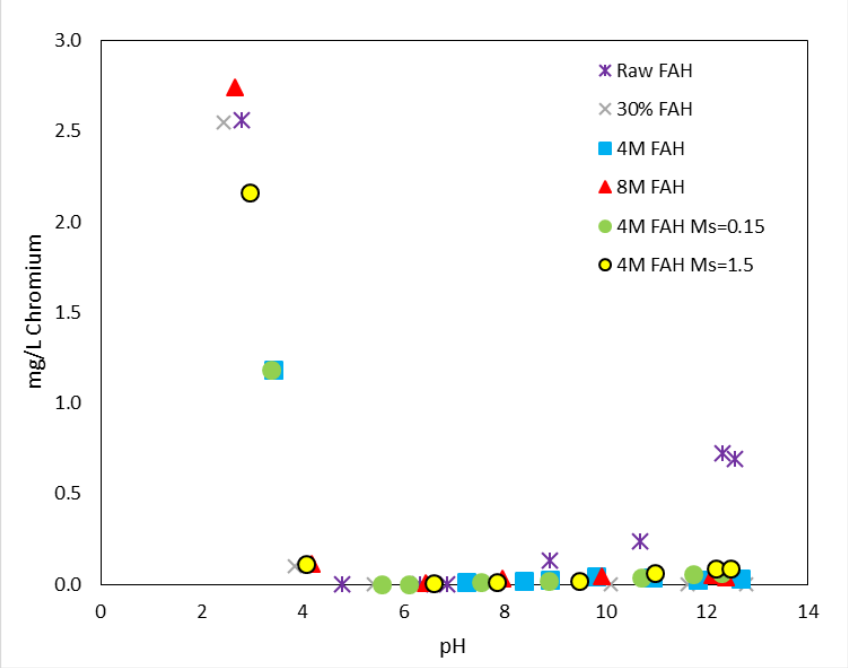

Figure A.32: Raw Chromium Concentrations in Leachate from FAH Specimens versus pH

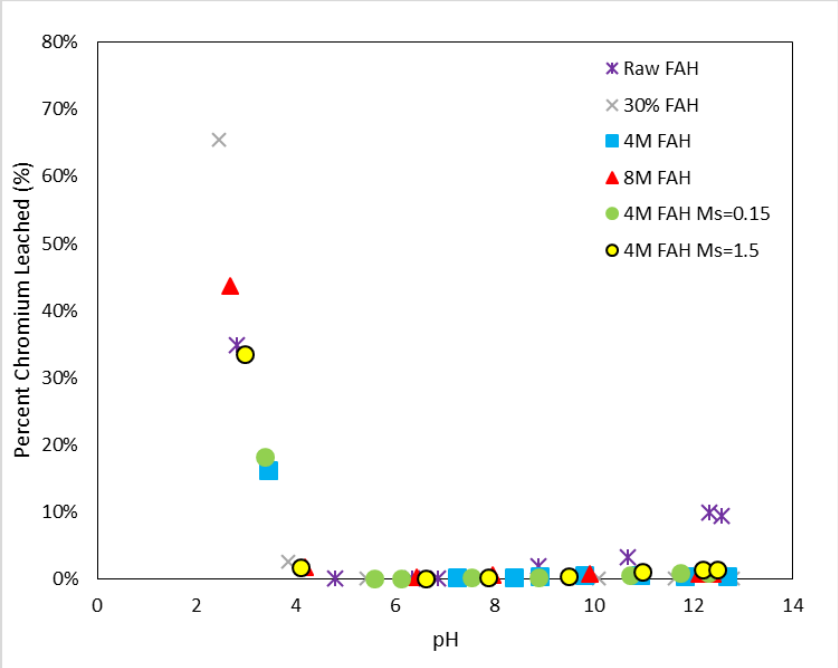

Figure A.33: Percent Chromium Leached from FAH Specimens versus pH

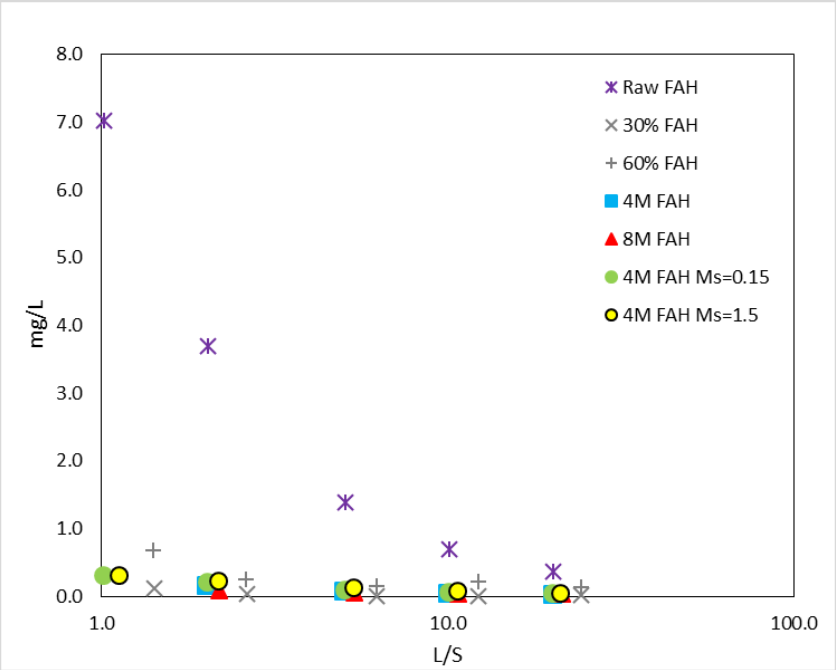

Figure A.34: Raw Chromium Concentrations in Leachate from FAH Specimens versus L/S

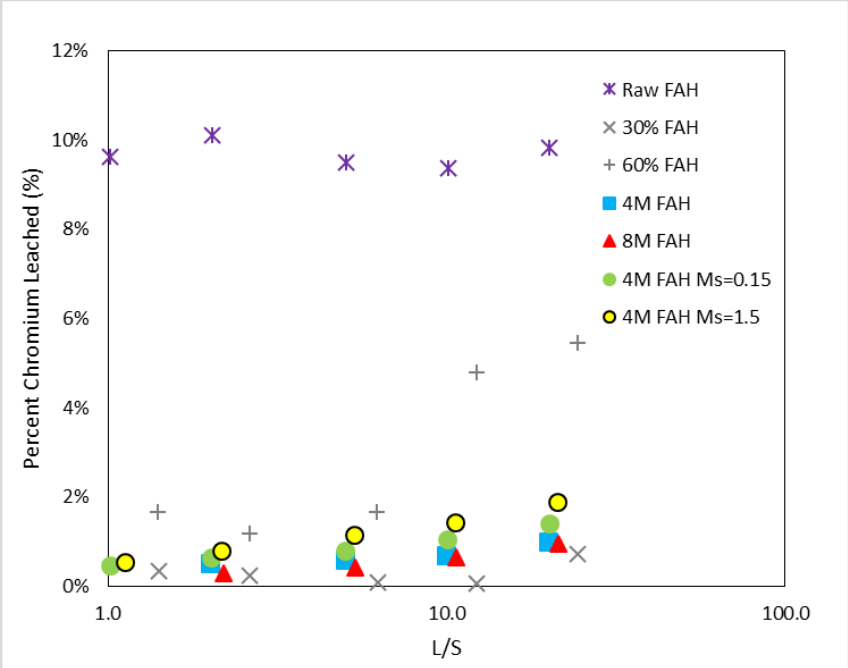

Figure A.35: Percent Chromium Leached from FAH Specimens versus L/S

A.10 FAB, CHROMIUM

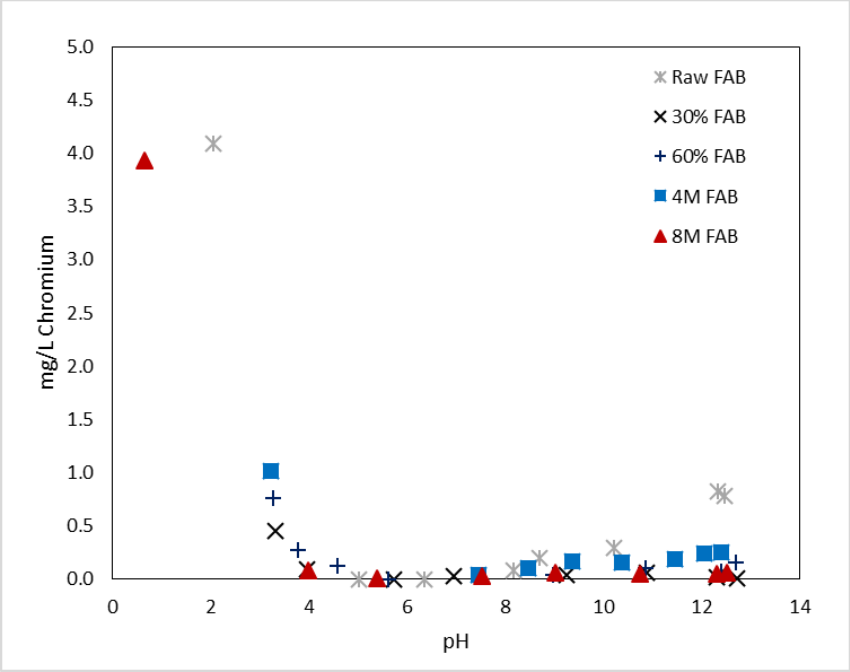

Figure A.36: Raw Chromium Concentrations in Leachate from FAB Specimens versus pH

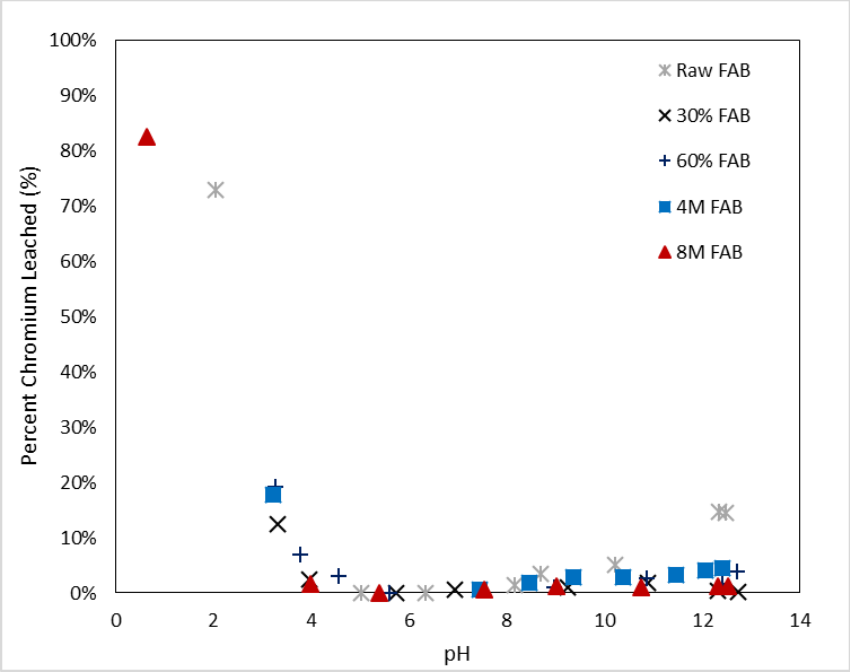

Figure A.37: Percent Chromium Leached from FAB Specimens versus pH

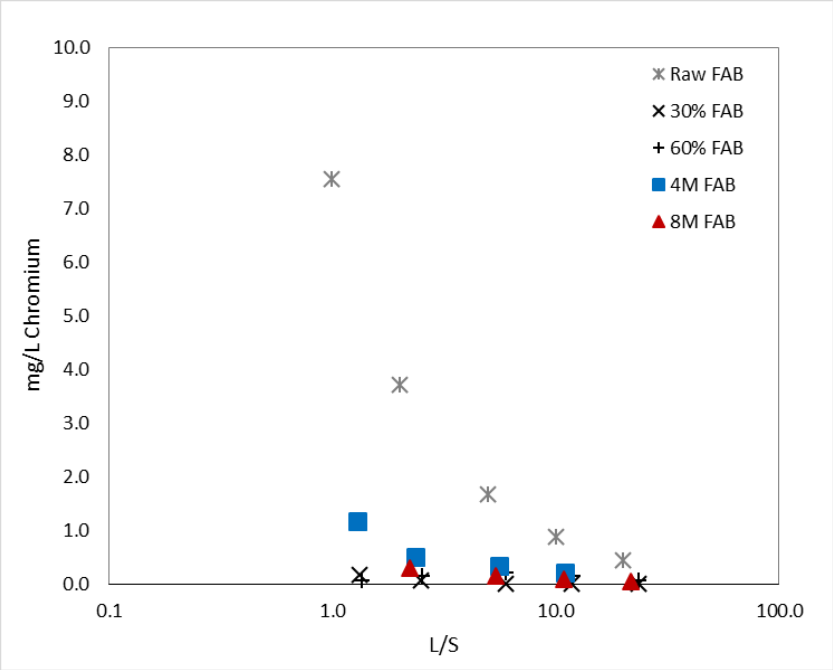

Figure A.38: Raw Chromium Concentrations in Leachate from FAB Specimens versus L/S

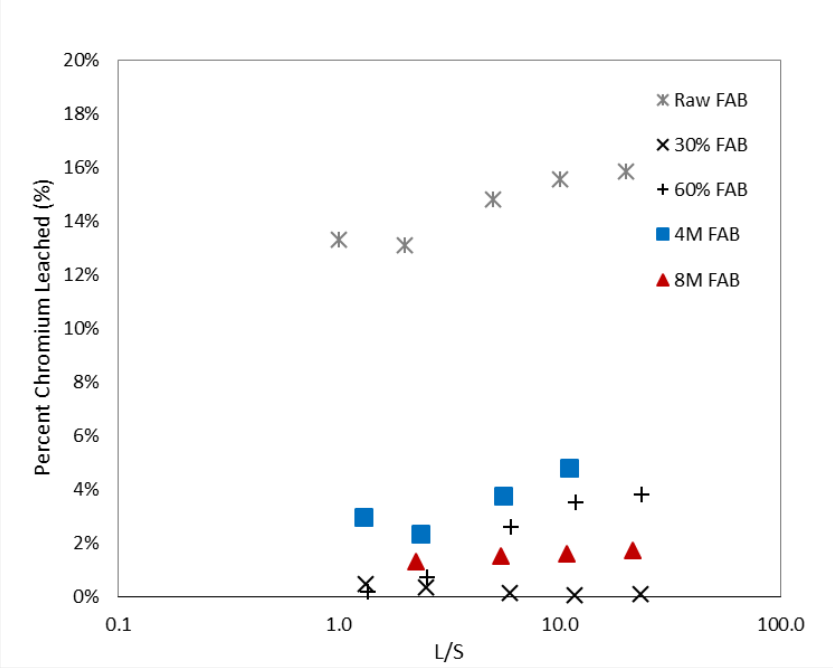

Figure A.39: Percent Chromium Leached from FAB Specimens versus L/S

A.11 FAH, NICKEL

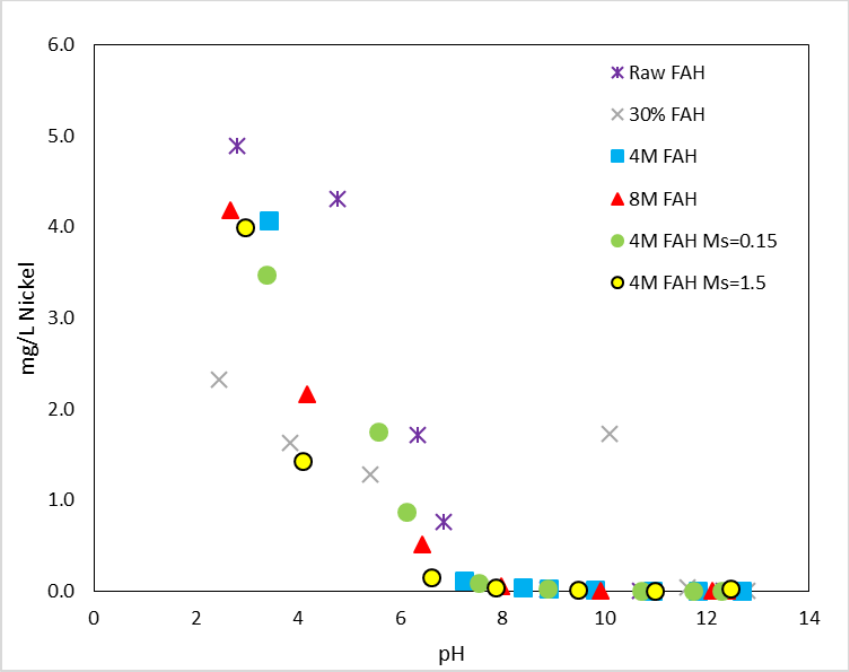

Figure A.40: Raw Nickel Concentrations in Leachate from FAH Specimens versus pH

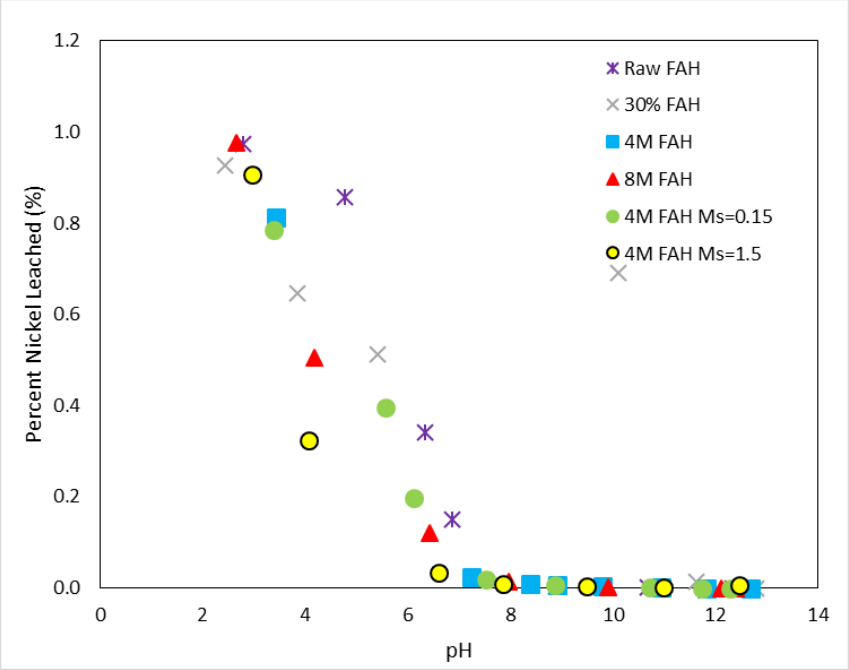

Figure A.41: Percent Nickel Leached from FAH Specimens versus pH

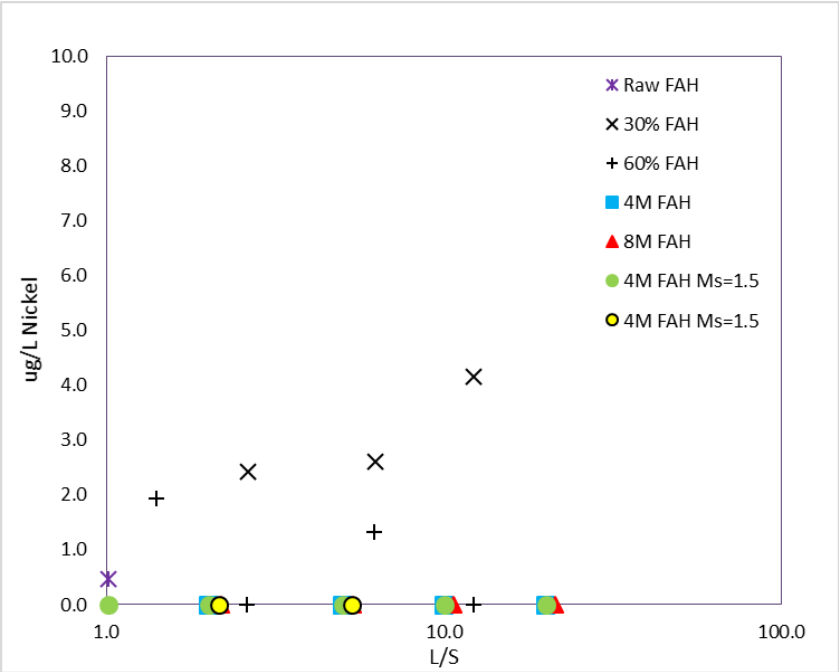

Figure A.42: Raw Nickel Concentrations in Leachate from FAH Specimens versus L/S

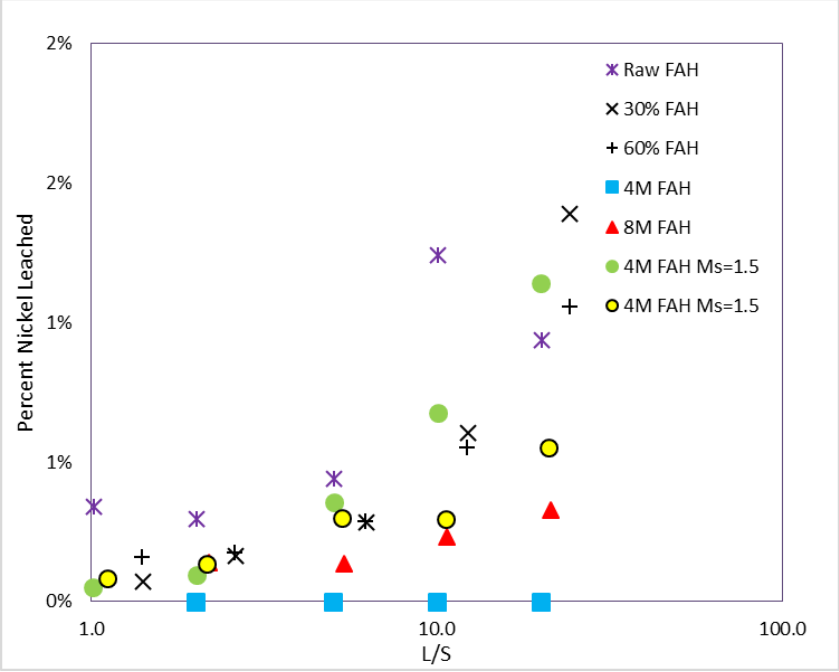

Figure A.43: Percent Nickel Leached from FAH Specimens versus L/S

A.12 FAB, NICKEL

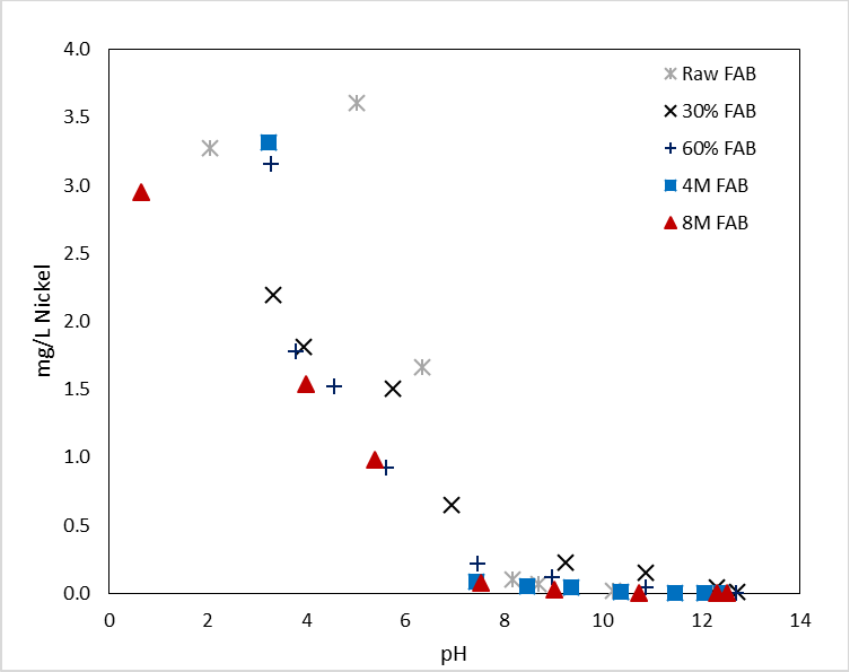

Figure A.44: Raw Nickel Concentrations in Leachate from FAB Specimens versus pH

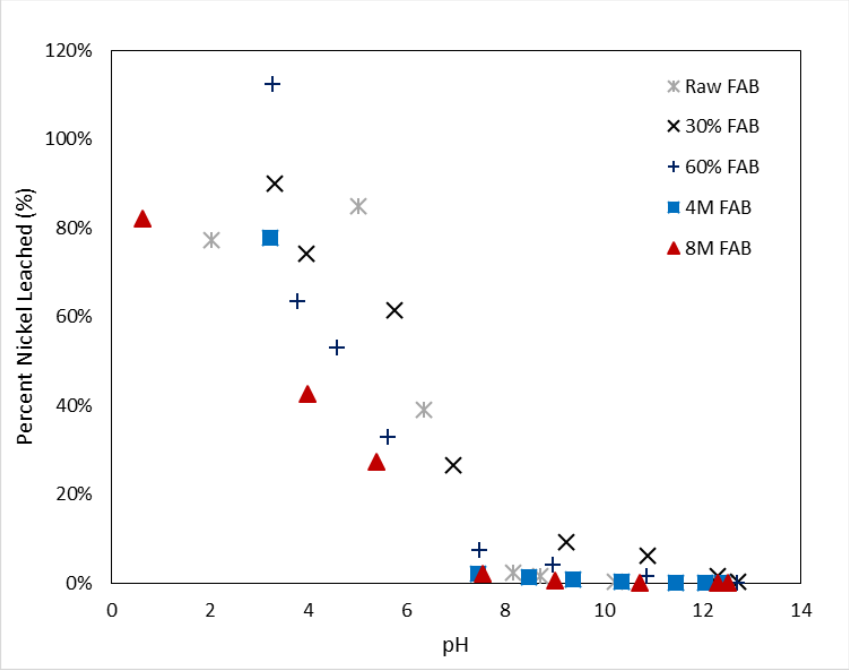

Figure A.45: Percent Nickel Leached from FAB Specimens versus pH

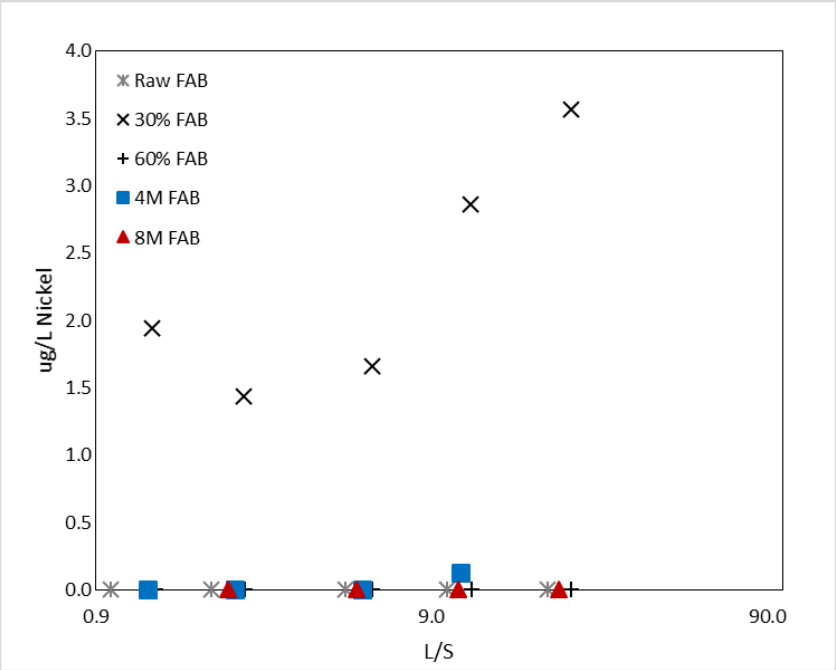

Figure A.46: Raw Nickel Concentrations in Leachate from FAB Specimens versus L/S

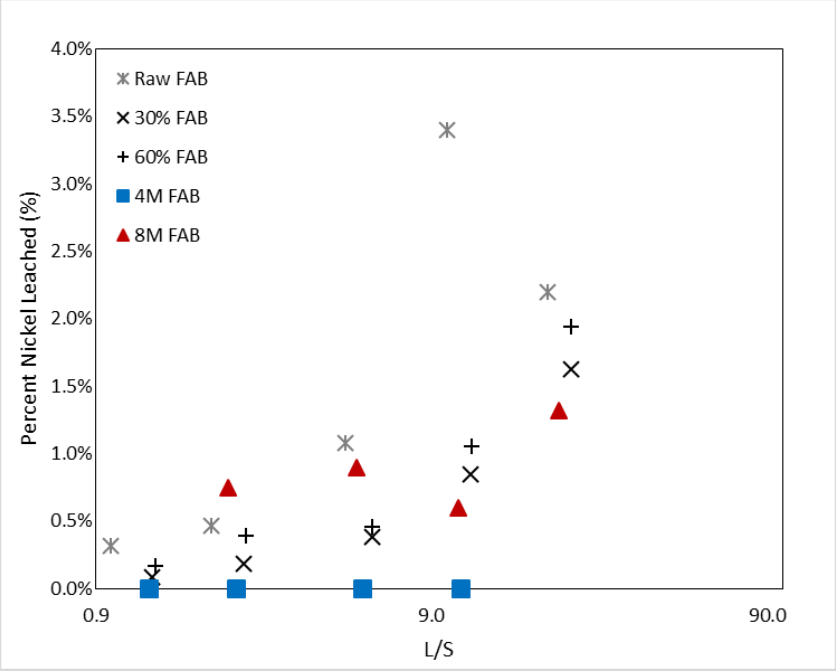

Figure A.47: Percent Nickel Leached from FAB Specimens versus L/S

A.13 FAH, LEAD

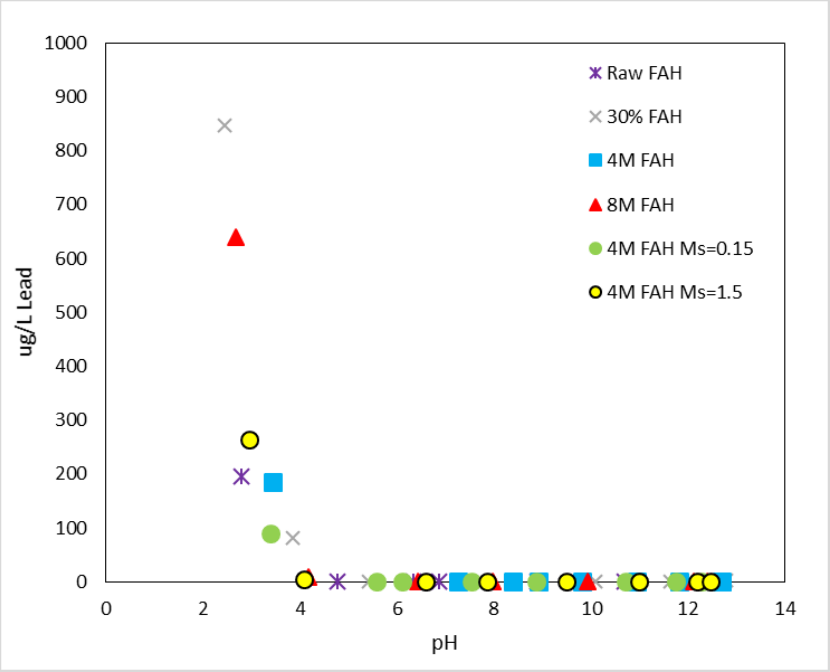

Figure A.48: Raw Lead Concentrations in Leachate from FAH Specimens versus pH

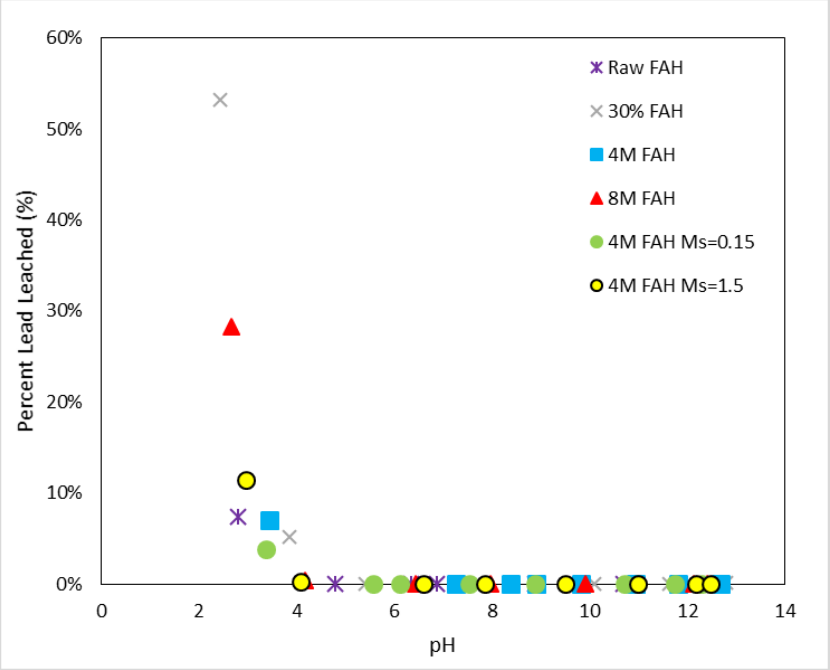

Figure A.49: Percent Lead Leached from FAH Specimens versus pH

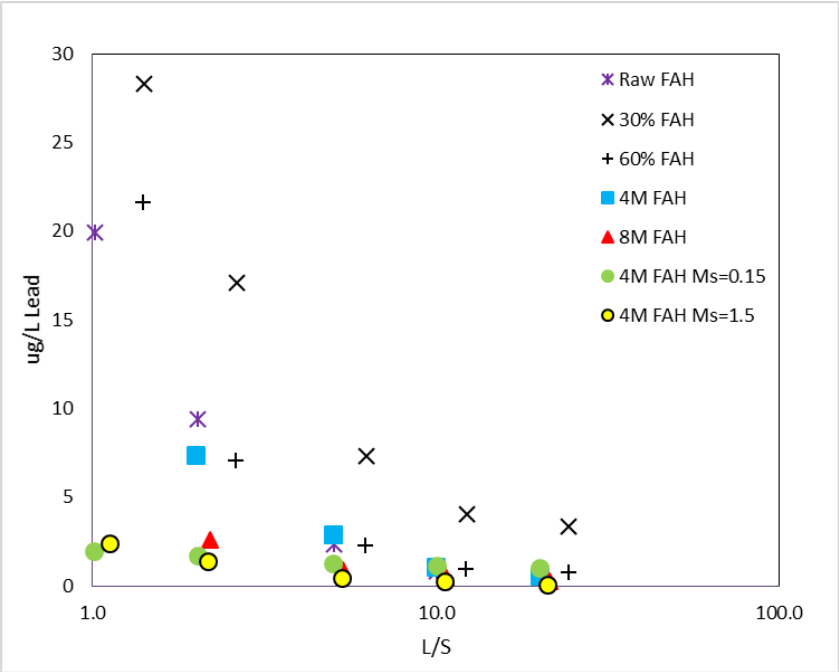

Figure A.50: Raw Lead Concentrations in Leachate from FAH Specimens versus L/S

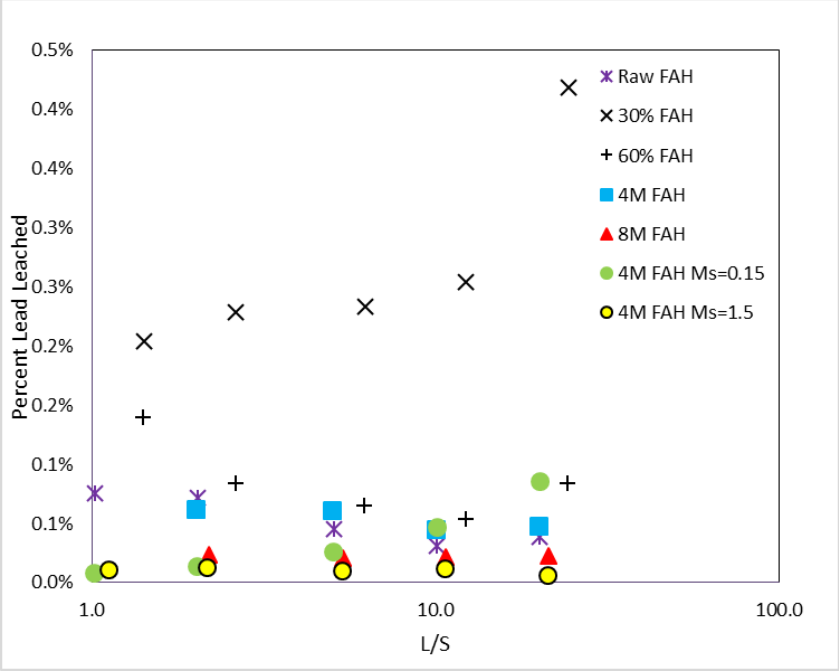

Figure A.51: Percent Lead Leached from FAH Specimens versus L/S

A.14 FAB, LEAD

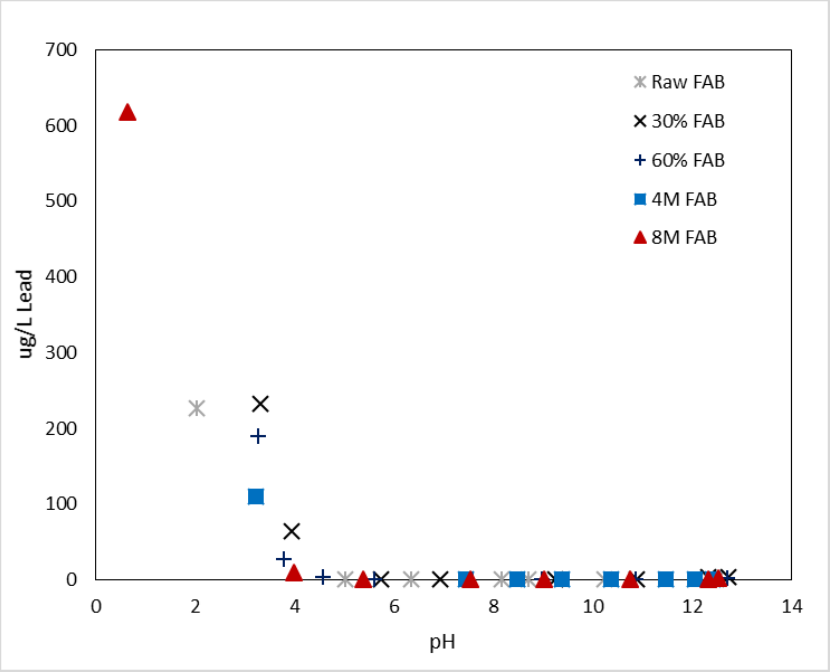

Figure A.52: Raw Lead Concentrations in Leachate from FAB Specimens versus pH

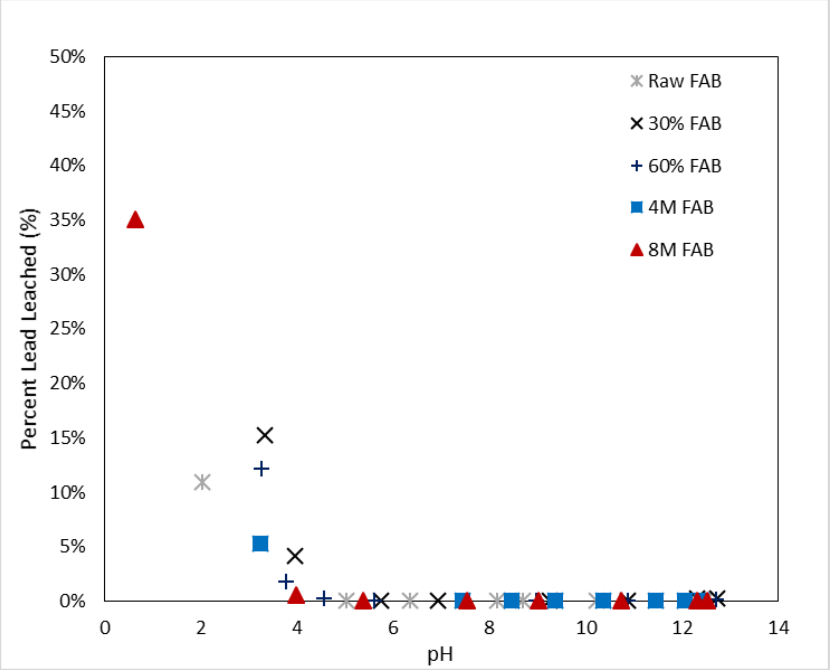

Figure A.53: Percent Lead Leached from FAB Specimens versus pH

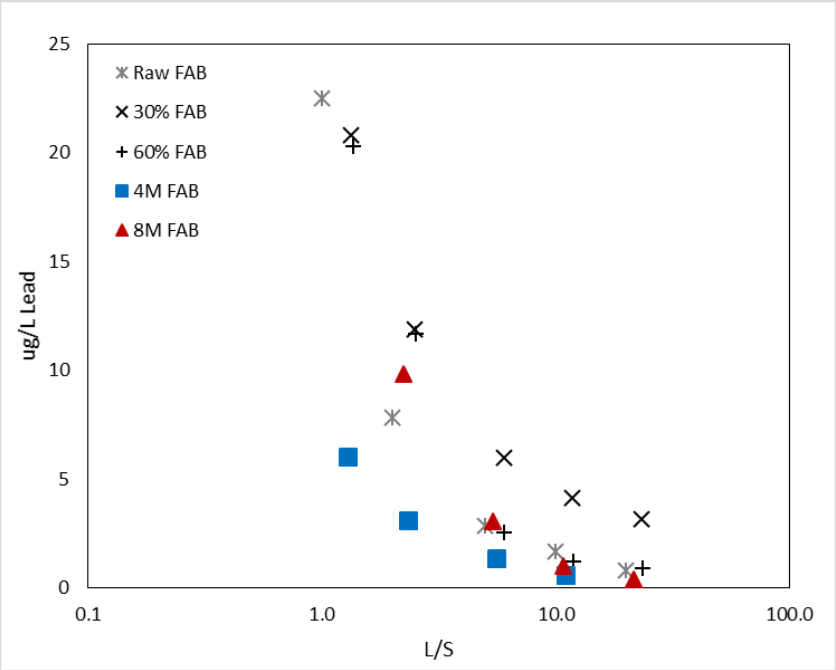

Figure A.54: Raw Lead Concentrations in Leachate from FAB Specimens versus L/S

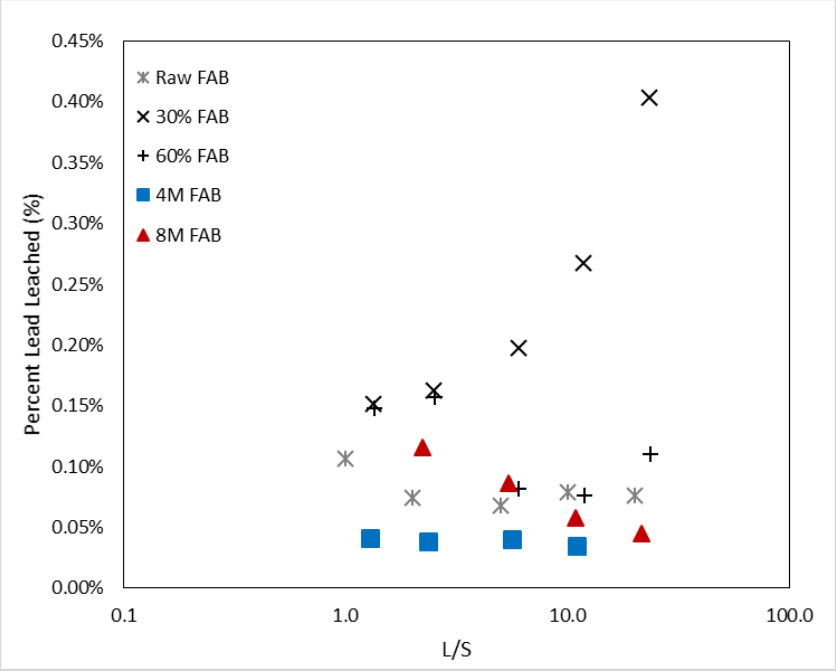

Figure A.55: Percent Lead Leached from FAB Specimens versus L/S

A.15 FAH, SELENIUM

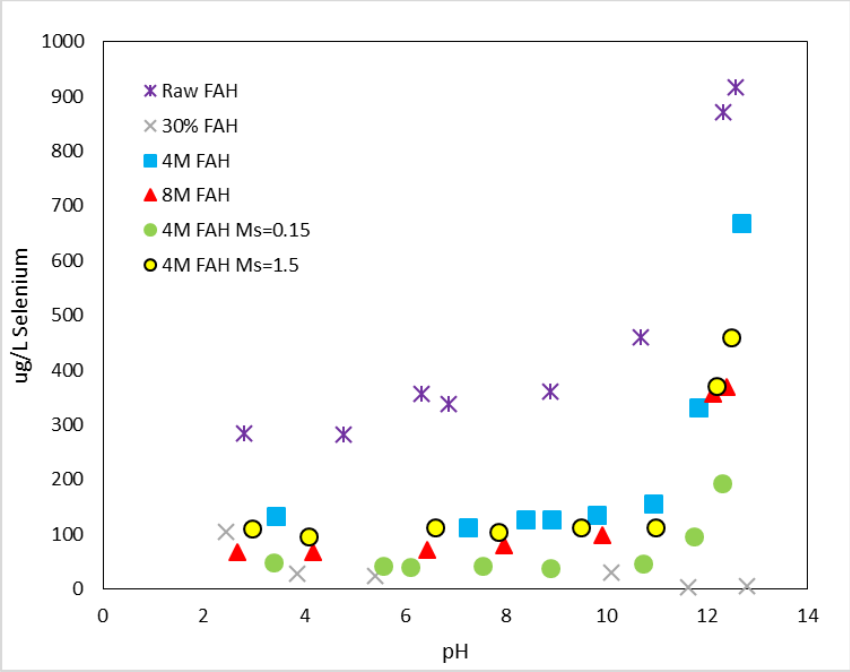

Figure A.56: Raw Selenium Concentrations in Leachate from FAH Specimens versus pH

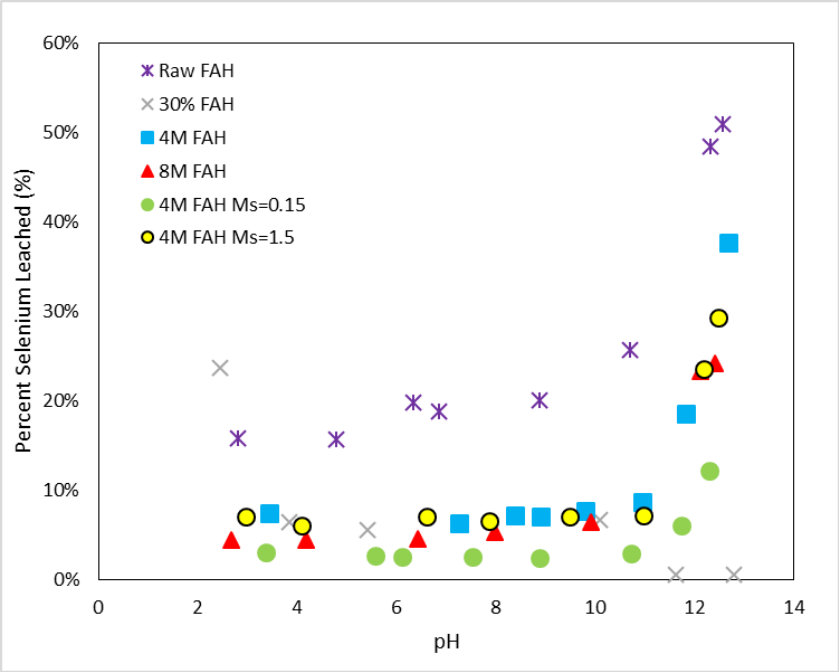

Figure A.57: Percent Selenium Leached from FAH Specimens versus pH

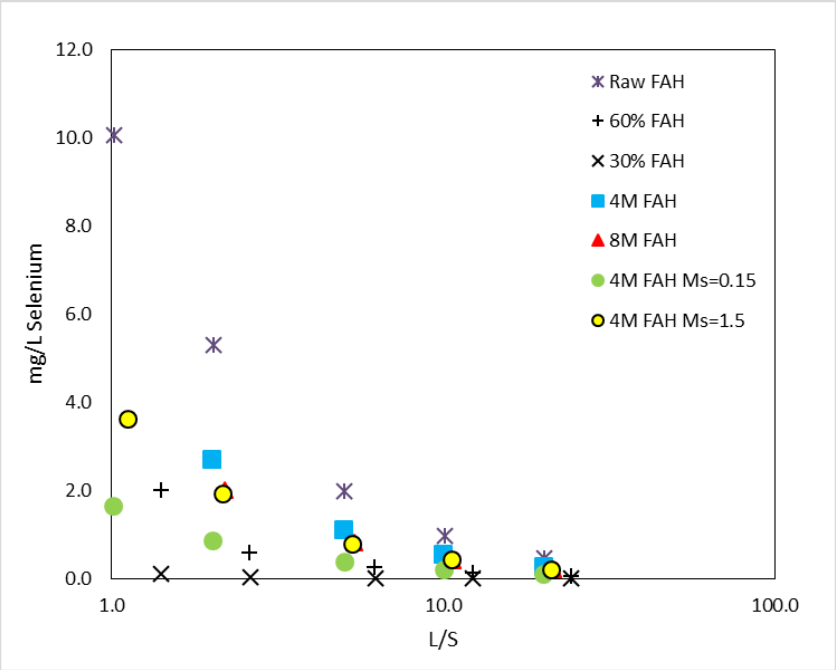

Figure A.58: Raw Selenium Concentrations in Leachate from FAH Specimens versus L/S

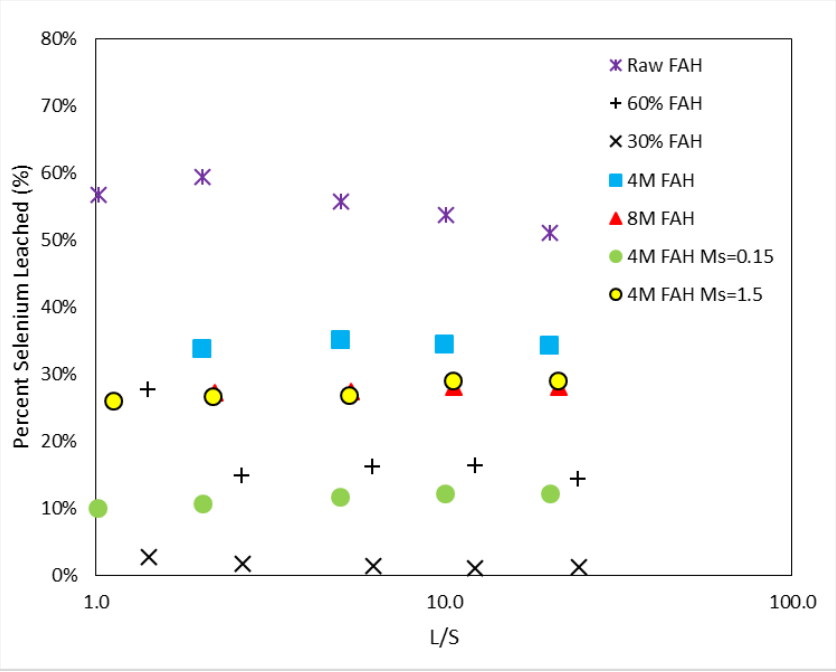

Figure A.59: Percent Selenium Leached from FAH Specimens versus L/S

A.16 FAB, SELENIUM

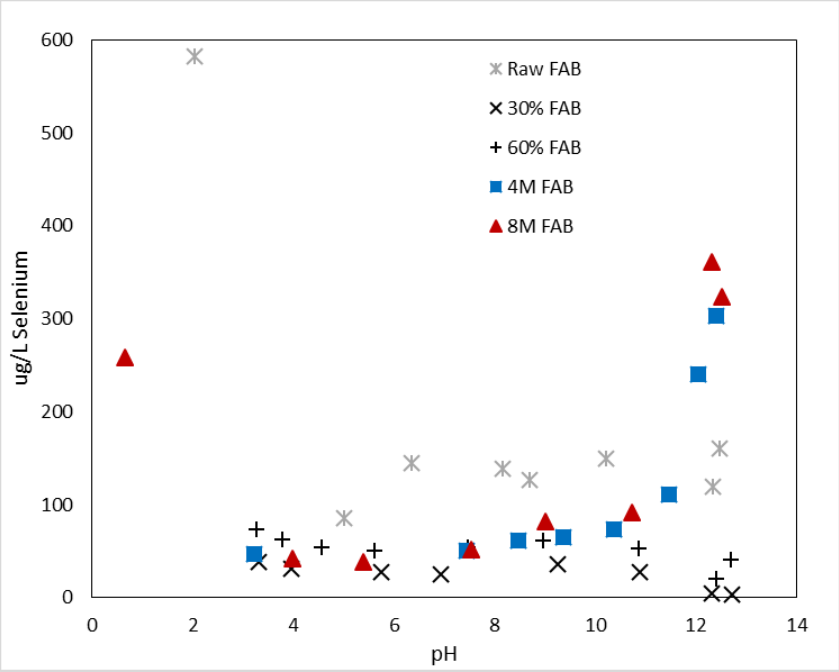

Figure A.60: Raw Selenium Concentrations in Leachate from FAB Specimens versus pH

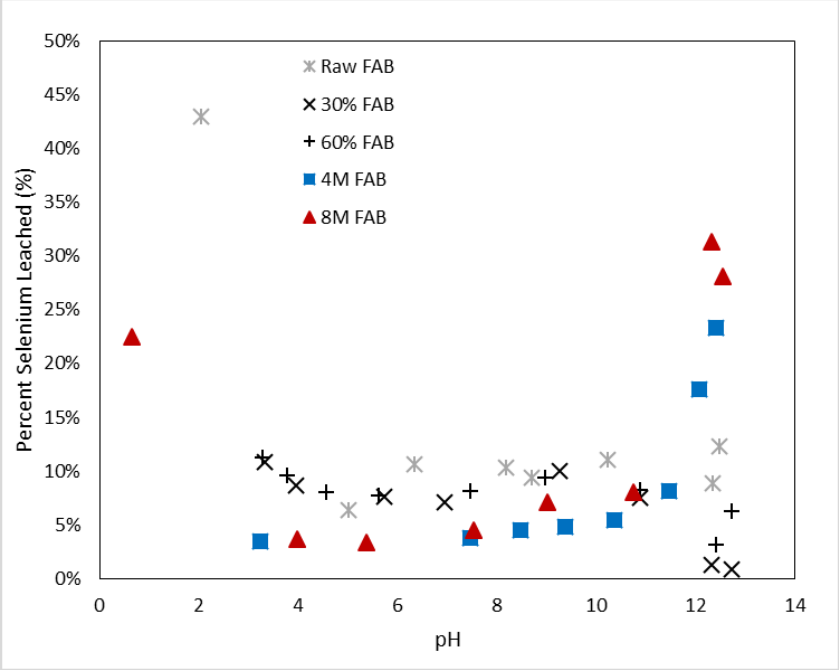

Figure A.61: Percent Selenium Leached from FAB Specimens versus pH

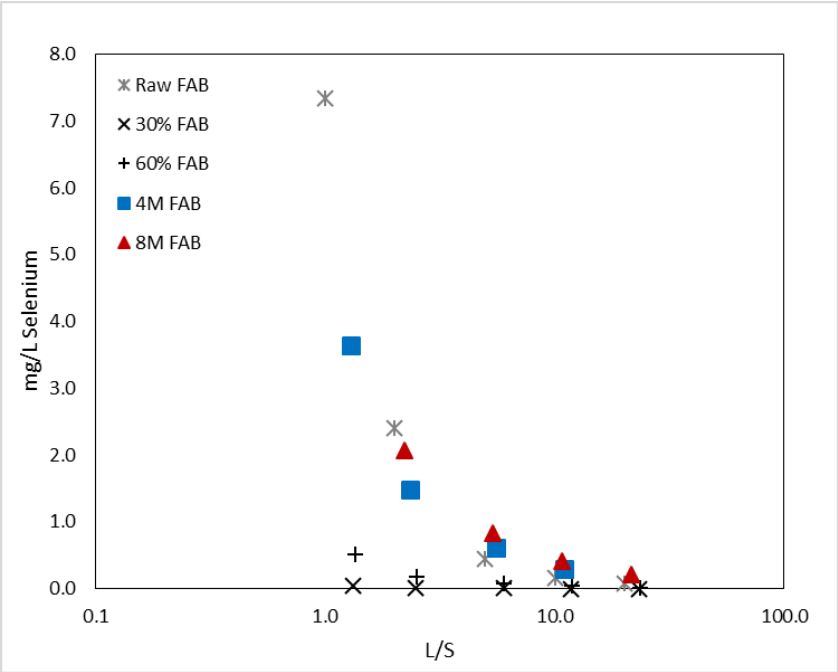

Figure A.62: Raw Selenium Concentrations in Leachate from FAB Specimens versus L/S

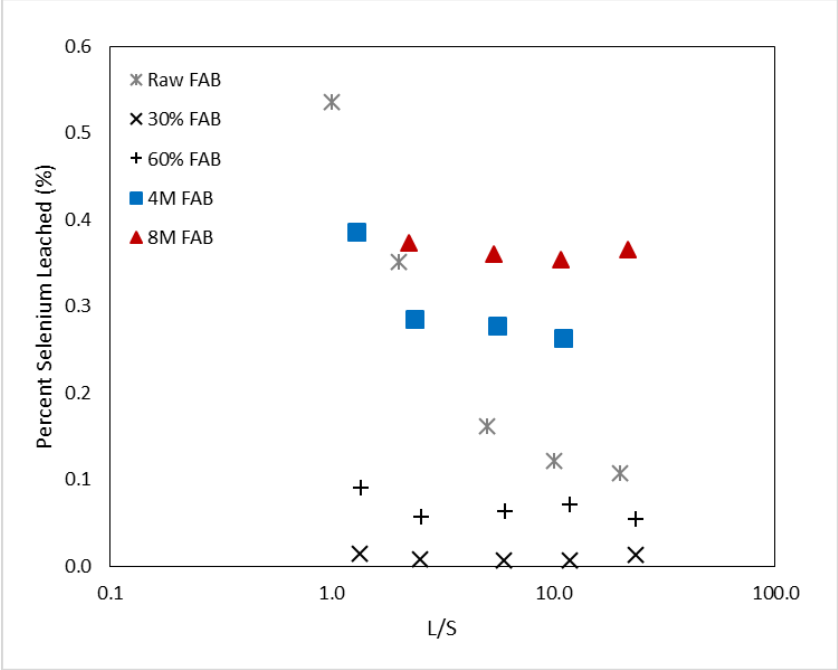

Figure A.63: Percent Selenium Leached from FAB Specimens versus L/S

A.17 FAH, ZINC

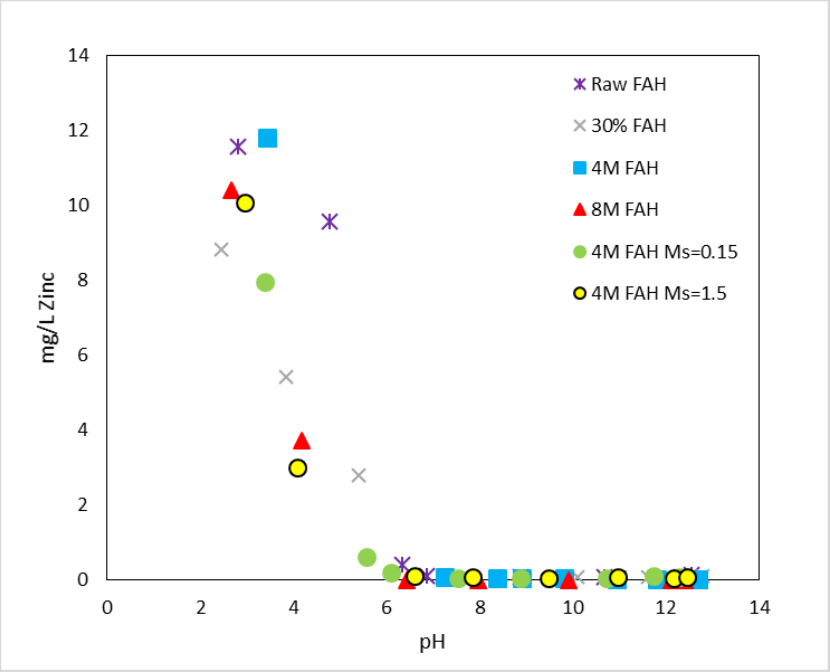

Figure A.64: Raw Zinc Concentrations in Leachate from FAH Specimens versus pH

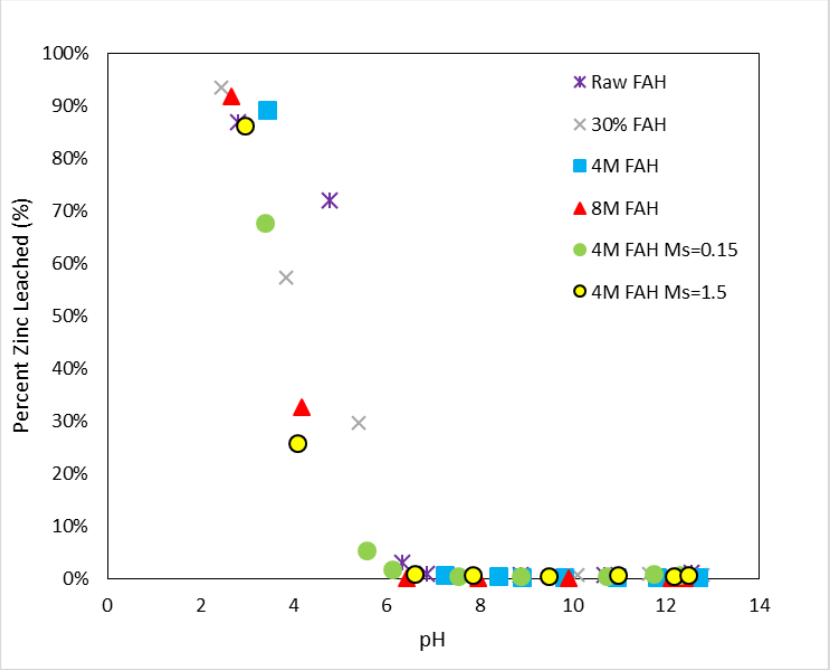

Figure A.65: Percent Zinc Leached from FAH Specimens versus pH

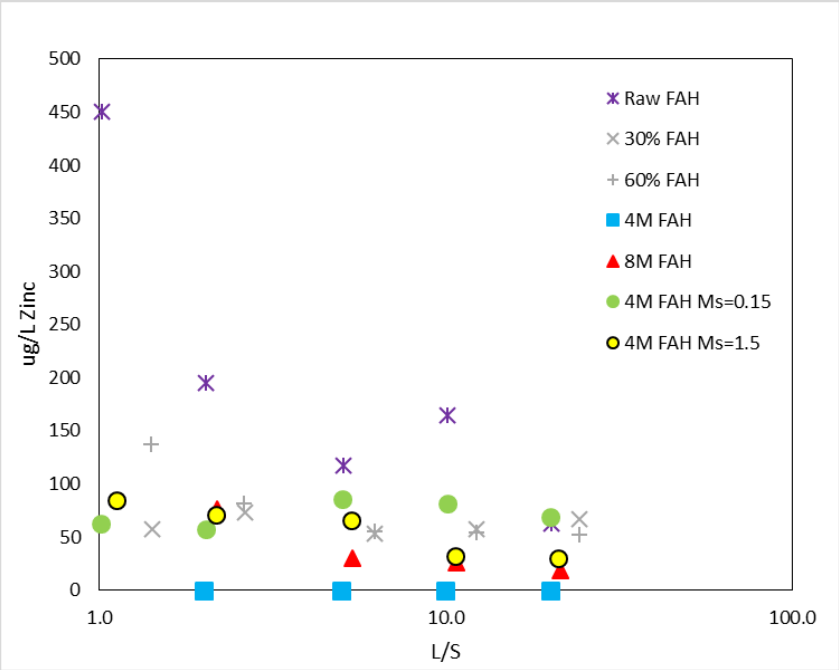

Figure A.66: Raw Zinc Concentrations in Leachate from FAH Specimens versus L/S

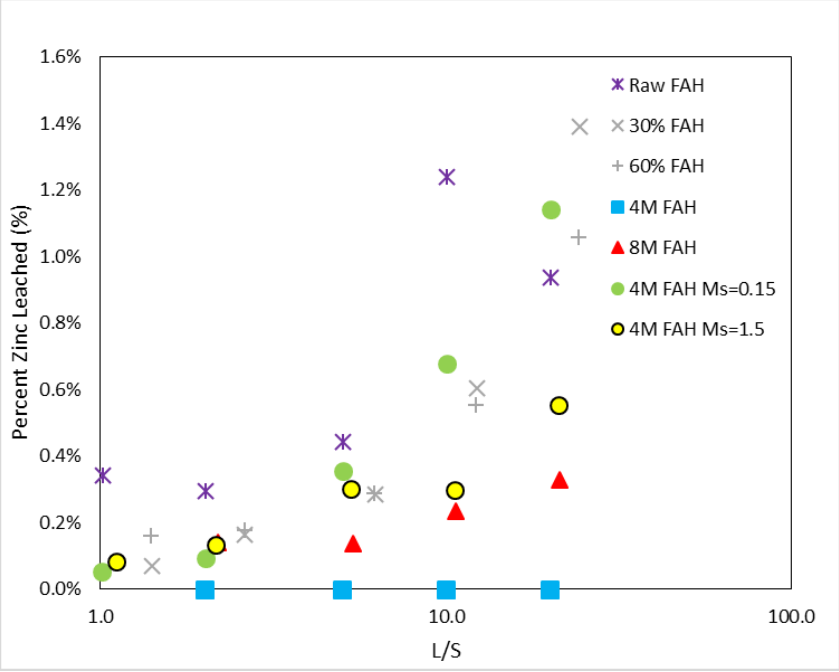

Figure A.67: Percent Zinc Leached from FAH Specimens versus L/S

A.18 FAB, ZINC

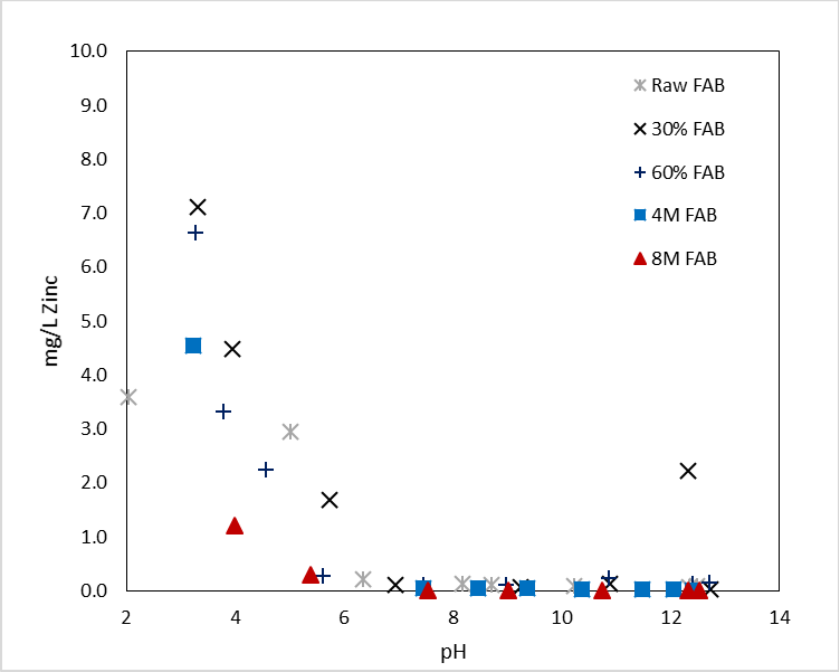

Figure A.68: Raw Zinc Concentrations in Leachate from FAB Specimens versus pH

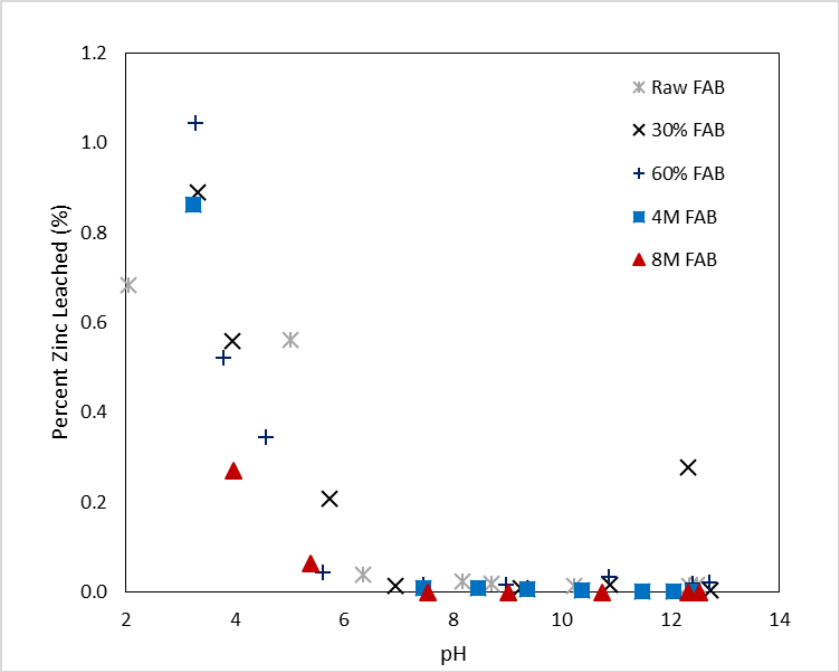

Figure A.69: Percent Zinc Leached from FAB Specimens versus pH

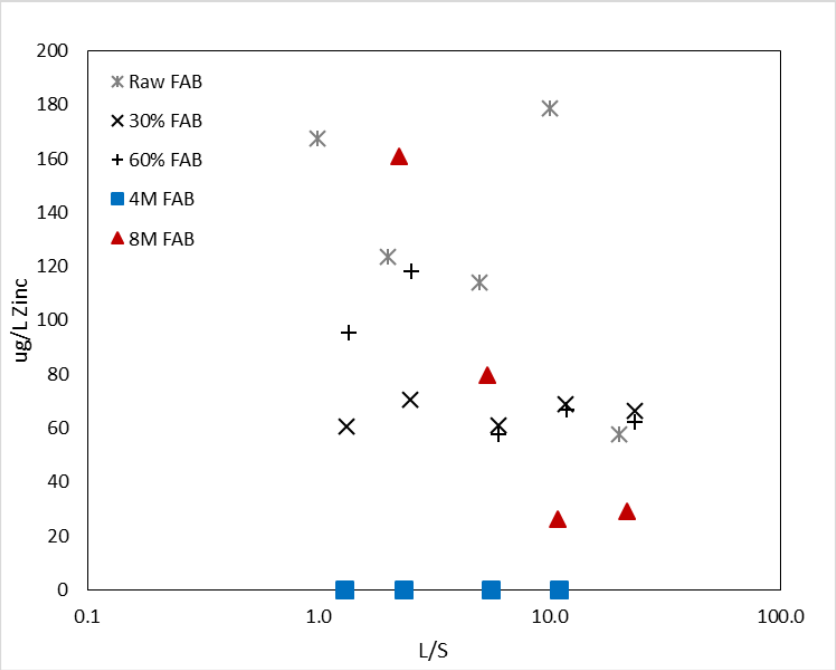

Figure A.70: Raw Zinc Concentrations in Leachate from FAB Specimens versus L/S

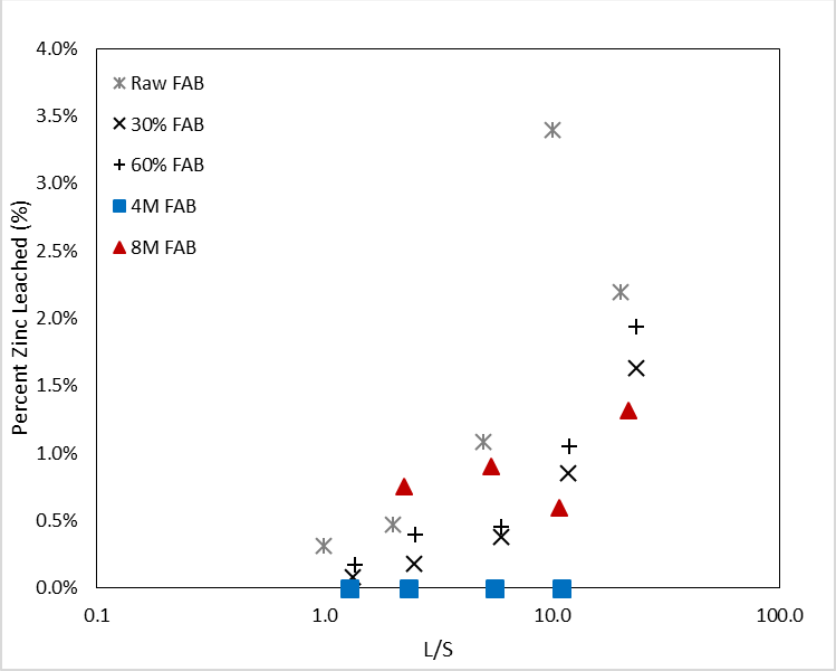

Figure A.71: Percent Zinc Leached from FAB Specimens versus L/S

Appendix B – Characterization Results

B.1 Supplementary Cementitious Materials XRF Results

Table B.1: Lafarge Slag and Calcium Aluminate Cement XRF Results

Oxide	Lafarge Slag	Calcium Aluminate Cement
SiO_2	36.27%	5.08%
Al_2O_3	9.23%	50.52%
Fe_2O_3	0.33%	2.25%
CaO	38.70%	36.89%
MgO	11.50%	0.57%
Na_2O	0.46%	0.08%
K_2O	0.45%	0.30%
TiO_2	0.41%	2.08%
Mn_2O_3	0.26%	0.04%
P_2O_5	0.01%	0.14%
SrO	0.05%	0.06%
BaO	0.05%	0.00%
SO_3	2.18%	0.02%

B.2 RAW CCP XRD

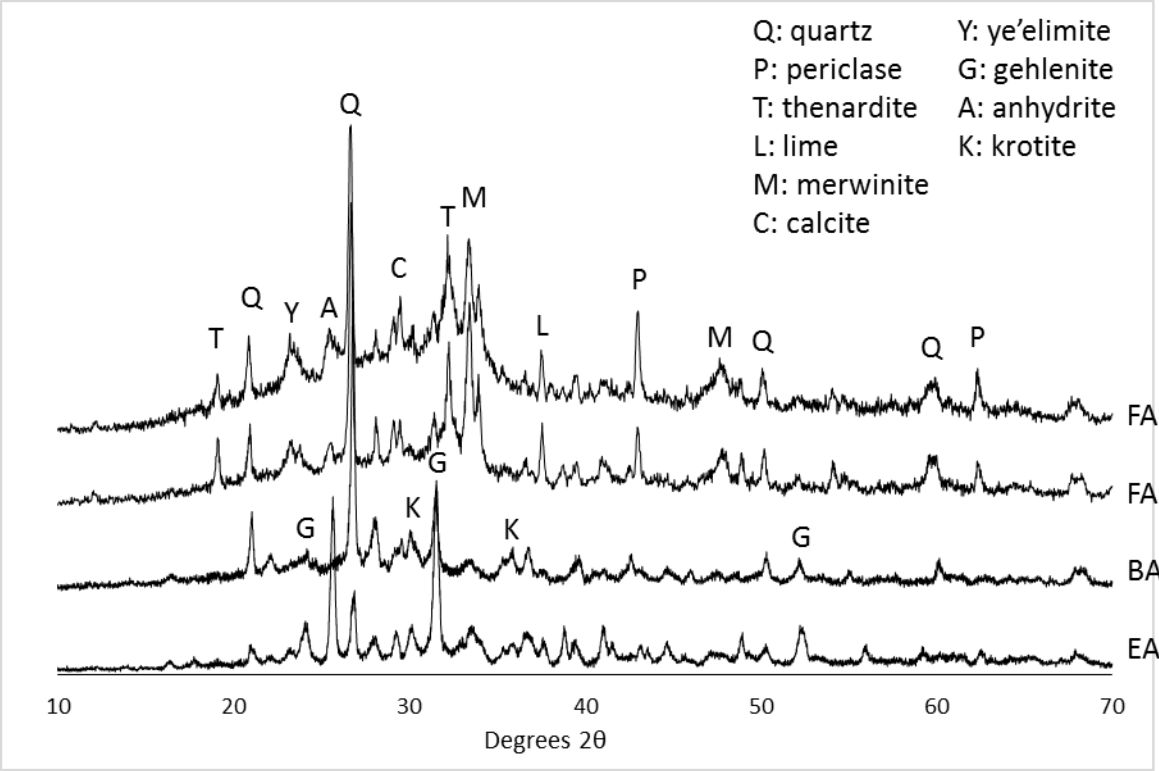

Figure B.1: Raw FAH, FAB, EA, and BA XRD Diffractograms

Table B.2: Raw FAH and FAB XRD Results

Phase Name	Phase Formula	PDF#	FAH Phase Percent (%)	FAB Phase Percent (%)
Amorphous	N/A	-	65.1	59.6
Anhydrite	$CaSO_4$	37-1496	1.6	13.1
Calcite	$CaCO_3$	5-586	2.3	2.3
Gehlenite	$Ca_2Al(AlSiO_7)$	37-755	-	6.3
Lime	CaO	37-1497	2.3	2.3
Merwinite	$Ca_3Mg(SiO_4)_2$	35-591	8.6	27.2

Periclase	MgO	45-0946	4.0	5.7
Quartz	SiO_2	33-1161	9.3	4.5
Thenardite	Na_2SO_4		4.1	1.9
Ye'elimite	$Ca_4(AlO_2)_6SO_4$	33-0256	2.7	1.7
Rwp			8.43	11.8
Rp			6.49	8.77
Chi^2			1.23	1.67

Table B.3: Economizer Ash and Bottom Ash XRD Results

Phase Name	**Phase Formula**	**PDF#**	**EA Phase Percent (%)**	**BA Phase Percent (%)**
Amorphous	N/A	-	39.9	52.5
Anhydrite	$CaSO_4$	37-1496	4.3	-
Anorthite	$CaAl_2Si_2O_8$	01-086-1705	3.8	2.8
Augite	$Ca(Fe,Mg)Si_2O_6$	24-0201	12.1	2.4
Calcite	$CaCO_3$	5-586	-	3.6
Gehlenite	$Ca_2Al(AlSiO_7)$	37-755	19.4	9.6
Hematite	Fe_2O_3	33-664		1.2
Lime	CaO	37-1497	0.4	-
Maghemite	Fe_2O_3	39-1346		1.8
Merwinite	$Ca_3Mg(SiO_4)_2$	35-591	10.9	.15
Periclase	MgO	45-0946	1.7	-
Quartz	SiO_2	33-1161	7.4	12.8

Thaumasite	$Ca_3Si(OH)_6(CO_3)(SO_4)\cdot 12H_2O$	01-074-3266	-	1.4
Ye'elimite	$Ca_4(AlO_2)_6SO_4$	33-0256	-	1.7
Rwp			13.54	13.58
Rp			10.15	10.51
Chi^2				2.47

B.3 FAH GEOPOLYMER XRD

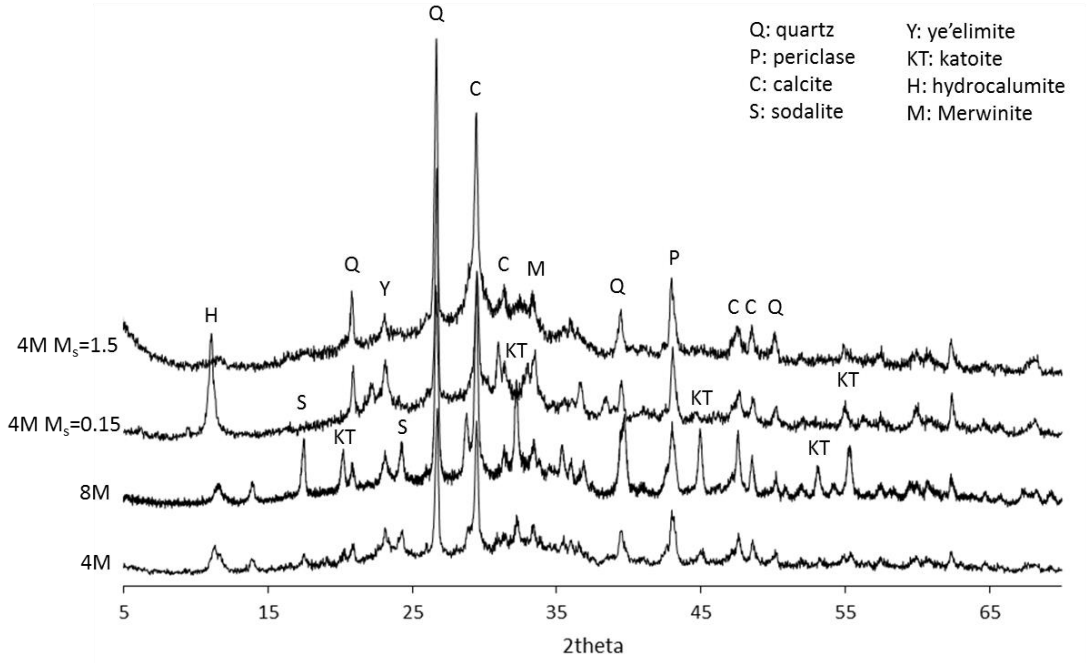

Figure B.2: 4M M_s = 0, 0.15, 1.5 and 8M M_s = 0 FAH Geopolymer XRD Diffractograms

Table B.4: 4M M_s = 0, 0.15, 1.5 and 8M M_s = 0 FAH Geopolymer XRD Phases and Phase Percent

Phase Name	Phase Formula	4M FAH Phase %	8M FAH Phase %	4M FAH M_s = 0.15 Phase %	4M FAH M_s = 1.5 Phase %
Amorphous C-S-H	N/A	61.6	60.8	47.9	70.2
Calcite	$CaCO_3$	10.7	10.8	11.5	15.2
Katoite	$Ca_3Al_2(SiO_4)_{(3-x)}(OH)_{4x}$	5.7	13.1	-	-
Hydrocalumite	$Ca_2Al(OH)_6[Cl\text{-}x(OH)_x]\text{-}3H_2O$	3.8	1.5	13.8	-
Merwinite	$Ca_3Mg(SiO_4)_2$	3.6	2.1	-	-
Periclase	MgO	3.2	2.8	4.0	2.6
Quartz	SiO_2	4.2	4.4	11.2	7.7
Sodalite	$Na_8Al_6Si_6O_{24}Cl_2$	3.0	2.6	-	-
Ye'elimite	$Ca_4(AlO_2)_6SO_4$	4.3	1.8	0.0	4.3
Rwp		8.75	9.46	9.22	8.84
Rp		6.72	7.16	7.16	6.69
Chi^2		1.07	1.75	2.14	1.97

B.4 FAH CEMENT PASTE XRD

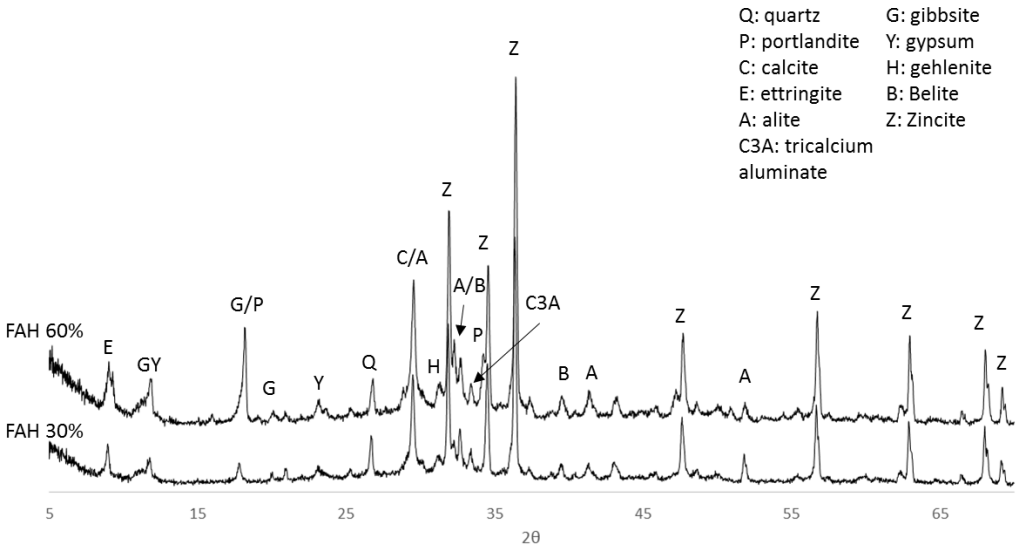

Figure B.3: 30% and 60% FAH Cement Paste XRD Diffractograms with Zincite

Table B.5: 30% and 60% FAH Cement Paste Crystalline Phases and Phase Percent

Phase Name	**Phase Formula**	**PDF#**	**30% FAH Phase Percent (%)**	**60% FAH Phase Percent (%)**
Amorphous	N/A	-	51.1	63.5
Alite	Ca_3SiO_5	42-551	4.6	6.0
Belite	Ca_2SiO_4	23-1042	6.5	1.3
Calcite	$CaCO_3$	5-586	14.9	9.3
C3A	$Ca_3Al_2O_6$	38-1429	1.4	1.1
Ettringite	$Ca_6Al_2(SO_4)_3(OH)_{12}(H_2O)_{26}$	41-1451	2.5	1.5
Gehlenite	$Ca_2Al(AlSi)O_7$	35-755	0.6	3.8
Gibbsite	$Ca_3Mg(SiO_4)_2$	01-070-2038	8.1	8.3
Gypsum	$CaSO_4$-$2H_2O$	33-311	3.9	2.9

Portlandite	$Ca(OH)_2$	4-733	4.9	-
Quartz	SiO_2	33-1161	1.6	2.3
Rwp			11.5	11.8
Rp			8.82	8.93
Chi^2			3.72	2.65

B.5 FAB GEOPOLYMER XRD

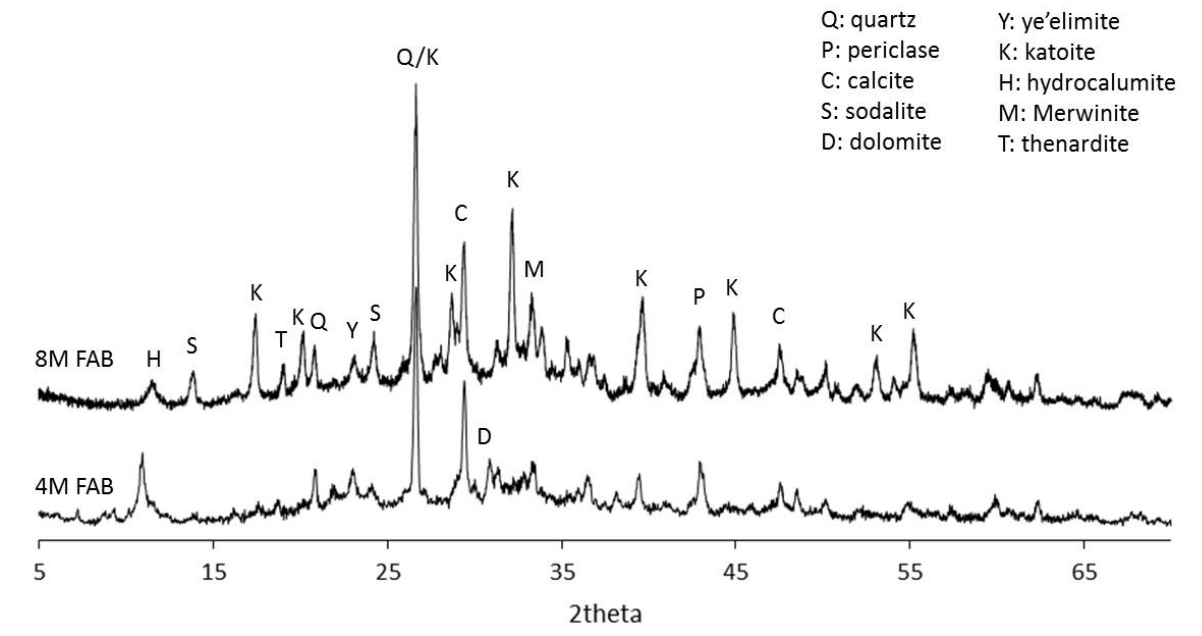

Figure B.4: 4M and 8M FAB Geopolymer XRD Diffractograms

Table B.6: 4M and 8M FAB Geopolymer Crystalline Phases and Phase Percent

Phase Name	**Phase Formula**	**PDF#**	**4M FAB Phase Percent (%)**	**8M FAB Phase Percent (%)**
Amorphous	N/A	-	68.4	48.9
Brucite	$Mg(OH)_2$	7-239	1.3	-
Calcite	$CaCO_3$	5-586	7.5	9.1

Ettringite	$Ca_6Al_2(SO_4)_3(OH)_{12}(H_2O)_{26}$	41-1451	1.1	-
Hydrocalumite	$Ca_6Al_4(OH)_{24}(CO_3)\ Cl_2(H_2O)_{9.6}$	42-558	5.2	1.4
Katoite	$Ca_3Al_2(OH)_{12}$	01-074-3031	-	13.0
Lime	CaO	37-1497	-	-
Merwinite	$Ca_3Mg(SiO_4)_2$	35-591	2.9	12.6
Periclase	MgO	45-0946	2.5	4.1
Quartz	SiO_2	33-1161	5.6	6.0
Sodalite	$Na_8Al_6Si_6O_{24}Cl_2$		-	4.9
Rwp			9.62	9.20
Rp			7.36	7.10
Chi^2			1.30	1.57

B.6 FAB CEMENT PASTE XRD

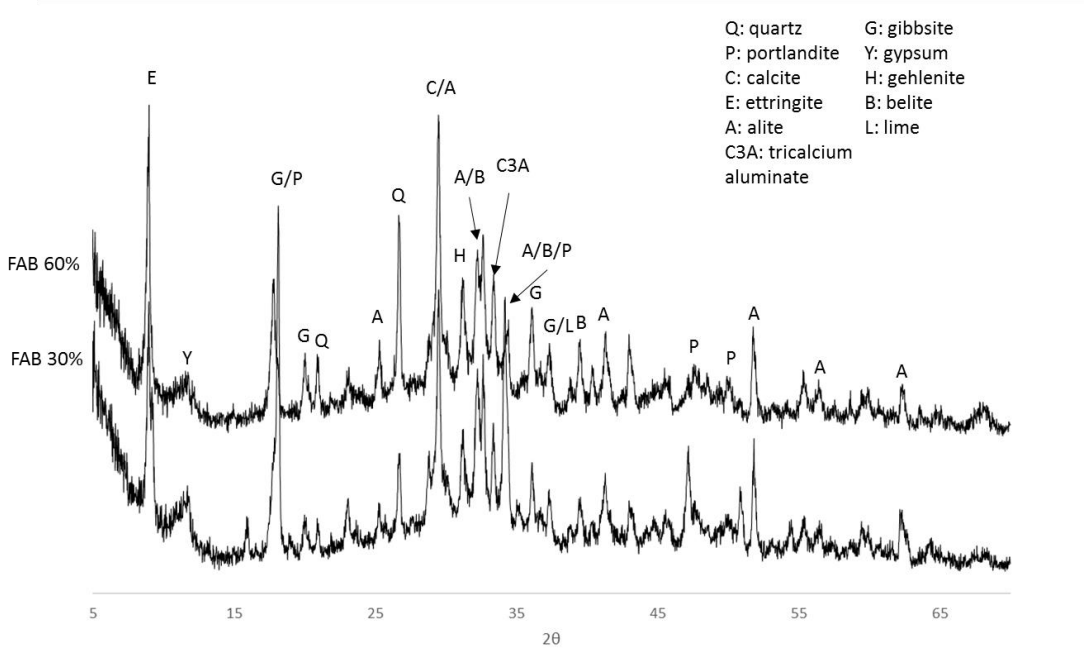

Figure B.5: 30% and 60% FAB Cement Paste XRD Diffractograms without Zincite

Table B.7: 30% and 60% FAH Cement Paste Phases and Phase Percent

Phase Name	**Phase Formula**	**PDF#**	**30% FAB Phase Percent (%)**	**60% FAB Phase Percent (%)**
Amorphous	N/A	-	55.8	71.2
Alite	Ca_3SiO_5	42-551	10.2	9.8
Dolomite	$CaMg(CO_3)_2$	33-628	1.1	0.6
Ettringite	$Ca_6Al_2(SO_4)_3(OH)_{12}(H_2O)_{26}$	41-1451	7.6	2.7
Gibbsite	$Ca_3Mg(SiO_4)_2$	01-070-2038	13.8	8.8
Gypsum	$CaSO_4$-$2H_2O$	33-311	1.7	1.3

Merwinite	$Ca_3Mg(SiO_4)_2$	35-391	3.5	2.3
Portlandite	$Ca(OH)_2$	4-733	5.2	-
Quartz	SiO_2	33-1161	1.2	3.5
Rwp			13.47	15.80
Rp			10.18	11.96
Chi^2			3.26	4.78

Appendix C – Water Quality Data

C.1 Conductivity Measurements

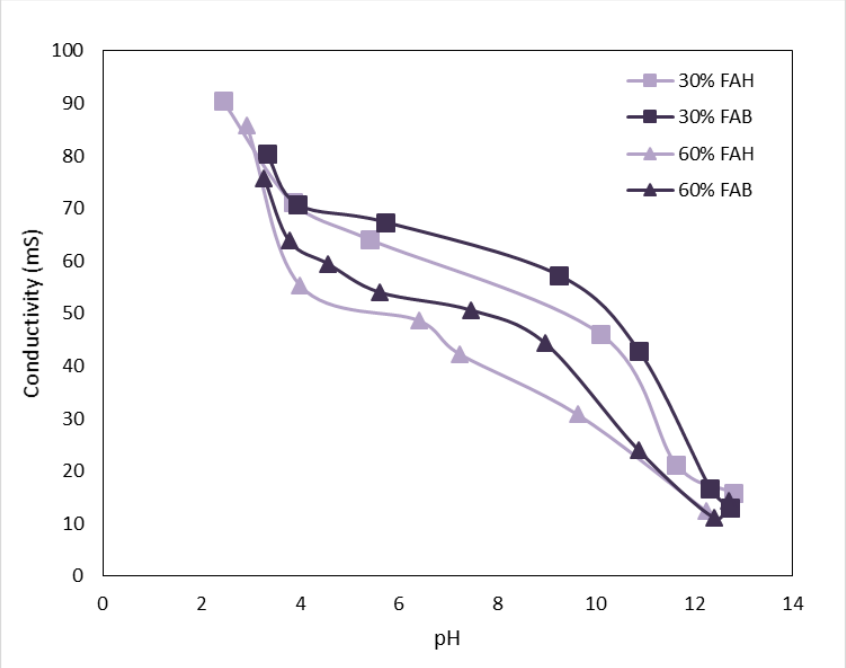

Figure C.1: Conductivity Measurements for Cement Paste Specimens versus pH with an L/S of 10

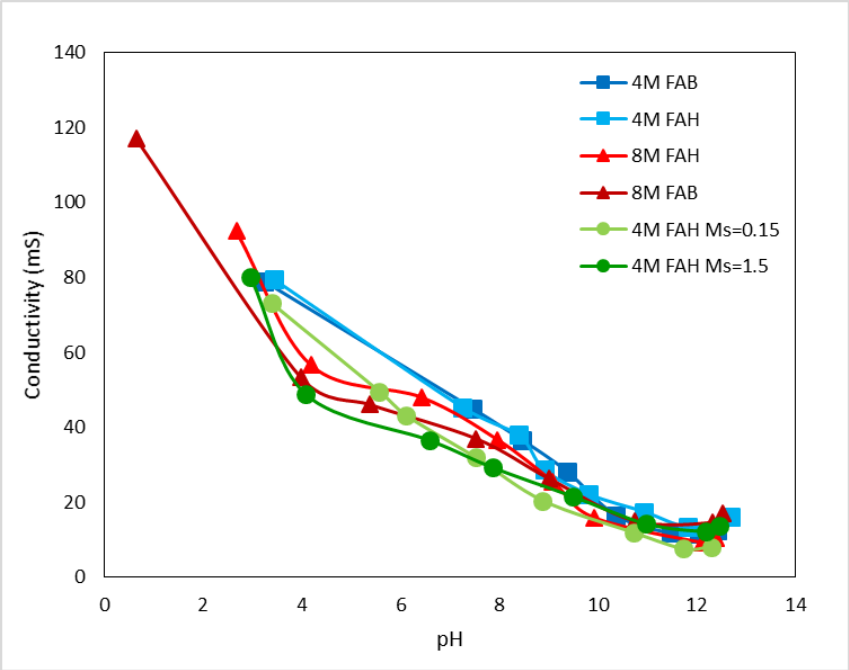

Figure C.2: Conductivity Measurements for Geopolymer Specimens versus pH with an L/S of 10

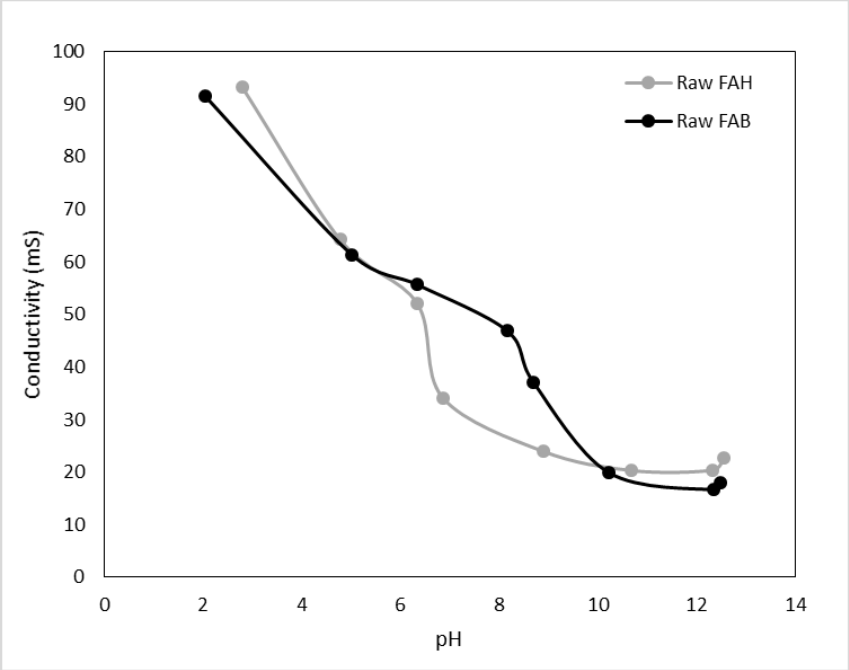

Figure C.3: Conductivity Measurements for Raw Ashes versus pH with an L/S of 10

C.2 TITRATION CURVES

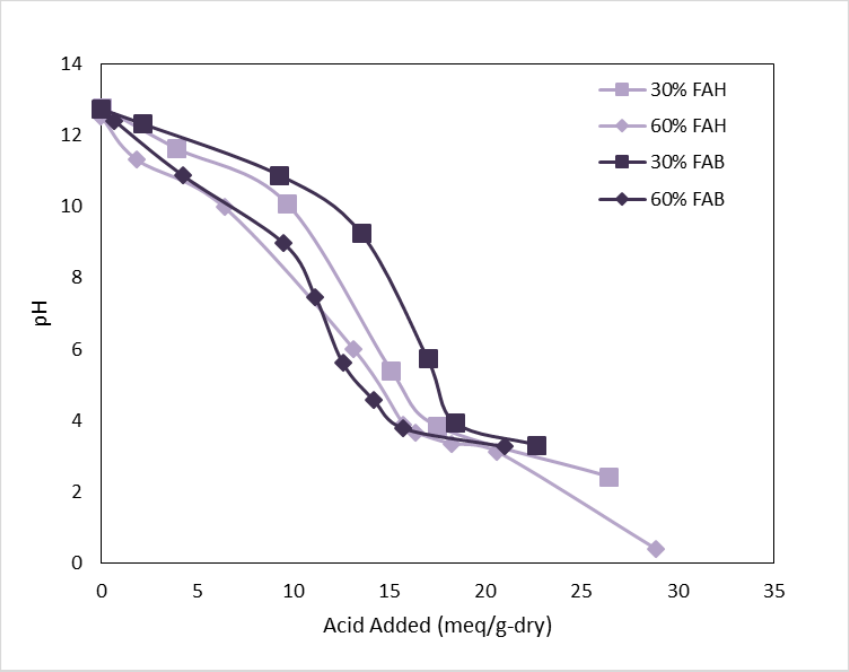

Figure C.4: Titration Curves for Cement Paste Specimens with an L/S of 10

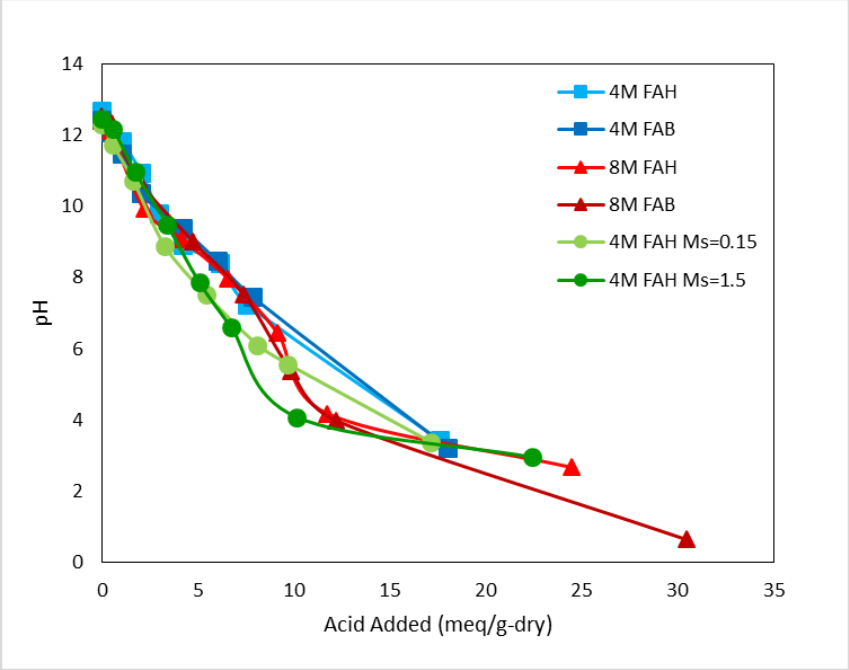

Figure C.5: Titration Curves for Geopolymer Specimens with an L/S of 10

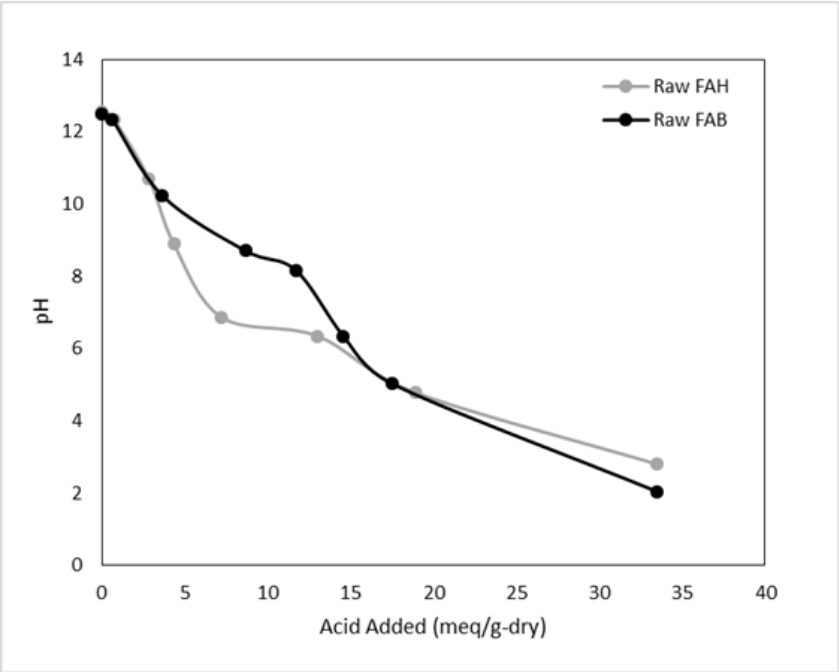

Figure C.6: Titration Curves for Raw CCPs with an L/S of 10

C.3 ORP DATA

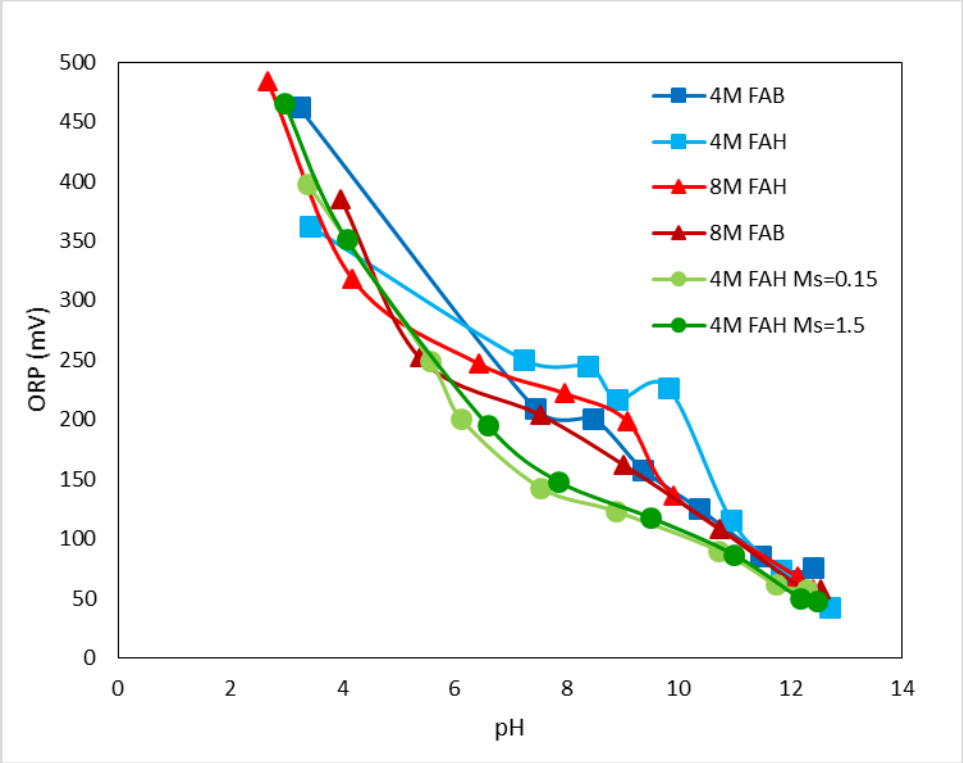

Figure C.7: ORP for Geopolymer Specimens in Reagent Water versus pH with an L/S of 10

References

A. Allahverdi, E. Najafi Kani, & S. Esmaeilpoor. (2008). Effects of Silica Modulus and Alkali Concentration on Activation of Blast-Furnace Slag. *Iranian Journal of Materials Science & Engineering*, *5*(2), 32–35. Retrieved from http://ijmse.iust.ac.ir/browse.php?a_code=A-10-3-26&slc_lang=en&sid=1

Akhter, H., Butler, L. G., Branz, S., Cartledge, F. K., & Tittlebaum, M. E. (1990). Immobilization of As, Cd, Cr and PB-containing soils by using cement or pozzolanic fixing agents. *Journal of Hazardous Materials*, *24*(2–3), 145–155. https://doi.org/10.1016/0304-3894(90)87006-4

Alexandratos, V., Elzinga, E.J., & Reeder, R.J. (2007). Arsenate uptake by calcite: Macroscopic and spectroscopic characterization of adsorption and incorpation mechanisms. *Ceochimica et Cosmochimica Acta, 71,* 4172-4187.

Al-Zboon, K., Al-Harahsheh, M. S., & Hani, F. B. (2011). Fly ash-based geopolymer for Pb removal from aqueous solution. *Journal of Hazardous Materials*. https://doi.org/10.1016/j.jhazmat.2011.01.133

Álvarez-Ayuso, E., Querol, X., Plana, F., Alastuey, A., Moreno, N., Izquierdo, M., … Barra, M. (2008). Environmental, physical and structural characterisation of geopolymer matrixes synthesised from coal (co-)combustion fly ashes. *Journal of Hazardous Materials*, *154*(1–3), 175–183. https://doi.org/10.1016/j.jhazmat.2007.10.008

Anseau, M. R., Leung, J. P., Sahai, N., & Swaddle, T. W. (2005). Interactions of Silicate Ions with Zinc(II) and Aluminum(III) in Alkaline Aqueous Solution. *Inorganic Chemistry*, *44*(22), 8023–8032. https://doi.org/10.1021/ic050594c

ASTM Standard C39. (2007). Compressive Strength for Cylindrical Concrete Specimens. *ASTM International, West Conshohocker, PA, 2003.*

ASTM Standard C192. (2016). Standard Practice for Making and Curing Concrete Test Specimens in the Laboratory. *ASTM International, West Conshohocker, PA, 2003.*

ASTM Standard C305. (2004). Mechanical Mixing of Hydraulic Cement Pastes and Mortars of Plastic Consistency. *ASTM International, West Conshohocker, PA, 2003.*

Bankowski, P., Zou, L., & Hodges, R. (2004). Reduction of metal leaching in brown coal fly ash using geopolymers, *114*, 59–67. https://doi.org/10.1016/j.jhazmat.2004.06.034

Barron, J.J. & Ashton, C. (2007). The Effect of Temperature on Conductivity Measurement. *Technical Services Department, Reagecon.* https://www.reagecon.com/pdf/technicalpapers/Effect_of_Temperature_TSP-07_Issue3.pdf

Blissett, R. S., & Rowson, N. A. (2012). A review of the multi-component utilisation of coal fly ash. *Fuel*, *97*, 1–23. https://doi.org/10.1016/j.fuel.2012.03.024

CDC (2011). Chromium Toxicity. *Agency for Toxic Substances and Disease Registry Case Studies in Environmental Medicine (CSEM).* https://www.atsdr.cdc.gov/csem/chromium/docs/chromium.pdf

CDC (2013). Cadmium Toxicity. *Agency for Toxic Substances and Disease Registry*

Case Studies in Environmental Medicine (CSEM). https://www.atsdr.cdc.gov/csem/cadmium/docs/cadmium.pdf
Chancey, R. T. (2008). Characterization of crystalline and amorphous phases and respective reactivities in a class F fly ash. http://hdl.handle.net/2152/18003
Christensen, T. H., Kjeldsen, P., Bjerg, P. L., Jensen, D. L., Christensen, J. B., Baun, A., … Heron, G. (2001). Biogeochemistry of landfill leachate plumes. *Applied Geochemistry*. https://doi.org/10.1016/S0883-2927(00)00082-2
Chu, K., & Thompson, A.R. (1962). Densities and Refractive Indices of Alcohol-Water Solutions. *Journal of Chemical and Engineering Data.* Vol 7, No.3, p358-360.
Comrie, D. C., Paterson, J. H., & Ritcey, D. J. (n.d.). Ppp 0024. *Scrap*.
Dan, Y., Zimmerman, C., Liu, K., Shi, H., & Wang, J. (2013). Increased leaching of As, Se, Mo, and v from high calcium coal ash containing trona reaction products. *Energy and Fuels*, *27*(3), 1531–1537. https://doi.org/10.1021/ef3020469
Davidovits, J. (1994). Properties of Geopolymer Cements. *First International Conference on Alkaline Cements and Concretes*, 131–149.
Day, R.L., & Marsh, B.K. (1987). Measurement of Porosity in Blended Cement Pastes. *Cement and Concrete Research*. Vol. 18, p63-73.
De Vargas, A. S., Dal Molin, D. C. C., Vilela, A. C. F., Silva, F. J. Da, Pavão, B., & Veit, H. (2011). The effects of Na2O/SiO2 molar ratio, curing temperature and age on compressive strength, morphology and microstructure of alkali-activated fly ash-based geopolymers. *Cement and Concrete Composites*, *33*(6), 653–660. https://doi.org/10.1016/j.cemconcomp.2011.03.006
Diaz, E. I., Allouche, E. N., & Eklund, S. (2010). Factors affecting the suitability of fly ash as source material for geopolymers. *Fuel*, *89*(5), 992–996. https://doi.org/10.1016/j.fuel.2009.09.012
Diez, J.M., Madrid, J. & Macias, A. (1997). Characterization of Cement-Stabilized Cd Wastes. *Cement and Concrete Research*, *27*(4), 479–485.
Dixit, S. & Hering, J. (2003). Comparison of Arsenic(V) and Arsenic(III) Sorption onto Iron Oxide Minerals: Implications for Arsenic Mobility. *Environmental Science and Technology, 37,* 4182-4189.
Dutré, V., & Vandecasteele, C. (1998). Immobilization mechanism of arsenic in waste solidified using cement and lime. *Environmental Science and Technology*, *32*(18), 2782–2787. https://doi.org/10.1021/es971090j
Dyer, J. a., Scrivner, N. C., & Dentel, S. K. (1998). A practical guide for determining the solubility of metal hydroxides and oxides in water. *Environmental Progress*, *17*(1), 1–8. https://doi.org/10.1002/ep.670170112
EPA Test Method 1311 (1992). TCLP, Toxicity Characteristic Leaching Procedure.
EPA Method 1313 (2012). Liquid-Solid Partitioning as a Function of Extract pH Using a Parallel Batch Extraction Procedure. *SW-846 Update V. Revision 0.*
EPA Method 1314 (2012). Liquid-Solid Partitioning as a Function of Liquid-Solid Ratio for Constituents in Solid Materials Using an Up-flow Percolation Column Procedure. *SW-846 Update V. Revision 0.*
EPA Method 1316 (2012). Liquid-Solid Partitioning as a Function of Liquid-to-Solid

Ratio in Solid Materials Using a Parallel Batch Procedure. *SW-846 Update V. Revision 0.*

EPA Method 3050b (1996). Acid Digestion of Sediments, Sludges, and Soils. CD-ROM. *Revision 2.*

Fagerlund, G. (2009) Chemically bound water as measure of degree of hydration method and potential errors. *Division of Building Materials, LTH, Lund University.* Report TVBM; Vol. 3150.

Fernández-Jiménez, A., Palomo, A., & Criado, M. (2005). Microstructure development of alkali-activated fly ash cement: A descriptive model. *Cement and Concrete Research*, *35*(6), 1204–1209. https://doi.org/10.1016/j.cemconres.2004.08.021

Gao, K., Lin, K. L., Wang, D., Hwang, C. L., Shiu, H. S., Chang, Y. M., & Cheng, T. W. (2014). Effects SiO2/Na2O molar ratio on mechanical properties and the microstructure of nano-SiO2 metakaolin-based geopolymers. *Construction and Building Materials*, *53*, 503–510. https://doi.org/10.1016/j.conbuildmat.2013.12.003

Ghosh, A., Sáez, A. E., & Ela, W. (2006). Effect of pH, competitive anions and NOM on the leaching of arsenic from solid residuals. *Science of the Total Environment*, *363*(1–3), 46–59. https://doi.org/10.1016/j.scitotenv.2005.06.018

Glasser, F. P. (1997). Fundamental aspects of cement solidification and stabilisation. *Journal of Hazardous Materials*, *52*(2–3), 151–170. https://doi.org/10.1016/S0304-3894(96)01805-5

Goldberg, S. & Glaubig, R.A. (1988). Anion Sorption on a calcareous, montmorillonitic soil-arsenic. *Soil Science Society of America Journal, 52,* 1297-1300.

Griffin, R.A., Anna, K. Au. & Frost, R.R. (1977). Effect of pH on adsorption of chromium from landfill leachate by clay minerals. *Journal of Env. Science and Health.* Vol 12 - Issue 8. http://dx.doi.org/10.1080/10934527709374769

Guo, X., & Shi, H. (2013). Self-Solidification / Stabilization of Heavy Metal Wastes of Class C Fly Ash – Based Geopolymers, (April), 491–496. https://doi.org/10.1061/(ASCE)MT.1943-5533.0000595.

Hanzlicek, T., & Steinerova-Vondrakova, M. (2006). Immobilization of toxic metals in solidified systems of siloxo-sial networks. *Journal of the American Ceramic Society*, *89*(3), 968–970. https://doi.org/10.1111/j.1551-2916.2005.00822.x

Hyun, D., Grubb, D. G., & Reilly, T. L. (2009). Stabilization / solidification of selenium-impacted soils using Portland cement and cement kiln dust, *168*, 944–951. https://doi.org/10.1016/j.jhazmat.2009.02.125

Ibrahim, A. (2016). Chemical characterization and mobility of metal species in fly ash – water system. *Water Science*, *29*(2), 109–122. https://doi.org/10.1016/j.wsj.2015.10.001

Iyer, R. (2002). The surface chemistry of leaching coal fly ash. *Journal of Hazardous Materials*, *93*(3), 321–329. https://doi.org/10.1016/S0304-3894(02)00049-3

Jewell, R. B., & Rathbone, R. F. (2009). Optical Properties of Coal Combustion Byproducts for Particle-Size Analysis by Laser Diffraction. *Coal Combustion and Gasification Products Journal.* Vol 1. https://doi.org/10.4177/CCGP-D-09-00001

Kazonich, G. (n.d.). EFFECTS OF pH , ORP , AND CONDUCTIVITY ON LEACHING

OF TRACE METALS FROM FLY ASH, 1–11. *U.S. Department of Energy, National Energy Technology Laboratory Environmental Science Division.*

Kogbara, R. B., Al-Tabbaa, A., & Stegemann, J. A. (2014). Comparisons of operating envelopes for contaminated soil stabilised/solidified with different cementitious binders. *Environmental Science and Pollution Research*, *21*(5), 3395–3414. https://doi.org/10.1007/s11356-013-2276-7

Kogbara, R. B., Al-Tabbaa, A., Yi, Y., & Stegemann, J. A. (2013). Cement-fly ash stabilisation/solidification of contaminated soil: Performance properties and initiation of operating envelopes. *Applied Geochemistry*, *33*, 64–75. https://doi.org/10.1016/j.apgeochem.2013.02.001

Kupwade-patil, K., Allouche, E. N., Islam, R., & Gunasekaran, A. (2014). Encapsulation of Solid Waste Incinerator Ash in Geopolymer Concretes and Its Applications, (111). https://doi.org/10.14359/51686834

Ladwig, K. E. N. (2007). Selenium and Arsenic Speciation in Fly Ash from Full-Scale Coal-Burning Utility Plants, *41*(9), 3284–3289.

Leist, M., Casey, R. J., & Caridi, D. (2003a). Evaluation of leaching tests for cement based immobilization of hazardous compounds. *Journal of Environmental Engineering-Asce*, *129*(7), 637–641. https://doi.org/10.1061/(ASCE)0733-9372(2003)129:7(637)

Leist, M., Casey, R. J., & Caridi, D. (2003b). The fixation and leaching of cement stabilized arsenic, *23*, 353–359.

Li, X. D., Poon, C. S., Sun, H., Lo, I. M. C., & Kirk, D. W. (2001). Heavy metal speciation and leaching behaviors in cement based solidified/stabilized waste materials. *Journal of Hazardous Materials*, *82*(3), 215–230. https://doi.org/10.1016/S0304-3894(00)00360-5

Li, Q., Sun, Z., Tao, D., Xu, Y., Li, P., Cui, H., & Zhai, J. (2013). Immobilization of simulated radionuclide 133Cs+ by fly ash-based geopolymer. *Journal of Hazardous Materials*, *262*, 325–331. https://doi.org/10.1016/j.jhazmat.2013.08.049

Mohebbi, M., Rajabipour, F., & Scheetz, B. E. (2015). Reliability of Loss on Ignition (LOI) Test for Determining the Unburned Carbon Content in Fly Ash. *World of Coal Ash (WOCA) Conferenc in Nasvhille, USA*.

Palmer, B. (2015). Coal Ash, Fly Ash, Bottom Ash, and Boiler Slag. *NDRC.* https://www.nrdc.org/onearth/coal-ash-fly-ash-bottom-ash-and-boiler-slag

Palomo, A., Ferna, A., Macphee, D. E., & Lachowski, E. E. (2005). Fixing Arsenic in Alkali-Activated Cementitious Matrices ′, *1126*, 1122–1126. https://doi.org/10.1111/j.1551-2916.2005.00224.x

Particle Analytical. (2017). BET. http://particle.dk/methods-analytical-laboratory/surface-area-bet-2/

Pflughoeft-hassett, D., Ladwig, K., Hassett, D. J., Heebink, L. V, Eylands, K., & Hoffarth, J. (2009). Characteristics and Performance of Fly Ash from Sodium Sorbent Scrubbing of SO 3 Emissions from Coal-Based Power Plants.

Poon, C. S., Clark, A. I., Perry, R., Barker, A. P., & Barnes, P. (1986). Permeability study on the cement based solidification process for the disposal of hazardous wastes.

Cement and Concrete Research, *16*(2), 161–172. https://doi.org/10.1016/0008-8846(86)90132-8
Porex Filtration Division (2017). Heavy Metal Removal from Wastewater by Precipitation and Microfiltration. http://www.porexfiltration.com/learning-center/technology/precipitation-microfiltration/
Provis, J.L. & van Deventer, J.S.J. *Geopolymers. Chapter 19, Immobilisation of Toxic Wastes in Geopolymers.* Woodhead Publishing Limited, 2009.
Rajurkar, N. S., Gokarn, A. N., & Dimya, K. (2011). Adsorption of Chromium(III), Nickel(II), and Copper(II) from aqueous solution by activated alumina. *Clean - Soil, Air, Water*, *39*(8), 767–773. https://doi.org/10.1002/clen.201000273
Ramezanianpour, A. A. (2014). *Cement Replacement Materials*. https://doi.org/10.1007/978-3-642-36721-2
Ratnaike, R. N. (2003). Acute and chronic arsenic toxicity. *Postgraduate Medical Journal*, *79*(933), 391–6. https://doi.org/10.1136/pmj.79.933.391
Roy, D. (1988). Relationships between Permeability, Porosity, Diffusion, and Microstructure of Cement Pastes, Mortar, and Concrete at Different Temperatures. *Materials Research Society, 137.* https://doi.org/10.1557/PROC-137-179
Ryu, G. S., Lee, Y. B., Koh, K. T., & Chung, Y. S. (2013). The mechanical properties of fly ash-based geopolymer concrete with alkaline activators. *Construction and Building Materials*, *47*(2013), 409–418. https://doi.org/10.1016/j.conbuildmat.2013.05.069
Schure, M. R., Soitys, P. A., Natusch, D. F. S., & Mauneys, T. (1985). Surface Area and Porosity of Coal Fly Ash. *Environmental Science and Technology*, *19*(1), 82–86. https://doi.org/10.1021/es00131a009
Scrivener, K., Snellings, R., & Lothenbach, B. (2015). A Practical Guide to Microstructural Analysis of Cementitious Materials. Chapter 5. CRC Press.
Shi, C., & Fernández-Jiménez, A. (2006). Stabilization/solidification of hazardous and radioactive wastes with alkali-activated cements. *Journal of Hazardous Materials*, *137*(3), 1656–1663. https://doi.org/10.1016/j.jhazmat.2006.05.008
States, U., Eia, T., States, U., & States, U. (2015). Trace Elements in Coal Ash, (May), 2–7.
Su, T., Shi, H., & Wang, J. (2011). Impact of trona-based SO2 control on the elemental leaching behavior of fly ash. *Energy and Fuels*, *25*(8), 3514–3521. https://doi.org/10.1021/ef2006035
Swanepoel, J. C., & Strydom, C. A. (2002). Utilisation of fly ash in a geopolymeric material. *Applied Geochemistry*, *17*(8), 1143–1148. https://doi.org/10.1016/S0883-2927(02)00005-7
Tiruta-Barna, L., Rakotoarisoa, Z., & Méhu, J. (2006). Assessment of the multi-scale leaching behaviour of compacted coal fly ash. *Journal of Hazardous Materials*, *137*(3), 1466–1478. https://doi.org/10.1016/j.jhazmat.2006.04.039
Van Jaarsveld, J. G. S., Van Deventer, J. S. J., Lorenzen, L., Jaarsveld, J. G. S. Van, & Deventer, J. S. J. Van. (1997). The Potential Use of Geopolymeric Materials to Immobilise Toxic Metals : Part 1. Theory and Applications. *Minerals Engineering*,

10(7), 1–10. https://doi.org/10.1016/S0892-6875(97)00046-0
Van Zomeren, A., & Comans, R. N. J. (2004). Contribution of natural organic matter to copper leaching from municipal solid waste incinerator bottom ash. *Environmental Science and Technology*, *38*(14), 3927–3932. https://doi.org/10.1021/es035266v
Wang, L. F., Habibul, N., He, D. Q., Li, W. W., Zhang, X., Jiang, H., & Yu, H. Q. (2015). Copper release from copper nanoparticles in the presence of natural organic matter. *Water Research*, *68*, 12–23. https://doi.org/10.1016/j.watres.2014.09.031
Wei, Z., Liang, K., Wu, Y., Zou, Y., Zuo, J., Arriagada, D. C., … Hu, G. (2016). The effect of pH on the adsorption of arsenic(III) and arsenic(V) at the TiO2 anatase [101] surface. *Journal of Colloid and Interface Science*, *462*, 252–259. https://doi.org/10.1016/j.jcis.2015.10.018
WHO (2011). Selenium in Drinking Water. http://www.who.int/water_sanitation_health/dwq/chemicals/selenium.pdf
Williamson, T. & Juenger, M. (2016). The role of activating solution concentration on alkali-silica reaction in alkali-activated fly ash concrete. *Cement and Concrete Research, 83,* 124-130.
Winnefeld, F., Leemann, A., Lucuk, M., Svoboda, P., & Neuroth, M. (2010). Assessment of Phase Formation in alkali activated low and high calcium fly ashes in building materials. *Construction and Building Materials, 24(6),* 1086-1093.
Zhang, J., Provis, J. L., Feng, D., & van Deventer, J. S. J. (2008a). Geopolymers for immobilization of Cr6+, Cd2+, and Pb2+. *Journal of Hazardous Materials*, *157*(2–3), 587–598. https://doi.org/10.1016/j.jhazmat.2008.01.053
Zhang, J., Provis, J. L., Feng, D., & van Deventer, J. S. J. (2008b). The role of sulfide in the immobilization of Cr(VI) in fly ash geopolymers. *Cement and Concrete Research*, *38*(5), 681–688. https://doi.org/10.1016/j.cemconres.2008.01.006
Zhang, Y., Cetin, B., Likos, W. J., & Edil, T. B. (2016). Impacts of pH on leaching potential of elements from MSW incineration fly ash. *Fuel*. https://doi.org/10.1016/j.fuel.2016.07.089
Zhao, S., Chen, Z., Shen, J., Kang, J., Zhang, J., & Shen, Y. (2017). Leaching mechanisms of constituents from fly ash under the influence of humic acid. *Journal of Hazardous Materials*, *321*, 647–660. https://doi.org/10.1016/j.jhazmat.2016.09.054